

OROELASTODYNAMIC SOLUTIONS OF
TRANSVERSELY ISOTROPIC
MULTI-LAYERED MEDIA



Mr. Suraparb Keawsawasvong

จุฬาลงกรณ์มหาวิทยาลัย
CHULALONGKORN UNIVERSITY

A Dissertation Submitted in Partial Fulfillment of the Requirements
for the Degree of Doctor of Philosophy in Civil Engineering
Department of Civil Engineering
Faculty of Engineering
Chulalongkorn University
Academic Year 2018
Copyright of Chulalongkorn University

ผลเฉลยทางพลวัตของตัวกลางโพโรอีลาสติกหลายชั้นที่มีคุณสมบัติเหมือนกันตามขวาง



วิทยานิพนธ์นี้เป็นส่วนหนึ่งของการศึกษาตามหลักสูตรปริญญาวิศวกรรมศาสตรดุษฎีบัณฑิต

สาขาวิชาวิศวกรรมโยธา ภาควิชาวิศวกรรมโยธา

คณะวิศวกรรมศาสตร์ จุฬาลงกรณ์มหาวิทยาลัย

ปีการศึกษา 2561

ลิขสิทธิ์ของจุฬาลงกรณ์มหาวิทยาลัย

สุภาพ แก้วสวัสดิ์วงศ์ : ผลเฉลยทางพลวัตของตัวกลางโพโรเอลาสติกหลายชั้นที่มีคุณสมบัติเหมือนกันตามขวาง.
(
POROELASTODYNAMIC SOLUTIONS OF TRANSVERSELY ISOTROPIC MULTI-LAYERED MEDIA) อ.ที่ปรึกษาหลัก : ศ. ดร.ธีรพงศ์ เสนจันทร์ดีไชย

วิทยานิพนธ์ฉบับนี้นำเสนอผลเฉลยทางพลวัตของตัวกลางโพโรเอลาสติกที่มีคุณสมบัติเหมือนกันตามขวาง ผลเฉลยทั่วไปภายใต้สภาวะระนาบความเครียดและสมมาตรรอบแกน ได้มาจากการแก้สมการกำกับโดยใช้วิธีการแปลงฟูเรียร์และแองเกิลตามลำดับ ผลเฉลยทั่วไปดังกล่าวได้ถูกนำไปใช้ในการหาผลเฉลยมูลฐานของตัวกลางกึ่งปริภูมิที่เป็นเนื้อเดียวกันโดยการแก้ปัญหาค่าขอบเขต ผลเฉลยทั่วไปยังได้ถูกนำไปใช้ในการพัฒนาวิธีเมทริกซ์แน่นอนตรงเพื่อหาผลเฉลยมูลฐานของตัวกลางแบบหลายชั้นที่มีคุณสมบัติต่างกัน ผลเฉลยมูลฐานสำหรับตัวกลางทั้งสองแบบจะถูกนำมาใช้วิเคราะห์ปัญหาการรับแรงร่วมกันระหว่างฐานรากและดินโพโรเอลาสติกที่มีคุณสมบัติเหมือนกันตามขวาง โปรแกรมสำหรับการวิเคราะห์ปัญหาเหล่านี้ได้ถูกพัฒนาขึ้น และความถูกต้องของโปรแกรมได้ถูกตรวจสอบโดยการเปรียบเทียบกับผลการศึกษาในอดีต ผลเฉลยเชิงตัวเลขสำหรับปัญหามูลฐานต่างๆ ได้ถูกนำเสนอเพื่อแสดงถึงอิทธิพลของคุณสมบัติแอนไอโซทรอปิกและโพโรเอลาสติกต่อการตอบสนองทางพลวัตของดินภายใต้แรงกระทำแบบโทมส์ฮาร์มอนิก นอกจากนี้ปัญหาการรับแรงร่วมกันระหว่างดินโพโรเอลาสติกที่มีคุณสมบัติเหมือนกันตามขวางและฐานรากแถบและฐานรากวงกลมได้ถูกวิเคราะห์โดยอาศัยผลเฉลยมูลฐานและการแบ่งชิ้นส่วนย่อยเพื่อนำเสนออิทธิพลของแอนไอโซทรอปิกของดิน ความยืดหยุ่นของฐานราก ระยะฝั่งของฐานราก และความถี่ของแรงที่กระทำ ต่อการตอบสนองทางพลวัตของฐานราก



สาขาวิชา วิศวกรรมโยธา
ปีการศึกษา 2561

ลายมือชื่อนิสิต
ลายมือชื่อ อ.ที่ปรึกษาหลัก

5971468021 : MAJOR CIVIL ENGINEERING

KEYWORD Anisotropy, Fundamental Solutions, Poroelasticity, Soil-structure
D: Interaction, Vibrations

Suraparb Keawsawasvong :
POROELASTODYNAMIC SOLUTIONS OF TRANSVERSELY ISOTROPIC
MULTI-LAYERED MEDIA. Advisor: Prof. Teerapong
Senjuntichai, Ph.D.

This dissertation presents poroelastodynamic fundamental solutions of transversely isotropic poroelastic materials. Analytical general solutions for transversely isotropic poroelastic media under time-harmonic loading are derived for plane strain and axisymmetric problems by applying Fourier and Hankel integral transforms respectively. The fundamental solutions for a homogeneous half-space are then explicitly obtained by solving relevant boundary value-problems based on the derived general solutions. An exact stiffness matrix method is also employed based on the present general solutions to determine the fundamental solutions corresponding to multi-layered transversely isotropic poroelastic media. The obtained fundamental solutions are then employed in the analysis of dynamic interaction problems between foundations and transversely isotropic poroelastic soils. A computer code is developed to obtain numerical solutions for each problem, and its accuracy is verified by comparing with existing solutions. Selected numerical results are presented to portray the influence of anisotropic and poroelastic properties on dynamic response of transversely isotropic poroelastic media under time-harmonic loading. In addition, numerical solutions on soil-structure interaction problems involving strip and circular foundations are also obtained by employing a semi-analytical discretization scheme based on the present fundamental solutions to demonstrate the influence of soil properties, the foundation flexibility, the embedded depth, and the frequency of excitation on the foundation response.

จุฬาลงกรณ์มหาวิทยาลัย
CHULALONGKORN UNIVERSITY

Field of Study: Civil Engineering

Student's Signature

Academic 2018

Advisor's Signature

Year:

.....

ACKNOWLEDGEMENTS

The work presented in this dissertation was supported by the Thailand Research Fund (TRF) under the Royal Golden Jubilee Ph.D. (RGJ-Ph.D.) scholarship, and the research assistantship from Applied Mechanics and Structures Research Unit, Department of Civil Engineering, Faculty of Engineering, Chulalongkorn University. Those supports are gratefully acknowledged.

The author wishes to express his sincere appreciation to his advisor, Professor Dr. Teerapong Senjuntichai, for their kind guidance and long-term support throughout this work. He also wishes to express his gratitude to Professor Dr. Nimal Rajapakse at the Simon Fraser University, Canada, for his kindness and invaluable advice on the research work and very warm welcome during the visit at SFU from September, 2018 to January, 2019.

The author also would like to express his sincere thanks to all committee members: Professor Dr. Thaksin Thepchatri; Associate Professor Dr. Jaroon Rungamornrat; Assistant Professor Dr. Watanachai Smittakorn; and Assistant Professor Dr. Yasothorn Sapsathiarn for their helpful suggestions and comments.

Special thanks are also due to everyone who has helped directly and indirectly in the preparation of this dissertation. Finally, the author would like to express his gratitude to his parents for their support and love.

จุฬาลงกรณ์มหาวิทยาลัย
CHULALONGKORN UNIVERSITY

Suraparb Keawsawasvong

TABLE OF CONTENTS

	Page
ABSTRACT (THAI)	iii
ABSTRACT (ENGLISH).....	iv
ACKNOWLEDGEMENTS	v
TABLE OF CONTENTS.....	vi
LIST OF TABLES	viii
LIST OF FIGURES	ix
LIST OF SYMBOLS	xiii
CHAPTER 1 INTRODUCTIONS.....	1
1.1 General.....	1
1.2 Objectives of Present Study.....	2
CHAPTER 2 LITERATURE REVIEWS.....	5
2.1 Literature Reviews of Fundamental Solutions	5
2.2 Literature Reviews of Soil-Structure Interaction Problems.....	7
CHAPTER 3 BASIC EQUATIONS AND GENERAL SOLUTIONS.....	9
3.1 Basic Equations	9
3.2 General Solutions for Plane Strain Deformations	13
3.3 General Solutions for Axisymmetric Deformations	17
CHAPTER 4 PLANE STRAIN FUNDAMENTAL SOLUTIONS OF TRANSVERSELY ISOTROPIC POROELASTIC MEDIA	23
4.1 Fundamental Solutions for Homogeneous Half-Plane	23
4.2 Fundamental Solutions for Multi-Layered Half-Plane	31
4.3 Conclusion	37
CHAPTER 5 AXISYMMETRIC FUNDAMENTAL SOLUTIONS OF TRANSVERSELY ISOTROPIC POROELASTIC MEDIA	47
5.1 Fundamental Solutions for Homogeneous Half-Space.....	47
5.2 Fundamental Solutions for Multi-Layered Half-Space	50

5.3 Conclusion	54
CHAPTER 6 INTERACTION BETWEEN STRIP FOUNDATIONS AND TRANSVERSELY ISOTROPIC PORORELASTIC SOILS	61
6.1 Rigid Strip Foundation in Homogeneous Half-Plane	61
6.2 Multiple Rigid Strip Foundations on Homogeneous Layer with Rigid Base	66
6.3 Multiple Flexible Strip Foundations on Multi-Layered Half-Plane	72
6.4 Conclusion	79
CHAPTER 7 INTERACTION BETWEEN CIRCULAR FOUNDATION AND TRANSVERSELY ISOTROPIC PORORELASTIC SOILS	98
7.1 Rigid Circular Foundation on Homogeneous Layer with Rigid Base	98
7.2 Flexible Circular Foundation in Homogeneous Half-Space.....	103
7.3 Flexible Circular Foundation in Multi-Layered Half-Space.....	111
7.4 Conclusion	112
CHAPTER 8 CONCLUSIONS	133
APPENDIX.....	135
REFERENCES	141
VITA.....	145

LIST OF TABLES

Table 4.1 Material properties of System A.....38



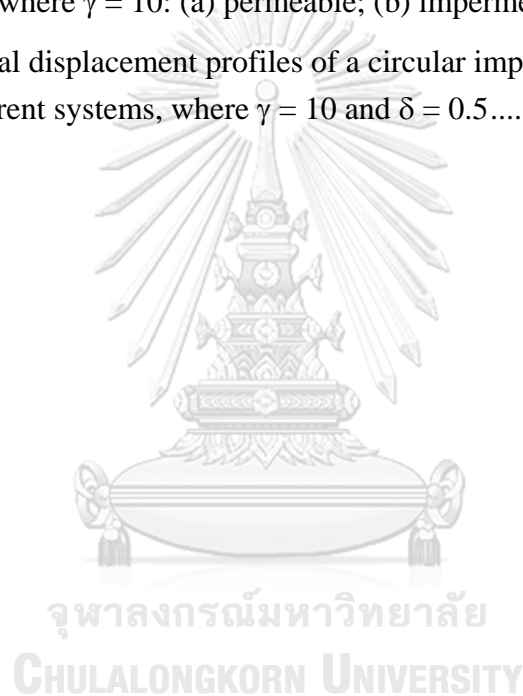
LIST OF FIGURES

Figure 1.1 Amplitude versus frequency relations for vertical oscillation of a rigid circular footing on an elastic half-space (After Richart 1962)	4
Figure 3.1 Homogeneous transversely isotropic poroelastic half-space.....	22
Figure 4.1 Comparisons of normalized vertical displacement profiles of an isotropic poroelastic half-plane under buried loading ($z/a = 1$): (a) applied vertical load; (b) applied fluid pressure	39
Figure 4.2 Comparisons of normalized elastic fields of transversely isotropic elastic half-planes: (a) vertical displacements and vertical stress under surface vertical loading; (b) horizontal displacement and horizontal stress under buried horizontal loading ($z/a = 1$)	40
Figure 4.3 Normalized displacement profiles along the x-axis under buried loading ($z/a = 1$): (a) vertical displacements under vertical loading; (b) horizontal displacement under horizontal loading	41
Figure 4.4 Normalized vertical stress profiles along the z-axis under buried loading ($z/a = 1$): (a) applied vertical load; and (b) applied fluid pressure.....	42
Figure 4.5 Normalized pore pressure profiles along the z-axis under buried loading ($z/a = 1$): (a) applied vertical load and (b) applied fluid pressure.....	43
Figure 4.6 Geometry of a multi-layered transversely isotropic poroelastic half-plane under time-harmonic loading	44
Figure 4.7 Comparison of: (a) normalized vertical displacement profiles of a multi-layered transversely isotropic half-plane under surface vertical loading ($h/a = 0$); (b) normalized vertical displacement of a multi-layered poroelastic half-plane under buried loading ($h/a = 1$)	45
Figure 4.8 Non-dimensional displacements due to surface ($h/a = 0$) and buried loading ($h/a = 1$): (a) vertical displacement due to vertical loading; (b) horizontal displacement due to horizontal loading	46
Figure 5.1 Comparison of non-dimensional vertical displacements of isotropic poroelastic half-space under applied vertical load.....	56
Figure 5.2 (a) Vertical displacement; (b) pore pressure and (c) vertical stress along z-axis under a surface vertical load.....	57
Figure 5.3 Geometry of a multi-layered transversely isotropic poroelastic half-space under time-harmonic loading	58

Figure 5.4 Comparison of normalized vertical displacement profiles of a multi-layered isotropic poroelastic half-plane under buried loading at $h = 2$	59
Figure 5.5 Non-dimensional displacements due to surface ($h/a = 0$) and buried loading ($h/a = 1$): (a) vertical displacement due to vertical loading; (b) radial displacement due to vertical loading	60
Figure 6.1 (a) Rigid strip foundation embedded in a transversely isotropic poroelastic half-plane under time-harmonic loading; (b) Discretization of contact area.....	80
Figure 6.2 Comparison of (a) non-dimensional vertical compliances of a rigid strip resting on a transversely isotropic half-plane; and (b) non-dimensional impedances of a rigid strip resting on an isotropic poroelastic half-plane.....	81
Figure 6.3 Non-dimensional vertical compliances of surface strip foundation ($h/a = 0$): (a) permeable foundation; (b) impermeable foundation	82
Figure 6.4 Non-dimensional vertical compliances of strip foundation embedded in Mat B with various embedded depths: (a) permeable foundation; (b) impermeable foundation	83
Figure 6.5 Non-dimensional compliances of surface strip foundation ($h/a = 0$): (a) rocking compliance; (b) horizontal compliance; (c) coupling compliance	84
Figure 6.6 (a) A system of N rigid strips on a transversely isotropic poroelastic layer under time-harmonic loading; (b) Discretization of the contact surface under strip i .	85
Figure 6.7 Comparison of non-dimensional compliances of a rigid strip on a transversely isotropic elastic layer ($h/a = 1$)	86
Figure 6.8 Comparison of non-dimensional impedances of a rigid strip on an isotropic poroelastic layer ($h/a = 1$)	87
Figure 6.9 Two-strip system considered in the numerical study	88
Figure 6.10 Non-dimensional compliances of Strip 1 with $d/a = 0.5$ on different transversely isotropic poroelastic layers with $h/a = 1$	89
Figure 6.11 Non-dimensional compliances of Strip 1 with various distances (d/a) on transversely Layer C with $h/a = 1$	90
Figure 6.12 Non-dimensional compliances of Strip 1 with $d/a = 0.5$ on Layer C with various thicknesses (h/a)	91
Figure 6.13 Multiple flexible strip foundations on a multi-layered transversely isotropic poroelastic half-plane under time-harmonic loading	92
Figure 6.14 Comparison of central displacement of surface strips on: (a) transversely isotropic half-plane; (b) poroelastic half-plane.....	93

Figure 6.15 (a) Central vertical displacement and (b) Bending moment at the center of a flexible impermeable strip on System A for different foundation flexibilities.....	94
Figure 6.16 Profiles of contact traction and pore pressure jump under flexible impermeable strip with $\gamma = 100$ on System A.....	95
Figure 6.17 Dynamic responses of a flexible impermeable strip with $\gamma = 1$ resting on different system: (a) center vertical displacement; (b) bending moment at the center	96
Figure 6.18 Central vertical displacement of two flexible impermeable strips on System A with various distance (d/a): (a) $\gamma = 0.2$; (b) $\gamma = 100$	97
Figure 7.1 Rigid circular foundation on transversely isotropic poroelastic layer.....	114
Figure 7.2 Unit vertical ring load f_z and applied ring fluid pressure f_p	115
Figure 7.3 Comparison with existing solutions for: (a) isotropic poroelastic half-space; (b) transversely isotropic elastic half-space.....	116
Figure 7.4 Influence of $n_1 = E_v/E_h$ on non-dimensional vertical compliance with $h/a = 1$ and $n_2 = 1$: (a) permeable foundation; (b) impermeable foundation	117
Figure 7.5 Influence of $n_2 = b_v/b_h$ on non-dimensional vertical compliance with $h/a = 1$ and $n_1 = 1$: (a) permeable foundation; (b) impermeable foundation	118
Figure 7.6 Influence of layer thickness on non-dimensional vertical compliance with $n_1 = n_2 = 0.5$: (a) permeable foundation; (b) impermeable foundation.....	119
Figure 7.7 Vertically loaded circular foundation in a transversely isotropic poroelastic soil.....	120
Figure 7.8 Vertical annular load f_z and annular fluid pressure f_p acting in the interior of soil half-space	121
Figure 7.9 Comparison of central displacement of embedded foundations on isotropic poroelastic soil ($h/a = 1$)	122
Figure 7.10 Effect of foundation permeability on vertical compliance of a rigid foundation ($h/a = 0$)	123
Figure 7.11 Central vertical compliance of a rigid impermeable foundation for different depths of embedment: (a) $n = 1$; (b) $n = 2$	124
Figure 7.12 Profiles of vertical stress and pore pressure jumps under a rigid impermeable foundation with $h/a = 2$	125
Figure 7.13 Central vertical compliance of a rigid impermeable foundation for different foundation flexibilities ($h/a = 0$): (a) $n = 1$; (b) $n = 2$	126

Figure 7.14 Bending moment at the center of foundation for different foundation flexibilities ($h/a = 0$): (a) $n = 1$; (b) $n = 2$	127
Figure 7.15 (a) Dimensionless amplitude of and (b) dimensionless force transferred to soil for a rigid impermeable massive foundation on different soils ($h/a = 0$).....	128
Figure 7.16 Vertically loaded circular foundation in a multi-layered transversely isotropic poroelastic half-space.....	129
Figure 7.17 Comparison of displacement profile of flexible circular foundations on multilayered transversely isotropic elastic half-space	130
Figure 7.18 Central vertical displacement of a circular foundation at $h/a = 0$ and 1 for different systems, where $\gamma = 10$: (a) permeable; (b) impermeable.....	131
Figure 7.19 Vertical displacement profiles of a circular impermeable foundation at $h/a = 0$ and 1 for different systems, where $\gamma = 10$ and $\delta = 0.5$	132



LIST OF SYMBOLS

A_z	amplitude of vertical vibration.
b_h	parameter accounting for the internal friction in the plane of isotropy.
b_v	parameter accounting for the internal friction in the normal plane.
c_{ij}	elastic moduli of solid skeleton.
C_H	horizontal compliance.
C_{HM}	coupling compliance.
C_M	rocking compliance.
C_V	vertical compliance.
E_h	drained Young's modulus in the plane of isotropy.
E_v	drained Young's modulus in the plane normal to the plane of isotropy.
D	relative flexibility parameter.
\bar{F}	potential function.
G	shear modulus.
J_n	Bessel function of the first kind of order n
M	Biot's parameters accounting for compressibility of the two-phased material.
m	mass of massive foundation.
m_i	density-like parameter.
Q_0	amplitude of the time-harmonic force acting on the massive foundation.
P_0	amplitude of the force transferred to soil.
p	excess pore fluid pressure.
r	radial coordinate.
T_i	traction in the i -direction.
T_p	pore pressure jump.
u_i	solid displacement of the solid matrix.
w	vertical displacement of the foundation.
w_i	fluid displacement relative to the solid matrix.
x	horizontal coordinate.

z	vertical coordinate.
α_h	Biot's coefficients in the plane of isotropy.
α_v	Biot's coefficients in the plane normal to the plane of isotropy.
ε_{ij}	strain component of the solid matrix.
ϕ	amplitude of the rotation about the y -axis.
μ	local coordinate of each strip foundation.
ν_h	Poisson's ratio in the plane of isotropy to a stress acting parallel to it.
ν_{vh}	Poisson's ratio in the plane of isotropy to a stress acting normal to it.
ρ	mass densities of the bulk material.
ρ^f	mass densities of the pore fluid.
σ_{ij}	total stress component of the bulk material.
ω	frequency of the motion.
ξ	Fourier and Hankel transform parameters.
Δ_i	displacement amplitude in the i -direction.

CHAPTER 1

INTRODUCTIONS

1.1 General

The theory of elasticity has long been used in geomechanics to estimate settlements and stresses of soil-structure interaction problems under static working loads. Although soils are not ideally elastic materials, they behave in a reasonably elastic manner when subjected to shearing strains of the magnitude ordinarily developed under machine, offshore and other foundations. The linear theory of elasticity has also been used to study the time-harmonic dynamic response of foundations in layered soils under small strains. One of key quantities in dynamic analysis of foundations is the amplitude of vibration of foundation. Richart (1962) developed a set of curves to demonstrate general limits of displacement amplitude for a given frequency as shown in Figure 1.1. These limits range from not noticeable to people to the extreme danger to structures. The amplitude of vibration and the maximum force transferred to soil are two key elements of foundation design.

Early studies on soil-structure interaction problems based on classical elasticity theory considered soils as homogenous isotropic elastic solids. However, geo-materials are often two-phase materials consisting of elastic solid skeleton with voids filled with water, commonly known as poroelastic materials. In addition, natural soils and rocks normally exhibit some degrees of anisotropy owing to various effects such as deposition or overburden. A simplified form of anisotropic properties, called transversely isotropic, has widely been accepted for the study of wave propagations in anisotropic materials including soils and rocks. The consideration of both anisotropic and two-phased properties of geo-materials is thus important in the study of dynamic interaction between foundations and soils. The theory of elastic wave propagations in poroelastic materials was proposed by Biot (1956) by adding the inertia terms to his three-dimensional consolidation theory (Biot 1941), in which the coupling between the solid and fluid stresses and strains are taken into account based on the classical theory of linear elastic and Darcy's law. To consider the effects of both anisotropy and poroelasticity, Biot proposed the constitutive model for anisotropic poroelastic

materials (Biot 1955), and later presented governing equations for wave propagations in transversely isotropic poroelastic media (Biot 1962).

In this dissertation, poroelastodynamics theory given by Biot (1962) is employed to obtain the fundamental solutions of transversely isotropic poroelastic media under plane strain and axisymmetric deformations by using the techniques of Fourier and Hankel integral transforms respectively. For homogeneous media, boundary-value problems corresponding to a transversely isotropic poroelastic half-space subjected to time-harmonic buried loading are established, and the plane strain and axisymmetric fundamental solutions are presented explicitly. For multi-layered media, an exact stiffness approach is employed to obtain the fundamental solutions for both cases. The obtained fundamental solutions are then employed as the influence foundations required in the formulation of various dynamic interaction problems between foundations and transversely isotropic poroelastic media. In addition, the influence of anisotropic and poroelastic material properties on foundation responses is also discussed.

1.2 Objectives of Present Study

The main objectives of the present study are given as follows:

- i. To obtain the analytical general solutions of transversely isotropic poroelastic materials under plane strain and axisymmetric deformations by using the techniques of Fourier and Hankel integral transforms respectively.
- ii. To obtain the fundamental solutions of homogeneous transversely isotropic poroelastic half-spaces under plane-strain and axisymmetric deformations.
- iii. To obtain the fundamental solutions of multi-layered transversely isotropic poroelastic media under plane-strain and axisymmetric deformations by adopting the exact stiffness matrix method.
- iv. To present numerical solutions of several boundary value problems based on the obtained fundamental solutions to demonstrate the influence of anisotropic and poroelastic material properties and other relevant parameters on dynamic response of transversely isotropic poroelastic media.

- v. To investigate several dynamic interaction problems between strip and circular foundations and transversely isotropic poroelastic soils by employing a semi-analytical discretization technique based on the obtained fundamental solutions.



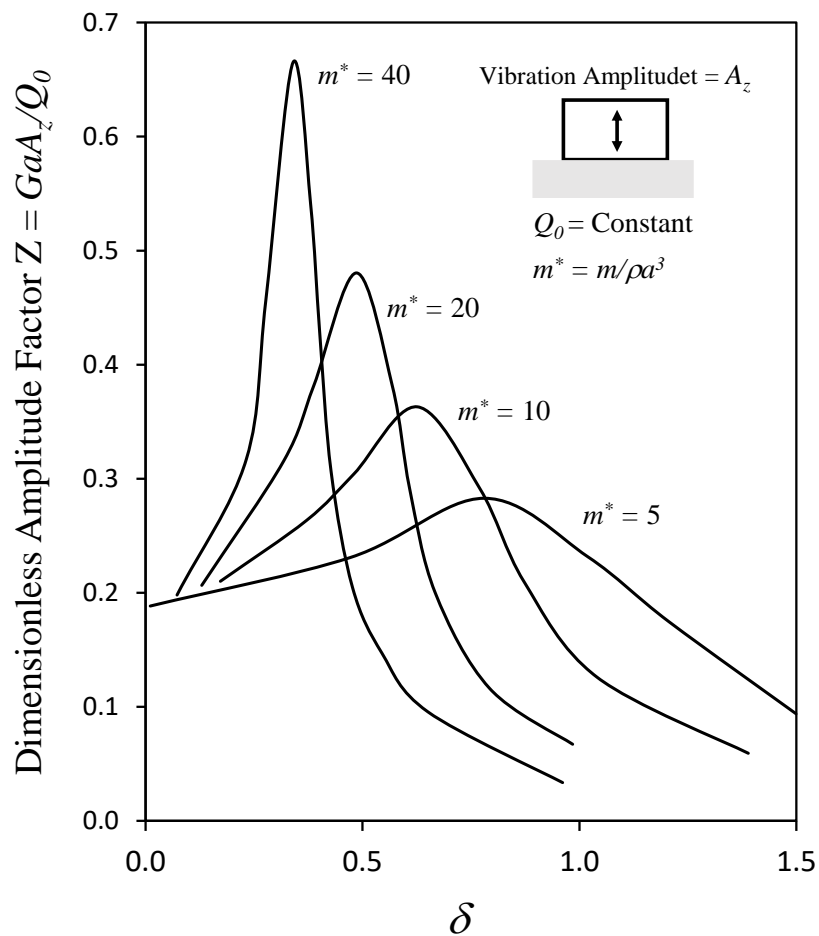


Figure 1.1 Amplitude versus frequency relations for vertical oscillation of a rigid circular footing on an elastic half-space (After Richart 1962)

CHAPTER 2 LITERATURE REVIEWS

2.1 Literature Reviews of Fundamental Solutions

Geo-materials such as rocks and soils often consists of a two-phase material consisting of an elastic solid skeleton with voids saturated with water commonly known as poroelastic materials. A salient feature of poroelastic materials is generation and dissipation of excess pore water pressure under applied loading. The study of wave propagations in poroelastic materials is of considerable importance in various disciplines such as civil engineering, earthquake engineering, and offshore engineering. The theory of elastic wave propagations in poroelastic materials was proposed by Biot (1956). Several researchers have employed Biot's poroelastodynamics theory to study a variety of problems related to poroelastic media. For example, dynamic response of homogeneous isotropic poroelastic media subjected to time harmonic loading under plane strain (Paul 1976; Philippacopoulos 1988; Senjuntichai and Rajapakse 1994); and axisymmetric (Philippacopoulos 1989; Zeng and Rajapakse 1999) deformations; and for three-dimensional response (Halpern and Christiano 1986a). For studies related to multi-layered poroelastic media under time harmonic loading, Lu and Hanyga (2005) and Zheng et al. (2013) adopted the transmission and reflection matrix (TRM) approach to investigate the response of multi-layered media under axisymmetric and asymmetric deformations respectively. The exact stiffness matrix approach was employed by Rajapakse and Senjuntichai (1995) to investigate dynamic response of a multi-layered isotropic poroelastic half-plane. The similar technique was used by Liu et al. (2015) and Ai and Wang (2017) to present dynamic response of a multi-layered isotropic poroelastic half-space under axisymmetric deformation. In addition, Senjuntichai et al. (2018) presented the dynamic response of multi-layered poroelastic media in three-dimensional Cartesian coordinate by using the exact stiffness matrix approach.

Geo-materials generally exhibit certain degrees of anisotropic properties that occur from deposition or sedimentation processes. As a result, the mechanical

properties of natural soils and rocks in their vertical and horizontal directions are different, and these materials are commonly known as transversely isotropic elastic materials. The theory of wave propagations in transversely isotropic elastic materials was presented by Stoneley (1949). Rajapakse and Wang (1991, 1993) derived Green's functions for a homogeneous transversely isotropic elastic half-space subjected to time-harmonic loading under plane-strain and axisymmetric conditions respectively. Subsequently, several studies on axisymmetric wave propagation problems involving homogeneous transversely isotropic elastic media were carried out by Liu (1997) and Wang and Liao (1999). In addition, Shodja and Eskandari-Ghadi (2007) presented a study on dynamic response of two-layered transversely isotropic elastic media under axisymmetric deformation. By using the elastodynamic potential method (Rahimian et al. 2007), asymmetric dynamic Green's functions for transversely isotropic elastic media were derived for single-layered (Khojasteh et al. 2008a) and two-layered (Khojasteh et al. 2008b) half-spaces. For studies on multi-layered transversely isotropic elastic media under time harmonic loading, Khojasteh et al. (2011) adopted the transmission and reflection matrix (TRM) approach to investigate dynamic response of multi-layered media under asymmetric deformations. The exact stiffness method was used by Wang and Rajapakse (1994) to obtain fundamental solutions of a multi-layered transversely isotropic elastic half-plane. The similar method was employed by Ai and Li (2014), Ai et al. (2014) and Ai and Zhang (2015) to investigate the response of multi-layered media under time-harmonic loading for asymmetric, axisymmetric and plane strain deformations respectively.

In order to combine the effects of anisotropy and poroelasticity, Biot (1955) proposed the constitutive relations for transversely isotropic and orthotropic poroelastic materials. Biot (1962) later extended his poroelastodynamics theory (Biot 1956) to study wave propagations in transversely isotropic and anisotropic poroelastic media. Based on Biot's constitutive models (Biot 1955), Kumar et al. (2003; 2004) obtained the time-harmonic response of a homogeneous transversely isotropic poroelastic full-space subjected to vertical concentrated forces under axisymmetric and plane strain deformations. The material parameters in Biot's models were later reformulated by Cheng (1997) to be more easily identifiable from the laboratory

measurement. Sahebkar and Eskandari-Ghadi (2016) employed the parameters proposed by Cheng (1997) to study dynamic response of a transversely isotropic poroelastic half-space subjected to asymmetric time-harmonic surface loading. Pooladi et al. (2017) then revisited the problem by Sahebkar and Eskandari-Ghadi (2016) to investigate the influence of permeable and impermeable surfaces of the asymmetric half-space under surface loading. The exact stiffness method was adopted by Ba et al. (2017) to study dynamic response of a multi-layered transversely isotropic poroelastic half-plane. To the best of the authors' knowledge, the fundamental solutions of a transversely isotropic poroelastic medium subjected to time-harmonic buried loads and fluid sources have never been presented explicitly in the literature even for the case of plane strain or axisymmetric deformation. In addition, the fundamental solutions of a multi-layered transversely isotropic poroelastic medium under axisymmetric deformations have never been reported in the literature. These fundamental solutions can be employed as influence functions in the development of numerical solution scheme in the analysis of a variety of problems related to transversely isotropic poroelastic soils such as embedded foundations, anchors, and underground structures, etc.

2.2 Literature Reviews of Soil-Structure Interaction Problems

For soil-structure interaction problems between foundations and homogeneous isotropic poroelastic media, several previous works on the dynamic response of foundations subjected to time-harmonic loading were presented for rigid rectangular (Halpern and Christiano 1986b), circular (Kassir et al. 1989; Bougacha et al. 1993; Jin and Liu 1999; Zeng and Rajapakse 1999), and strip (Kassir and Xu 1988; Bougacha et al. 1993). In addition, Philippacopoulos (1989) also presented the study of a rigid circular foundation resting on two layered isotropic poroelastic half-space. For soil-structure interaction problems between foundations and multi-layered isotropic poroelastic media, Senjuntichai and Rajapakse (1996) proposed the solutions of a rigid strip foundation on a multi-layered isotropic poroelastic half-plane. In addition, Senjuntichai and Sapsathiarn (2003) and Senjuntichai and Kaewjuea (2008)

investigated dynamic interaction between flexible circular and strip foundations respectively and a multi-layered isotropic poroelastic medium.

In the context of transversely isotropic elastic media, the dynamic response of a rigid strip foundation bonded to a homogeneous half-plane was studied by Gazetas (1981). Later, Kirkner (1982), Eskandri-Ghadi et al. (2010) and Eskandri-Ghadi and Ardeshir-Behrestaghi (2010) developed semi-analytical solutions for vertical vibrations of a rigid circular foundation on a transversely isotropic elastic half-space. For multi-layered problems, vertical vibration of a circular foundation embedded in a multi-layered transversely isotropic elastic half-space was studied by Eskandri-Ghadi et al. (2014), and Ai et al. (2016). In addition, dynamic response of a rigid strip foundation on a multi-layered transversely isotropic elastic half-plane was investigated by Ai and Zhang (2016). For a study on flexible foundations, Ai and Liu (2014) and Ai et al. (2017) respectively presented an investigation on the dynamic response of a flexible circular foundation and a flexible strip foundation on a transversely isotropic multi-layered half-space and half plane. A rigid rectangular foundation on a transversely isotropic multi-layered half-space was also studied by Amiri-Hezaveh et al. (2013), where the required influence functions used in the analysis were based on the asymmetric coordinate system.

CHAPTER 3

BASIC EQUATIONS AND GENERAL SOLUTIONS

In this chapter, basic equations of a transversely isotropic poroelastic medium are presented. The general solutions for problems under plane strain and axisymmetric deformations are then obtained by using the techniques of Fourier and Hankel integral transforms respectively. These general solutions are later used to derive the fundamental solutions of homogeneous and multi-layered transversely isotropic poroelastic media in the subsequent chapters.

3.1 Basic Equations

Consider a transversely isotropic poroelastic material, where the x - and y -planes are chosen as the plane of isotropy, and the z -axis is thus perpendicular to the isotropic plane (see Figure 3.1). According to Cheng (1997), the constitutive relations of a transversely isotropic poroelastic medium can be expressed as,

$$\sigma_{xx} = c_{11}\varepsilon_{xx} + c_{12}\varepsilon_{yy} + c_{13}\varepsilon_{zz} - \alpha_h p \quad (3.1a)$$

$$\sigma_{yy} = c_{12}\varepsilon_{xx} + c_{11}\varepsilon_{yy} + c_{13}\varepsilon_{zz} - \alpha_h p \quad (3.1b)$$

$$\sigma_{zz} = c_{13}\varepsilon_{xx} + c_{13}\varepsilon_{yy} + c_{33}\varepsilon_{zz} - \alpha_v p \quad (3.1c)$$

$$\sigma_{xy} = (c_{11} - c_{12})(\varepsilon_{xy} + \varepsilon_{yx}) / 2 \quad (3.1d)$$

$$\sigma_{xz} = c_{44}(\varepsilon_{xz} + \varepsilon_{zx}) \quad (3.1e)$$

$$\sigma_{yz} = c_{44}(\varepsilon_{yz} + \varepsilon_{zy}) \quad (3.1f)$$

$$p = -M(\alpha_h \varepsilon_{xx} + \alpha_h \varepsilon_{yy} + \alpha_v \varepsilon_{zz} - w_{i,i}), \quad i = x, y, z \quad (3.1g)$$

$$\varepsilon_{ij} = (u_{i,j} + u_{j,i}) / 2, \quad i, j = x, y, z \quad (3.1h)$$

In the above equations, σ_{ij} ($i = j = x, y, z$) is the total stress component of the bulk material; ε_{ij} ($i = j = x, y, z$) is the strain component, which is related to the solid displacement u_i ($i = x, y, z$); p is the excess pore fluid pressure (suction is considered

negative); w_i ($i = x, y, z$) is the fluid displacement relative to the solid matrix); α_i ($i = v, h$) and M are Biot's parameters accounting for compressibility of the two-phased material, where α_h and α_v are Biot's coefficients of effective stress in the plane of isotropy (x - y plane) and in the plane normal to the plane of isotropy (z -direction), respectively. In addition, c_{11} , c_{12} , c_{13} , c_{33} and c_{44} are elastic moduli of solid skeleton being held for a transversely isotropic medium in the following manner.

$$c_{11} = \frac{E_h (E_v - E_h \nu_{vh}^2)}{(1 + \nu_h)(E_v - E_v \nu_h - 2E_h \nu_{vh}^2)} \quad (3.2a)$$

$$c_{12} = \frac{E_h (E_v \nu_h + E_h \nu_{vh}^2)}{(1 + \nu_h)(E_v - E_v \nu_h - 2E_h \nu_{vh}^2)} \quad (3.2b)$$

$$c_{13} = \frac{E_h E_v \nu_{vh}}{E_v - E_v \nu_h - 2E_h \nu_{vh}^2} \quad (3.2c)$$

$$c_{33} = \frac{E_v^2 (1 - \nu_{vh})}{E_v - E_v \nu_h - 2E_h \nu_{vh}^2} \quad (3.2d)$$

$$c_{44} = G \quad (3.2e)$$

In the above equations, E_h and E_v are drained Young's modulus in the plane of isotropy (x - y plane) and in the plane normal to the plane of isotropy (z -direction), respectively; G is the shear modulus; ν_h is the Poisson's ratio characterizing the lateral strain response in the plane of transverse isotropy to a stress acting parallel to it; ν_{vh} is the Poisson's characterizing the lateral strain response in the plane of transverse isotropy to a stress acting normal to it.

The equations of motions of a transversely isotropic poroelastic medium, in absence of body forces and a fluid source, can be expressed as,

$$c_{11} \frac{\partial^2 u_x}{\partial x^2} + \frac{(c_{11} - c_{12})}{2} \frac{\partial^2 u_x}{\partial y^2} + c_{44} \frac{\partial^2 u_x}{\partial z^2} + \frac{(c_{11} + c_{12})}{2} \frac{\partial^2 u_y}{\partial x \partial y} \quad (3.3a)$$

$$+ (c_{13} + c_{44}) \frac{\partial^2 u_z}{\partial x \partial z} - \alpha_h \frac{\partial p}{\partial x} = \rho \frac{\partial^2 u_x}{\partial t^2} + \rho_f \frac{\partial^2 w_x}{\partial t^2}$$

$$\frac{(c_{11} - c_{12})}{2} \frac{\partial^2 u_y}{\partial x^2} + c_{11} \frac{\partial^2 u_y}{\partial y^2} + c_{44} \frac{\partial^2 u_y}{\partial z^2} + \frac{(c_{11} + c_{12})}{2} \frac{\partial^2 u_x}{\partial x \partial y} \quad (3.3b)$$

$$+ (c_{13} + c_{44}) \frac{\partial^2 u_z}{\partial y \partial z} - \alpha_h \frac{\partial p}{\partial y} = \rho \frac{\partial^2 u_y}{\partial t^2} + \rho_f \frac{\partial^2 w_y}{\partial t^2}$$

$$c_{44} \frac{\partial^2 u_z}{\partial x^2} + c_{44} \frac{\partial^2 u_z}{\partial y^2} + c_{33} \frac{\partial^2 u_z}{\partial z^2} + (c_{13} + c_{44}) \frac{\partial^2 u_x}{\partial x \partial z} \quad (3.3c)$$

$$+ (c_{13} + c_{44}) \frac{\partial^2 u_y}{\partial y \partial z} - \alpha_v \frac{\partial p}{\partial z} = \rho \frac{\partial^2 u_z}{\partial t^2} + \rho_f \frac{\partial^2 w_z}{\partial t^2} - \frac{\partial p}{\partial x} = \rho_f \frac{\partial^2 u_x}{\partial t^2} + m_h \frac{\partial^2 w_x}{\partial t^2} + b_h \frac{\partial w_x}{\partial t} \quad (3.3d)$$

$$- \frac{\partial p}{\partial y} = \rho_f \frac{\partial^2 u_y}{\partial t^2} + m_h \frac{\partial^2 w_y}{\partial t^2} + b_h \frac{\partial w_y}{\partial t} \quad (3.3e)$$

$$- \frac{\partial p}{\partial z} = \rho_f \frac{\partial^2 u_z}{\partial t^2} + m_v \frac{\partial^2 w_z}{\partial t^2} + b_v \frac{\partial w_z}{\partial t} \quad (3.3f)$$

where ρ and ρ_f are the mass densities of the bulk material and the pore fluid, respectively; m_i ($i = v, h$) is a density-like parameter that depends on ρ_f and the geometry of the pores; b_i ($i = v, h$) is a parameter accounting for the internal friction due to the relative motion between the solid matrix and the pore fluid.

A homogeneous transversely isotropic poroelastic material is defined with a cylindrical coordinate system (r, θ, z) as shown in Figure 3.1. In the present study, the $r\theta$ plane is chosen as the plane of isotropy, and the z -axis is thus perpendicular to the isotropic plane. The constitutive relations of a transversely isotropic poroelastic medium can be expressed in the cylindrical coordinate system as,

$$\sigma_{rr} = c_{11} \frac{\partial u_r}{\partial r} + c_{12} \left(\frac{u_r}{r} + \frac{1}{r} \frac{\partial u_\theta}{\partial \theta} \right) + c_{13} \frac{\partial u_z}{\partial z} - \alpha_h p \quad (3.4a)$$

$$\sigma_{\theta\theta} = c_{12} \frac{\partial u_r}{\partial r} + c_{11} \left(\frac{u_r}{r} + \frac{1}{r} \frac{\partial u_\theta}{\partial \theta} \right) + c_{13} \frac{\partial u_z}{\partial z} - \alpha_h p \quad (3.4b)$$

$$\sigma_{zz} = c_{13} \left(\frac{\partial u_r}{\partial r} + \frac{u_r}{r} + \frac{1}{r} \frac{\partial u_\theta}{\partial \theta} \right) + c_{33} \frac{\partial u_z}{\partial z} - \alpha_v p \quad (3.4c)$$

$$\sigma_{rz} = c_{44} \left(\frac{\partial u_z}{\partial r} + \frac{\partial u_r}{\partial z} \right) \quad (3.4d)$$

$$\sigma_{\theta z} = c_{44} \left(\frac{1}{r} \frac{\partial u_z}{\partial \theta} + \frac{\partial u_\theta}{\partial z} \right) \quad (3.4e)$$

$$\sigma_{r\theta} = \frac{c_{11} - c_{12}}{2} \left(\frac{1}{r} \frac{\partial u_r}{\partial \theta} + \frac{\partial u_\theta}{\partial r} - \frac{u_\theta}{r} \right) \quad (3.4f)$$

$$p = -M \alpha_h \left(\frac{\partial u_r}{\partial r} + \frac{u_r}{r} + \frac{1}{r} \frac{\partial u_\theta}{\partial \theta} \right) - M \left(\alpha_v \frac{\partial u_z}{\partial z} + \frac{\partial w_r}{\partial r} + \frac{w_r}{r} + \frac{1}{r} \frac{\partial w_\theta}{\partial \theta} + \frac{\partial w_z}{\partial z} \right) \quad (3.4g)$$

In the above equations, σ_{rr} , $\sigma_{\theta\theta}$, σ_{zz} , $\sigma_{r\theta}$, $\sigma_{\theta z}$ and $\sigma_{r\theta}$ denote the total stress components of the bulk material; u_i and w_i denote the displacement of the solid matrix and fluid displacement relative to the solid matrix respectively in the i -direction ($i = r, \theta, z$).

The equations of motions of a transversely isotropic poroelastic medium can be expressed in the cylindrical coordinate, in absence of body forces and a fluid source as,

$$c_{11} \left(\frac{\partial^2 u_r}{\partial r^2} + \frac{\partial u_r}{r \partial r} - \frac{u_r}{r^2} \right) + \left(\frac{c_{11} - c_{12}}{2} \right) \frac{\partial^2 u_r}{r^2 \partial \theta^2} + c_{44} \frac{\partial^2 u_r}{\partial z^2} + \left(\frac{c_{11} + c_{12}}{2} \right) \left(\frac{\partial^2 u_\theta}{r \partial r \partial \theta} + \frac{\partial u_\theta}{r^2 \partial \theta} \right) - 2c_{11} \left(\frac{\partial u_\theta}{r^2 \partial \theta} \right) + (c_{13} + c_{44}) \frac{\partial^2 u_z}{\partial r \partial z} - \alpha_h \frac{\partial p}{\partial r} = \rho \frac{\partial^2 u_r}{\partial t^2} + \rho_f \frac{\partial^2 w_r}{\partial t^2} \quad (3.5a)$$

$$\left(\frac{c_{11} - c_{12}}{2} \right) \left(\frac{\partial^2 u_\theta}{\partial r^2} + \frac{\partial u_\theta}{r \partial r} - \frac{u_\theta}{r^2} \right) + c_{11} \frac{\partial^2 u_\theta}{r^2 \partial \theta^2} + c_{44} \frac{\partial^2 u_\theta}{\partial z^2} + \left(\frac{c_{11} + c_{12}}{2} \right) \left(\frac{\partial^2 u_r}{r \partial r \partial \theta} - \frac{\partial u_r}{r^2 \partial \theta} \right) + 2c_{11} \left(\frac{\partial u_r}{r^2 \partial \theta} \right) + (c_{13} + c_{44}) \frac{\partial^2 u_z}{r \partial \theta \partial z} - \alpha_h \frac{\partial p}{r \partial \theta} = \rho \frac{\partial^2 u_\theta}{\partial t^2} + \rho_f \frac{\partial^2 w_\theta}{\partial t^2} \quad (3.5b)$$

$$c_{44} \left(\frac{\partial^2 u_z}{\partial r^2} + \frac{\partial u_z}{r \partial r} + \frac{\partial^2 u_z}{r^2 \partial \theta^2} \right) + c_{33} \frac{\partial^2 u_z}{\partial z^2} + (c_{13} + c_{44}) \left(\frac{\partial^2 u_r}{\partial r \partial z} + \frac{\partial u_r}{r \partial z} + \frac{\partial^2 u_\theta}{r \partial \theta \partial z} \right) - \alpha_v \frac{\partial p}{\partial z} = \rho \frac{\partial^2 u_z}{\partial t^2} + \rho_f \frac{\partial^2 w_z}{\partial t^2} \quad (3.5c)$$

$$-\frac{\partial p}{\partial r} = \rho_f \frac{\partial^2 u_r}{\partial t^2} + m_h \frac{\partial^2 w_r}{\partial t^2} + b_h \frac{\partial w_r}{\partial t} \quad (3.5d)$$

$$-\frac{\partial p}{r \partial \theta} = \rho_f \frac{\partial^2 u_\theta}{\partial t^2} + m_h \frac{\partial^2 w_\theta}{\partial t^2} + b_h \frac{\partial w_\theta}{\partial t} \quad (3.5e)$$

$$-\frac{\partial p}{\partial z} = \rho_f \frac{\partial^2 u_z}{\partial t^2} + m_v \frac{\partial^2 w_z}{\partial t^2} + b_v \frac{\partial w_z}{\partial t} \quad (3.5f)$$

3.2 General Solutions for Plane Strain Deformations

Consider a homogeneous transversely isotropic poroelastic material with a Cartesian coordinate system (x, y, z) . Let assume that the deformations are plane strain in the xz -plane, i.e. $\varepsilon_{xy} = \varepsilon_{yy} = \varepsilon_{yz} = 0$. In addition, the xy -plane is chosen as the plane of isotropy, and the z -axis is thus perpendicular to the isotropic plane. Thus, the constitutive relations for a transversely isotropic poroelastic material, given by Eq. (3.1), can be expressed as,

$$\sigma_{xx} = c_{11}\varepsilon_{xx} + c_{13}\varepsilon_{zz} - \alpha_h p \quad (3.6a)$$

$$\sigma_{yy} = c_{12}\varepsilon_{xx} + c_{13}\varepsilon_{zz} - \alpha_h p \quad (3.6b)$$

$$\sigma_{zz} = c_{13}\varepsilon_{xx} + c_{33}\varepsilon_{zz} - \alpha_v p \quad (3.6c)$$

$$\sigma_{xz} = c_{44}(\varepsilon_{xz} + \varepsilon_{zx}) \quad (3.6d)$$

$$p = -M(\alpha_h \varepsilon_{xx} + \alpha_v \varepsilon_{zz} + \frac{\partial w_x}{\partial x} + \frac{\partial w_z}{\partial z}) \quad (3.6e)$$

The equations of motions of a transversely isotropic poroelastic material, given by Eq. (3.3), can be expressed for plane strain deformations as,

$$c_{11} \frac{\partial^2 u_x}{\partial x^2} + c_{44} \frac{\partial^2 u_x}{\partial z^2} + (c_{13} + c_{44}) \frac{\partial^2 u_z}{\partial x \partial z} - \alpha_h \frac{\partial p}{\partial x} = \rho \frac{\partial^2 u_x}{\partial t^2} + \rho_f \frac{\partial^2 w_x}{\partial t^2} \quad (3.7a)$$

$$c_{44} \frac{\partial^2 u_z}{\partial x^2} + c_{33} \frac{\partial^2 u_z}{\partial z^2} + (c_{13} + c_{44}) \frac{\partial^2 u_x}{\partial x \partial z} - \alpha_v \frac{\partial p}{\partial z} = \rho \frac{\partial^2 u_z}{\partial t^2} + \rho_f \frac{\partial^2 w_z}{\partial t^2} \quad (3.7b)$$

$$-\frac{\partial p}{\partial x} = \rho_f \frac{\partial^2 u_x}{\partial t^2} + m_h \frac{\partial^2 w_x}{\partial t^2} + b_h \frac{\partial w_x}{\partial t} \quad (3.7c)$$

$$-\frac{\partial p}{\partial z} = \rho_f \frac{\partial^2 u_z}{\partial t^2} + m_v \frac{\partial^2 w_z}{\partial t^2} + b_v \frac{\partial w_z}{\partial t} \quad (3.7d)$$

Let the motion under consideration be assumed to be time-harmonic of the form $e^{i\omega t}$, where ω is the frequency of the motion and $i = \sqrt{-1}$. The term $e^{i\omega t}$ is

omitted hereafter. The Fourier integral transform of a function with respect to the x -coordinate and its inverse relationship are defined respectively as (Sneddon 1951),

$$\bar{f}(\xi, z) = \frac{1}{\sqrt{2\pi}} \int_{-\infty}^{\infty} f(x, z) e^{-i\xi x} dx \quad (3.8a)$$

$$f(x, z) = \frac{1}{\sqrt{2\pi}} \int_{-\infty}^{\infty} \bar{f}(\xi, z) e^{i\xi x} d\xi \quad (3.8b)$$

where ξ is the Fourier transform parameter.

With the aid of Eqs. (3.6e) and (3.8a), the equations of motions, Eq. (3.7), can be reduced to three equations expressed in terms of Fourier transforms of the three unknowns \bar{u}_x , \bar{u}_z and \bar{p} as,

$$\left(s_1 + c_{44} \frac{d^2}{dz^2} \right) \bar{u}_x + \left((c_{13} + c_{44}) i\xi \frac{d}{dz} \right) \bar{u}_z - (i\xi \Lambda_h) \bar{p} = 0 \quad (3.9a)$$

$$\left((c_{13} + c_{44}) i\xi \frac{d}{dz} \right) \bar{u}_x + \left(s_2 + c_{33} \frac{d^2}{dz^2} \right) \bar{u}_z - \left(\Lambda_v \frac{d}{dz} \right) \bar{p} = 0 \quad (3.9b)$$

$$-(i\xi \Lambda_h) \bar{u}_x - \left(\Lambda_v \frac{d}{dz} \right) \bar{u}_z + \left(-s_3 - \beta_v \frac{d^2}{dz^2} \right) \bar{p} = 0 \quad (3.9c)$$

where

$$s_1 = -c_{11} \xi^2 - \rho_f^2 \omega^4 \beta_h + \rho \omega^2 \quad (3.10a)$$

$$s_2 = -c_{44} \xi^2 - \rho_f^2 \omega^4 \beta_v + \rho \omega^2 \quad (3.10b)$$

$$s_3 = -\xi^2 \beta_h + \frac{1}{M} \quad (3.10c)$$

$$\Lambda_j = \alpha_j - \rho_f \omega^2 \beta_j \quad (j = h, v) \quad (3.10d)$$

$$\beta_j = \frac{1}{(m_j \omega^2 - i b_j \omega)} \quad (j = h, v) \quad (3.10e)$$

To solve for the analytical solution of Eq. (3.9), a potential function $\bar{F}(\xi, z)$ is introduced, and the function \bar{F} is related to \bar{u}_x , \bar{u}_z and \bar{p} in the following manner:

$$\bar{u}_x = i\xi \left[-(c_{13} + c_{44}) \left(s_3 + \beta_v \frac{d^2}{dz^2} \right) - \Lambda_v \Lambda_h \right] \frac{d\bar{F}}{dz} \quad (3.11a)$$

$$\bar{u}_z = \left[\left(s_3 + \beta_v \frac{d^2}{dz^2} \right) \left(s_1 - (c_{13} + c_{44}) \frac{d^2}{dz^2} \right) - \Lambda_h^2 \xi^2 \right] \bar{F} \quad (3.11b)$$

$$\bar{p} = \left[-\Lambda_v \left(s_1 + c_{44} \frac{d^2}{dz^2} \right) - (c_{13} + c_{44}) \Lambda_h \xi^2 \right] \frac{d\bar{F}}{dz} \quad (3.11c)$$

Substitution of Eq. (3.11) into Eq. (3.9) leads to the following governing equation to determine \bar{F} ,

$$\gamma_1 \frac{d^6 \bar{F}}{dz^6} + \gamma_2 \frac{d^4 \bar{F}}{dz^4} + \gamma_3 \frac{d^2 \bar{F}}{dz^2} + \gamma_4 \bar{F} = 0 \quad (3.12)$$

where

$$\gamma_1 = c_{33} c_{44} \beta_v \quad (3.13a)$$

$$\gamma_2 = (s_2 c_{44} + s_1 c_{33} + (c_{13} + c_{44})^2 \xi^2) \beta_v + (s_3 c_{33} + \Lambda_v^2) c_{44} \quad (3.13b)$$

$$\gamma_3 = (s_2 \beta_v + \Lambda_v^2) s_1 + (s_2 c_{44} + s_1 c_{33} + (c_{13} + c_{44})^2 \xi^2) s_3 - (2(c_{13} + c_{44}) \Lambda_v \Lambda_h + \Lambda_h^2 c_{33}) \xi^2 \quad (3.13c)$$

$$\gamma_4 = (s_1 s_3 - \Lambda_h^2 \xi^2) s_2 \quad (3.13d)$$

The general solution to Eq. (3.12) can be obtained as follows:

$$\bar{F}(\xi, z) = A_j e^{\lambda_j z} + B_j e^{-\lambda_j z} \quad (j=1, 2, 3) \quad (3.14)$$

where A_j and B_j ($j = 1, 2, 3$) are the arbitrary functions, and

$$\lambda_1 = \sqrt{\Omega_3 - \frac{\Omega_1}{3\Omega_3} - \frac{\gamma_2}{3\gamma_1}}, \quad \lambda_2 = \sqrt{\Delta\Omega_3 - \frac{\Omega_1}{3\Delta\Omega_3} - \frac{\gamma_2}{3\gamma_1}}, \quad \lambda_3 = \sqrt{\Delta^2\Omega_3 - \frac{\Omega_1}{3\Delta^2\Omega_3} - \frac{\gamma_2}{3\gamma_1}} \quad (3.15a)$$

$$\Omega_1 = -\frac{\gamma_2^2}{3\gamma_1^2} + \frac{\gamma_3}{\gamma_1}, \quad \Omega_2 = \frac{2\gamma_2^3}{27\gamma_1^3} - \frac{3\gamma_2\gamma_3}{9\gamma_1^2} + \frac{\gamma_4}{\gamma_1}, \quad \Omega_3 = \left(-\frac{1}{2}\Omega_2 + \frac{1}{2}\sqrt{\Omega_2^2 + \frac{4\Omega_1^3}{27}} \right)^{1/3} \quad (3.15b)$$

$$\Delta = -\frac{1 - \sqrt{3}i}{2} \quad (3.15c)$$

In addition, λ_1 , λ_2 and λ_3 are the dimensionless complex wave numbers associated with the three kinds of dispersive and dissipative body waves. For an isotropic proelastic material under plane strain condition, there also exists three body waves, which are identified as two dilatation (fast and slow) waves and one rotational wave.

However, the motion associated with the wave numbers λ_i ($i = 1, 2, 3$) is neither purely dilatational nor purely rotational. In the case of transversely isotropic *elastic* materials, Eq. (3.11) is reduced to two equations for the two unknowns \bar{u}_x and \bar{u}_z expressed in term of a potential function \bar{F} , which is governed by a fourth-order differential equation. The general solution of \bar{F} involves two complex wave numbers that are identified as quasi-dilatational and quasi-distortional waves. Therefore, the three body waves propagating in transversely isotropic *poroelastic* materials under plane strain condition can be considered as two quasi-dilatation (fast and slow) waves and one quasi-distortional wave.

In view of Eqs. (3.11) and (3.14), the general solutions of \bar{u}_x , \bar{u}_z , \bar{p} , \bar{w}_z , $\bar{\sigma}_{xz}$ and $\bar{\sigma}_{zz}$ can be written as,

$$\bar{u}_x = \chi_j A_j e^{\lambda_j z} - \chi_j B_j e^{-\lambda_j z} \quad (3.16a)$$

$$\bar{u}_z = \psi_j A_j e^{\lambda_j z} + \psi_j B_j e^{-\lambda_j z} \quad (3.16b)$$

$$\bar{p} = \zeta_j A_j e^{\lambda_j z} - \zeta_j B_j e^{-\lambda_j z} \quad (3.16c)$$

$$\bar{w}_z = \varpi_j A_j e^{\lambda_j z} + \varpi_j B_j e^{-\lambda_j z} \quad (3.16d)$$

$$\bar{\sigma}_{xz} = \varphi_j A_j e^{\lambda_j z} + \varphi_j B_j e^{-\lambda_j z} \quad (3.16e)$$

$$\bar{\sigma}_{zz} = \eta_j A_j e^{\lambda_j z} - \eta_j B_j e^{-\lambda_j z} \quad (3.16f)$$

where

$$\chi_j = i\xi\lambda_j \left[-(c_{13} + c_{44})(s_3 + \beta_v \lambda_j^2) + \Lambda_v \Lambda_h \right] \quad (3.17a)$$

$$\psi_j = (s_3 + \beta_v \lambda_j^2)(s_1 + c_{44} \lambda_j^2) - \Lambda_h^2 \xi^2 \quad (3.17b)$$

$$\zeta_j = \lambda_j \left[-\Lambda_v (s_1 + c_{44} \lambda_j^2) - (c_{13} + c_{44}) \Lambda_h \xi^2 \right] \quad (3.17c)$$

$$\varpi_j = (\lambda_j \zeta_j - \rho_f \omega^2 \psi_j) \beta_v \quad (3.17a)$$

$$\varphi_j = c_{44} (\lambda_j \chi_j + i\xi \psi_j) \quad (3.17b)$$

$$\eta_j = i\xi c_{13} \chi_j + c_{33} \lambda_j \psi_j - \alpha_v \zeta_j \quad (3.17c)$$

The above general solutions are used in the derivation of fundamental solutions for transversely isotropic poroelastic media under plane strain deformations presented in Chapter 4.

3.3 General Solutions for Axisymmetric Deformations

The constitutive relations of a transversely isotropic poroelastic medium undergoing axisymmetric deformations can be reduced from Eq. (3.4) as follows:

$$\sigma_{rr} = c_{11} \frac{\partial u_r}{\partial r} + c_{12} \frac{u_r}{r} + c_{13} \frac{\partial u_z}{\partial z} - \alpha_h p \quad (3.18a)$$

$$\sigma_{\theta\theta} = c_{12} \frac{\partial u_r}{\partial r} + c_{11} \frac{u_r}{r} + c_{13} \frac{\partial u_z}{\partial z} - \alpha_h p \quad (3.18b)$$

$$\sigma_{zz} = c_{13} \left(\frac{\partial u_r}{\partial r} + \frac{u_r}{r} \right) + c_{33} \frac{\partial u_z}{\partial z} - \alpha_v p \quad (3.18c)$$

$$\sigma_{rz} = c_{44} \left(\frac{\partial u_z}{\partial r} + \frac{\partial u_r}{\partial z} \right) \quad (3.18d)$$

$$p = -M \alpha_h \left(\frac{\partial u_r}{\partial r} + \frac{u_r}{r} \right) - M \left(\alpha_v \frac{\partial u_z}{\partial z} + \frac{\partial w_r}{\partial r} + \frac{w_r}{r} + \frac{\partial w_z}{\partial z} \right) \quad (3.18e)$$

The equations of motions of a transversely isotropic poroelastic medium can be written for axisymmetric deformations as,

$$c_{11} \left(\nabla^2 - \frac{1}{r^2} \right) u_r + c_{44} \frac{\partial^2 u_r}{\partial z^2} + (c_{13} + c_{44}) \frac{\partial^2 u_z}{\partial r \partial z} - \alpha_h \frac{\partial p}{\partial r} = \rho \frac{\partial^2 u_r}{\partial t^2} + \rho_f \frac{\partial^2 w_r}{\partial t^2} \quad (3.19a)$$

$$(c_{13} + c_{44}) \left(\frac{\partial^2}{\partial r \partial z} + \frac{\partial}{r \partial z} \right) u_r + c_{33} \frac{\partial^2 u_z}{\partial z^2} + c_{44} \nabla^2 u_z - \alpha_v \frac{\partial p}{\partial z} = \rho \frac{\partial^2 u_z}{\partial t^2} + \rho_f \frac{\partial^2 w_z}{\partial t^2} \quad (3.19b)$$

$$-\frac{\partial p}{\partial r} = \rho_f \frac{\partial^2 u_r}{\partial t^2} + m_h \frac{\partial^2 w_r}{\partial t^2} + b_h \frac{\partial w_r}{\partial t} \quad (3.19c)$$

$$-\frac{\partial p}{\partial z} = \rho_f \frac{\partial^2 u_z}{\partial t^2} + m_v \frac{\partial^2 w_z}{\partial t^2} + b_v \frac{\partial w_z}{\partial t} \quad (3.19d)$$

$$\nabla^2 = \frac{1}{r} \frac{\partial}{\partial r} \left(r \frac{\partial}{\partial r} \right) \quad (3.19e)$$

The Hankel integral transform of a relevant variables with respect to the radial coordinate, and their inverse transforms can be expressed as follows:

$$\bar{u}_r(\xi, z) = \int_0^{\infty} u_r(r, z) J_1(\xi r) r dr \quad (3.20a)$$

$$\bar{u}_z(\xi, z) = \int_0^{\infty} u_z(r, z) J_0(\xi r) r dr \quad (3.20b)$$

$$\bar{p}(\xi, z) = \int_0^{\infty} p(r, z) J_0(\xi r) r dr \quad (3.20c)$$

$$\bar{w}_z(\xi, z) = \int_0^{\infty} w_z(r, z) J_1(\xi r) r dr \quad (3.20d)$$

$$\bar{\sigma}_{rz}(\xi, z) = \int_0^{\infty} \sigma_{rz}(r, z) J_0(\xi r) r dr \quad (3.20e)$$

$$\bar{\sigma}_{zz}(\xi, z) = \int_0^{\infty} \sigma_{zz}(r, z) J_1(\xi r) r dr \quad (3.20f)$$

and

$$u_r(r, z) = \int_0^{\infty} \bar{u}_r(\xi, z) J_1(\xi r) \xi d\xi \quad (3.20g)$$

$$u_z(r, z) = \int_0^{\infty} \bar{u}_z(\xi, z) J_0(\xi r) \xi d\xi \quad (3.20h)$$

$$p(r, z) = \int_0^{\infty} \bar{p}(\xi, z) J_0(\xi r) \xi d\xi \quad (3.20i)$$

$$w_z(r, z) = \int_0^{\infty} \bar{w}_z(\xi, z) J_1(\xi r) \xi d\xi \quad (3.20j)$$

$$\sigma_{rz}(r, z) = \int_0^{\infty} \bar{\sigma}_{rz}(\xi, z) J_0(\xi r) \xi d\xi \quad (3.20k)$$

$$\sigma_{zz}(r, z) = \int_0^{\infty} \bar{\sigma}_{zz}(\xi, z) J_1(\xi r) \xi d\xi \quad (3.20l)$$

where J_0 and J_1 denote the Bessel function of the first kind of order zero and one respectively, and ξ is the Hankel transform parameter.

By applying the Hankel integral transform given by Eqs. (3.20a) to (3.20f) together with the regularity condition in the radial direction, the equations of motions, Eq. (3.19), can be reduced to three equations with three unknowns, \bar{u}_r , \bar{u}_z and \bar{p} as follows:

$$\left(s_1 + c_{44} \frac{d^2}{dz^2} \right) \bar{u}_r + s_4 \xi \frac{d}{dz} \bar{u}_z + s_6 \xi \bar{p} = 0 \quad (3.21a)$$

$$s_4 \xi \frac{d}{dz} \bar{u}_r - \left(s_2 + c_{33} \frac{d^2}{dz^2} \right) \bar{u}_z + s_5 \frac{d}{dz} \bar{p} = 0 \quad (3.21b)$$

$$s_6 \xi \bar{u}_r + s_5 \frac{d}{dz} \bar{u}_z + \left(s_3 + \beta_v \frac{d^2}{dz^2} \right) \bar{p} = 0 \quad (3.21c)$$

where

$$s_1 = -\xi^2 c_{11} + \omega^2 \rho - \omega^4 \rho_f^2 \beta_h \quad (3.22a)$$

$$s_2 = -\xi^2 c_{44} + \omega^2 \rho - \omega^4 \rho_f^2 \beta_v \quad (3.22b)$$

$$s_3 = -\xi^2 \beta_h + \frac{1}{M} \quad (3.22c)$$

$$s_4 = -(c_{13} + c_{44}) \quad (3.22d)$$

$$s_5 = \alpha_v - \omega^2 \rho_f \beta_v \quad (3.22e)$$

$$s_6 = \alpha_h - \omega^2 \rho_f \beta_h \quad (3.22f)$$

$$\beta_j = \frac{1}{(m_j \omega^2 - i b_j \omega)} \quad (j = h, v) \quad (3.22g)$$

To solve for the three unknowns, a potential function \overline{F} is introduced by relating its Hankel transform to \overline{u}_r , \overline{u}_z and \overline{p} in the following manner:

$$\overline{u}_r = \xi \left[s_4 \left(s_3 + \beta_v \frac{d^2}{dz^2} \right) - s_6 s_5 \right] \frac{d\overline{F}}{dz} \quad (3.23a)$$

$$\overline{u}_z = \left[- \left(s_1 + c_{44} \frac{d^2}{dz^2} \right) \left(s_3 + \beta_v \frac{d^2}{dz^2} \right) + s_6^2 \xi^2 \right] \overline{F} \quad (3.23b)$$

$$\overline{p} = \left[s_5 \left(s_1 + c_{44} \frac{d^2}{dz^2} \right) - s_4 s_6 \xi^2 \right] \frac{d\overline{F}}{dz} \quad (3.23c)$$

With the substitution of Eq. (3.23) into Eq. (3.21), the following governing equation is obtained for the solution of \overline{F} ,

$$\gamma_1 \frac{d^6 \overline{F}}{dz^6} + \gamma_2 \frac{d^4 \overline{F}}{dz^4} + \gamma_3 \frac{d^2 \overline{F}}{dz^2} + \gamma_4 \overline{F} = 0 \quad (3.24)$$

where

$$\gamma_1 = c_{33} c_{44} \beta_v \quad (3.25a)$$

$$\gamma_2 = (s_2 c_{44} + s_1 c_{33} + s_4^2 \xi^2) \beta_v + (s_3 c_{33} + s_5^2) c_{44} \quad (3.25b)$$

$$\gamma_3 = (s_2 \beta_v + s_5^2) s_1 + (s_2 c_{44} + s_1 c_{33} + s_4^2 \xi^2) s_3 - (2s_4 s_5 s_6 + s_6^2 c_{33}) \xi^2 \quad (3.25c)$$

$$\gamma_4 = (s_1 s_3 - s_6^2 \xi^2) s_2 \quad (3.25d)$$

The general solution of \overline{F} is then determined from Eq. (3.24) as,

$$\overline{F}(\xi, z) = A_j e^{\lambda_j z} + B_j e^{-\lambda_j z} \quad (j=1, 2, 3) \quad (3.26)$$

where A_j and B_j ($j = 1, 2, 3$) are the arbitrary functions to be determined from appropriate boundary conditions. In addition, λ_1 , λ_2 and λ_3 are the dimensionless complex wave numbers associated with the three body waves which are similar to that in Eq. (3.15).

Finally, the general solutions of u_z , w_z , σ_{zz} , p , u_r and σ_{rz} can then be obtained as,

$$\bar{u}_r = \chi_j A_j e^{\lambda_j z} - \chi_j B_j e^{-\lambda_j z} \quad (3.27a)$$

$$\bar{u}_z = \psi_j A_j e^{\lambda_j z} + \psi_j B_j e^{-\lambda_j z} \quad (3.27b)$$

$$\bar{p} = \zeta_j A_j e^{\lambda_j z} - \zeta_j B_j e^{-\lambda_j z} \quad (3.27c)$$

$$\bar{w}_z = \varpi_j A_j e^{\lambda_j z} + \varpi_j B_j e^{-\lambda_j z} \quad (3.27d)$$

$$\bar{\sigma}_{rz} = \varphi_j A_j e^{\lambda_j z} + \varphi_j B_j e^{-\lambda_j z} \quad (3.27e)$$

$$\bar{\sigma}_{zz} = \eta_j A_j e^{\lambda_j z} - \eta_j B_j e^{-\lambda_j z} \quad (3.27f)$$

where

$$\chi_j = \xi \lambda_j \left[s_4 (s_3 + \beta_v \lambda_j^2) - s_5 s_6 \right] \quad (3.28a)$$

$$\psi_j = -(s_3 + \beta_v \lambda_j^2)(s_1 + c_{44} \lambda_j^2) + s_6^2 \xi^2 \quad (3.28b)$$

$$\zeta_j = \lambda_j \left[s_5 (s_1 + c_{44} \lambda_j^2) - s_4 s_6 \xi^2 \right] \quad (3.28c)$$

$$\varpi_j = (\lambda_j \zeta_j - \rho_f \omega^2 \psi_j) \beta_v \quad (3.28d)$$

$$\varphi_j = c_{44} (\lambda_j \chi_j - \xi \psi_j) \quad (3.28e)$$

$$\eta_j = \xi c_{13} \chi_j + c_{33} \lambda_j \psi_j - \alpha_v \zeta_j \quad (3.28f)$$

The above general solutions are used in the derivation of fundamental solutions for transversely isotropic poroelastic media under axisymmetric deformations presented in Chapter 5.

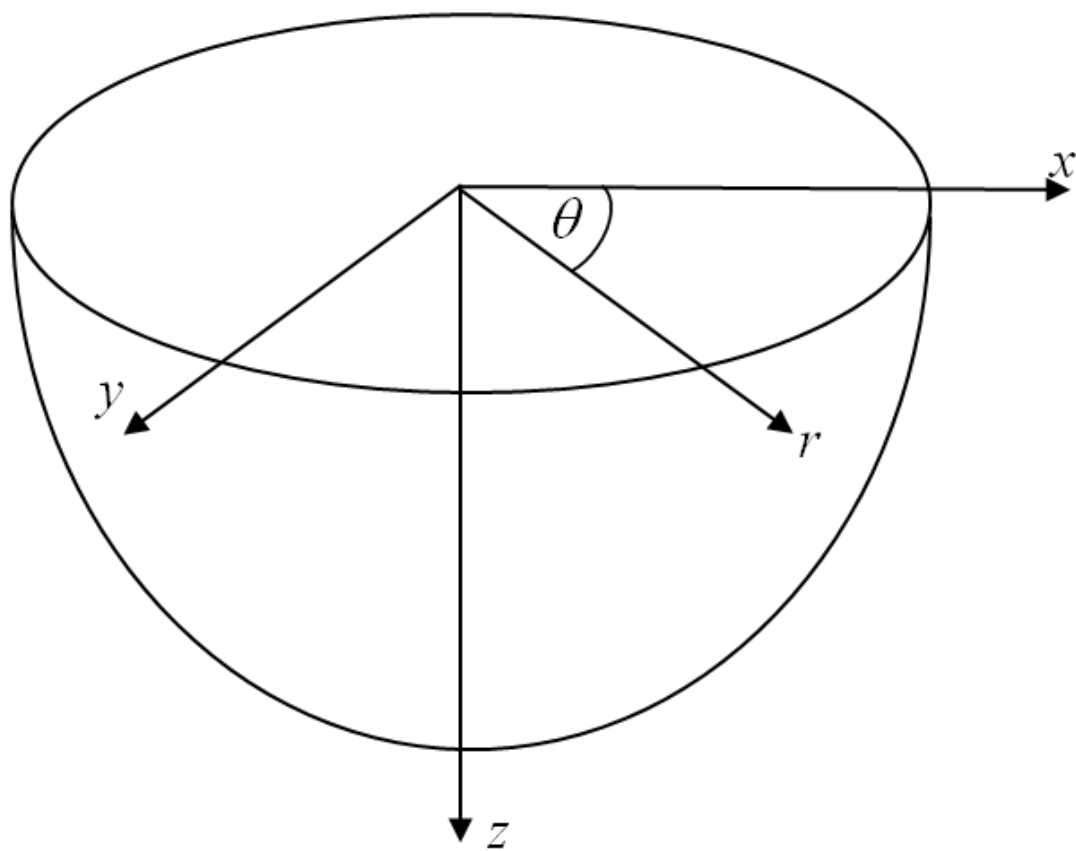


Figure 3.1 Homogeneous transversely isotropic poroelastic half-space



CHAPTER 4

PLANE STRAIN FUNDAMENTAL SOLUTIONS OF TRANSVERSELY ISOTROPIC POROELASTIC MEDIA

The general solutions for a transversely isotropic poroelastic medium under plane strain deformations derived in Chapter 3 are used in the derivation of the fundamental solutions of a homogeneous and multi-layered half-planes. The boundary-value problems corresponding to a homogeneous transversely isotropic poroelastic half-plane subjected to time-harmonic buried loading are considered. For a multi-layered medium, an exact stiffness matrix method is adopted to obtain fundamental solutions for a multi-layered transversely isotropic poroelastic half-plane. Selected numerical results are presented to portray the influence of anisotropic and poroelastic effects on dynamic response of transversely isotropic poroelastic media under plane strain deformations.

4.1 Fundamental Solutions for Homogeneous Half-Plane

4.1.1 *Boundary-value problems*

This section presents boundary-value problems corresponding to a homogeneous transversely isotropic poroelastic half-plane subjected to time-harmonic buried loading. Four loading types, i.e. a vertical load, a horizontal load, a fluid source and applied pore fluid pressure, applied at a depth $z = h$ below the free surface are considered. All loading types are assumed to be uniform in the y -direction so that the resulting deformations are of plane strain type. The boundary value problem can be solved by considering it as a two-domain boundary-value problem. The domain "1" is bounded by $0 \leq z \leq h$, and the domain "2" by $h \leq z \leq \infty$. The general solutions for the domain "1" are given by Eq. (3.16), whereas for the domain "2", the general solutions are also given by Eq. (3.16) with the arbitrary functions A_j and B_j ($j = 1, 2, 3$) being replaced by the arbitrary functions C_j and D_j ($j = 1, 2, 3$) respectively. Note that $C_j \equiv 0$ to ensure the regularity of the solutions at infinity. The boundary and continuity conditions corresponding to a transversely isotropic poroelastic half-plane subjected to buried vertical and horizontal loads, and a buried fluid source can be expressed as,

$$\overline{\sigma}_{zn}^{(1)}(x, 0) = 0 \quad (n = x, z) \quad (4.1a)$$

$$\overline{p}^{(1)}(x, 0) = 0 \quad (4.1b)$$

$$\overline{u}_n^{(1)}(x, h) - \overline{u}_n^{(2)}(x, h) = 0 \quad (n = x, z) \quad (4.1c)$$

$$\overline{p}^{(1)}(x, h) - \overline{p}^{(2)}(x, h) = 0 \quad (4.1d)$$

$$\overline{\sigma}_{zn}^{(1)}(x, h) - \overline{\sigma}_{zn}^{(2)}(x, h) = \overline{f}_n \quad (n = x, z) \quad (4.1e)$$

$$\overline{w}_z^{(1)}(x, h) - \overline{w}_z^{(2)}(x, h) = \frac{i \overline{f}_q}{\omega} \quad (4.1f)$$

where \overline{f}_x , \overline{f}_z , and \overline{f}_q denote the Fourier transforms of applied horizontal and vertical loads, and applied fluid source respectively. In addition, the superscript i ($i = 1, 2$) is used to denote the domain number. Substitution of the general solutions for displacements, stresses, pore pressure, and fluid displacement given by Eq. (3.16) into Eq. (4.1) yields a set of linear simultaneous equations to determine the arbitrary functions corresponding to the two domains. It is convenient to solve the boundary value problem corresponding to different loading cases separately.

In the case of a transversely isotropic poroelastic half-plane subjected to applied pore fluid pressure f_p at a depth $z = h$, the boundary and continuity conditions are given by Eqs. (4.1a) to (4.1c) together with the following continuity conditions:

$$\overline{p}^{(2)}(x, h) - \overline{p}^{(1)}(x, h) = \overline{f}_p \quad (4.2a)$$

$$\overline{\sigma}_{zz}^{(1)}(x, h) - \overline{\sigma}_{zz}^{(2)}(x, h) = \alpha_v \overline{f}_p \quad (4.2b)$$

$$\overline{\sigma}_{zx}^{(1)}(x, h) - \overline{\sigma}_{zx}^{(2)}(x, h) = 0 \quad (4.2c)$$

$$\overline{w}_z^{(1)}(x, h) - \overline{w}_z^{(2)}(x, h) = 0 \quad (4.2d)$$

If buried loading is uniformly distributed with intensity f_0 over a strip of width $2a$ at a depth $z = h$, the Fourier transform of applied loading \overline{f}_n ($n = z, x, q, p$) defined in Eqs. (4.1) and (4.2) is given by

$$\overline{f}_n(\xi) = \sqrt{\frac{2}{\pi}} \frac{\sin(a\xi)}{\xi} f_0; \quad (n = z, x, q, p) \quad (4.3a)$$

In addition, for buried line loading of intensity F_0 applied at a depth $z = h$,

$$\bar{f}_n(\xi) = \frac{F_0}{2\pi}; \quad (n = z, x, q, p) \quad (4.3b)$$

The solutions for the arbitrary functions corresponding to all loading cases are given explicitly as followed:

Arbitrary functions for vertical loading

$$A_1 = -\frac{\bar{f}_z \kappa_{v1}}{2\kappa_1 e^{\lambda_1 h}} \quad (4.4a)$$

$$A_2 = \frac{\bar{f}_z \kappa_{v2}}{2\kappa_1 e^{\lambda_2 h}} \quad (4.4b)$$

$$A_3 = -\frac{\bar{f}_z \kappa_{v3}}{2\kappa_1 e^{\lambda_3 h}} \quad (4.4c)$$

$$B_1 = \frac{\bar{f}_z}{2\kappa_1 \kappa_2} \left[\left(2e^{-\lambda_3 h} \varphi_3 \kappa_{v3} \kappa_8 \right) - \left(2e^{-\lambda_2 h} \varphi_2 \kappa_{v2} \kappa_8 \right) - \left(e^{-\lambda_1 h} \kappa_{v1} \kappa_5 \right) \right] \quad (4.4d)$$

$$B_2 = \frac{\bar{f}_z}{2\kappa_1 \kappa_2} \left[\left(-2e^{-\lambda_3 h} \varphi_3 \kappa_{v3} \kappa_9 \right) + \left(e^{-\lambda_2 h} \kappa_{v2} \kappa_4 \right) - \left(2e^{-\lambda_1 h} \varphi_1 \kappa_{v1} \kappa_9 \right) \right] \quad (4.4e)$$

$$B_3 = \frac{\bar{f}_z}{2\kappa_1 \kappa_2} \left[\left(e^{-\lambda_3 h} \kappa_{v3} \kappa_6 \right) - \left(2e^{-\lambda_2 h} \varphi_2 \kappa_{v2} \kappa_7 \right) + \left(2e^{-\lambda_1 h} \varphi_1 \kappa_{v1} \kappa_7 \right) \right] \quad (4.4f)$$

$$D_j = B_j + A_j e^{2\lambda_j h} \quad (j = 1, 2, 3) \quad (4.4g)$$

Arbitrary functions for horizontal loading

$$A_1 = -\frac{\bar{f}_x (\varpi_3 \psi_2 - \varpi_2 \psi_3)}{2\kappa_3 e^{\lambda_1 h}} \quad (4.5a)$$

$$A_2 = \frac{\bar{f}_x (\varpi_3 \psi_1 - \varpi_1 \psi_3)}{2\kappa_3 e^{\lambda_2 h}} \quad (4.5b)$$

$$A_3 = -\frac{\bar{f}_x (\varpi_2 \psi_1 - \varpi_1 \psi_2)}{2\kappa_3 e^{\lambda_3 h}} \quad (4.5c)$$

$$B_1 = -\frac{\bar{f}_x}{2\kappa_3 \kappa_2} \left[2\varpi_1 \kappa_8 (\varphi_3 \psi_2 e^{-\lambda_3 h} - \varphi_2 \psi_3 e^{-\lambda_2 h}) \right. \\ \left. + \varpi_3 (2\varphi_2 \psi_1 \kappa_8 e^{-\lambda_2 h} + \psi_2 \kappa_5 e^{-\lambda_1 h}) - \varpi_2 (2\varphi_3 \psi_1 \kappa_8 e^{-\lambda_3 h} + \psi_3 \kappa_5 e^{-\lambda_1 h}) \right] \quad (4.5d)$$

$$B_2 = -\frac{\bar{f}_x}{2\kappa_3\kappa_2} [2\varpi_2\kappa_9(\varphi_3\psi_1e^{-\lambda_3h} - \varphi_1\psi_3e^{-\lambda_1h}) \quad (4.5e)$$

$$+\varpi_3(2\varphi_1\psi_2\kappa_9e^{-\lambda_1h} - \psi_1\kappa_4e^{-\lambda_2h}) - \varpi_1(2\varphi_3\psi_2\kappa_9e^{-\lambda_3h} - \psi_3\kappa_4e^{-\lambda_2h})]$$

$$B_3 = -\frac{\bar{f}_x}{2\kappa_3\kappa_2} [2\varpi_3\kappa_7(\varphi_2\psi_1e^{-\lambda_2h} - \varphi_1\psi_2e^{-\lambda_1h}) \quad (4.5f)$$

$$+\varpi_2(2\varphi_1\psi_3\kappa_7e^{-\lambda_1h} - \psi_1\kappa_6e^{-\lambda_3h}) + \varpi_1(-2\varphi_2\psi_3\kappa_7e^{-\lambda_2h} + \psi_2\kappa_6e^{-\lambda_3h})]$$

$$D_j = B_j - A_j e^{2\lambda_j h} \quad (j=1,2,3) \quad (4.5g)$$

Arbitrary functions for fluid source

$$A_1 = \frac{i\bar{f}_q\kappa_{q1}}{2\kappa_{10}\delta e^{\lambda_1 h}} \quad (4.6a)$$

$$A_2 = -\frac{i\bar{f}_q\kappa_{q2}}{2\kappa_{10}\delta e^{\lambda_2 h}} \quad (4.6b)$$

$$A_3 = \frac{i\bar{f}_q\kappa_{q3}}{2\kappa_{10}\delta e^{\lambda_3 h}} \quad (4.6c)$$

$$B_1 = -\frac{i\bar{f}_q}{2\kappa_{10}\kappa_2\delta} \left[(2e^{-\lambda_3 h}\varphi_3\kappa_{q3}\kappa_8) - (2e^{-\lambda_2 h}\varphi_2\kappa_{q2}\kappa_8) - (e^{-\lambda_1 h}\kappa_{q1}\kappa_5) \right] \quad (4.6d)$$

$$B_2 = -\frac{i\bar{f}_q}{2\kappa_{10}\kappa_2\delta} \left[(-2e^{-\lambda_3 h}\varphi_3\kappa_{q3}\kappa_9) + (e^{-\lambda_2 h}\kappa_{q2}\kappa_4) - (2e^{-\lambda_1 h}\varphi_1\kappa_{q1}\kappa_9) \right] \quad (4.6e)$$

$$B_3 = -\frac{i\bar{f}_q}{2\kappa_{10}\kappa_2\delta} \left[(e^{-\lambda_3 h}\kappa_{q3}\kappa_6) - (2e^{-\lambda_2 h}\varphi_2\kappa_{q2}\kappa_7) + (2e^{-\lambda_1 h}\varphi_1\kappa_{q1}\kappa_7) \right] \quad (4.6f)$$

$$D_j = B_j - A_j e^{2\lambda_j h} \quad (j=1,2,3) \quad (4.6g)$$

Arbitrary functions for applied fluid pressure

$$A_1 = \frac{\bar{f}_p\kappa_{p1}}{2\kappa_1 e^{\lambda_1 h}} \quad (4.7a)$$

$$A_2 = -\frac{\bar{f}_p\kappa_{p2}}{2\kappa_1 e^{\lambda_2 h}} \quad (4.7b)$$

$$A_3 = \frac{\bar{f}_p \kappa_{p3}}{2\kappa_1 e^{\lambda_3 h}} \quad (4.7c)$$

$$B_1 = -\frac{\bar{f}_p}{2\kappa_1 \kappa_2} \left[(2e^{-\lambda_3 h} \varphi_3 \kappa_{p3} \kappa_8) - (2e^{-\lambda_2 h} \varphi_2 \kappa_{p2} \kappa_8) - (e^{-\lambda_1 h} \kappa_{p1} \kappa_5) \right] \quad (4.7d)$$

$$B_2 = -\frac{\bar{f}_p}{2\kappa_1 \kappa_2} \left[(-2e^{-\lambda_3 h} \varphi_3 \kappa_{p3} \kappa_9) + (e^{-\lambda_2 h} \kappa_{p2} \kappa_4) - (2e^{-\lambda_1 h} \varphi_1 \kappa_{p1} \kappa_9) \right] \quad (4.7e)$$

$$B_3 = -\frac{\bar{f}_p}{2\kappa_1 \kappa_2} \left[(e^{-\lambda_3 h} \kappa_{p3} \kappa_6) - (2e^{-\lambda_2 h} \varphi_2 \kappa_{p2} \kappa_7) + (2e^{-\lambda_1 h} \varphi_1 \kappa_{p1} \kappa_7) \right] \quad (4.7f)$$

$$D_j = B_j + A_j e^{2\lambda_j h} \quad (j=1,2,3) \quad (4.7g)$$

where

$$\kappa_1 = \eta_1 \chi_2 \zeta_3 + \eta_2 \chi_3 \zeta_1 + \eta_3 \chi_1 \zeta_2 - \eta_1 \chi_3 \zeta_2 - \eta_2 \chi_1 \zeta_3 - \eta_3 \chi_2 \zeta_1 \quad (4.8a)$$

$$\kappa_2 = \varphi_3 \eta_2 \zeta_1 - \varphi_2 \eta_3 \zeta_1 - \varphi_3 \eta_1 \zeta_2 + \varphi_1 \eta_3 \zeta_2 + \varphi_2 \eta_1 \zeta_3 - \varphi_1 \eta_2 \zeta_3 \quad (4.8b)$$

$$\kappa_3 = \varpi_1 \varphi_3 \psi_2 + \varpi_2 \varphi_1 \psi_3 + \varpi_3 \varphi_2 \psi_1 - \varpi_1 \varphi_2 \psi_3 - \varpi_2 \varphi_3 \psi_1 - \varpi_3 \varphi_1 \psi_2 \quad (4.8c)$$

$$\kappa_4 = \varphi_3 \eta_2 \zeta_1 + \varphi_2 \eta_3 \zeta_1 - \varphi_3 \eta_1 \zeta_2 + \varphi_1 \eta_3 \zeta_2 - \varphi_2 \eta_1 \zeta_3 - \varphi_1 \eta_2 \zeta_3 \quad (4.8d)$$

$$\kappa_5 = \varphi_3 \eta_2 \zeta_1 - \varphi_2 \eta_3 \zeta_1 - \varphi_3 \eta_1 \zeta_2 - \varphi_1 \eta_3 \zeta_2 + \varphi_2 \eta_1 \zeta_3 + \varphi_1 \eta_2 \zeta_3 \quad (4.8e)$$

$$\kappa_6 = \varphi_3 \eta_2 \zeta_1 + \varphi_2 \eta_3 \zeta_1 - \varphi_3 \eta_1 \zeta_2 - \varphi_1 \eta_3 \zeta_2 - \varphi_2 \eta_1 \zeta_3 + \varphi_1 \eta_2 \zeta_3 \quad (4.8f)$$

$$\kappa_7 = \eta_2 \zeta_1 - \eta_1 \zeta_2 \quad (4.8g)$$

$$\kappa_8 = \eta_3 \zeta_2 - \eta_2 \zeta_3 \quad (4.8h)$$

$$\kappa_9 = \eta_3 \zeta_1 - \eta_1 \zeta_3 \quad (4.8i)$$

$$\kappa_{10} = \delta_3 \varphi_2 \psi_1 - \delta_2 \varphi_3 \psi_1 - \delta_3 \varphi_1 \psi_2 + \delta_1 \varphi_3 \psi_2 + \delta_2 \varphi_1 \psi_3 - \delta_1 \varphi_2 \psi_3 \quad (4.8j)$$

$$\kappa_{v1} = \chi_3 \zeta_2 - \chi_2 \zeta_3 \quad (4.8k)$$

$$\kappa_{v2} = \chi_3 \zeta_1 - \chi_1 \zeta_3 \quad (4.8l)$$

$$\kappa_{v3} = \chi_2 \zeta_1 - \chi_1 \zeta_2 \quad (4.8m)$$

$$\kappa_{q1} = \varphi_3 \psi_2 - \varphi_2 \psi_3 \quad (4.8n)$$

$$\kappa_{q2} = \varphi_3 \psi_1 - \varphi_1 \psi_3 \quad (4.8o)$$

$$\kappa_{q3} = \varphi_2 \psi_1 - \varphi_1 \psi_2 \quad (4.8p)$$

$$\kappa_{p1} = \eta_3 \chi_2 - \eta_2 \chi_3 - \alpha_v \kappa_{v1} \quad (4.8q)$$

$$\kappa_{p2} = \eta_3 \chi_1 - \eta_1 \chi_3 - \alpha_v \kappa_{v2} \quad (4.8r)$$

$$\kappa_{p3} = \eta_2 \chi_1 - \eta_1 \chi_2 - \alpha_v \kappa_{v3} \quad (4.8s)$$

All variables in above arbitrary functions are given explicitly by Eq. (3.17) for a transversely isotropic poroelastic half-plane.

4.1.2 Numerical solutions and discussion

The solutions for displacements, stresses, pore pressure and fluid displacement, given by Eqs. (4.1) – (4.3) together with the arbitrary functions defined in Eqs. (4.4) – (4.7), appear in terms of infinite integrals in the form of Eq. (3.8b). The infinite integrals with respect to ξ can be evaluated by employing an accurate numerical integration scheme. For ideal elastic materials, influence functions have singularities along the ξ -axis. However, for poroelastic materials these singularities are complex-valued due to material damping associated with fluid friction. A globally adaptive numerical quadrature scheme (Piessens 1983) has been employed to numerically evaluate the semi-infinite integrals appearing in the influence functions. This quadrature scheme subdivides the interval of integrand and uses a 21-point Gauss–Kronrod rule to estimate the integral over each interval. All numerical results presented in Figures 4.1 to 4.5 correspond to the case where loading or fluid pressure of uniform intensity f_0 is applied over a strip of width $2a$. In addition, a non-dimensional frequency, defined as $\delta = \omega a \sqrt{\rho / G}$, is used in all numerical results presented in this paper; and other normalized material parameters are defined as: $E_i^* = E_i / G$; $M^* = M / G$; $\rho_f^* = \rho_f / \rho$; $m_i^* = m_i / \rho$ and $b_i^* = b_i a / \sqrt{\rho G}$, where $i = h$ and v .

The accuracy of the present solution scheme is first verified by comparing with existing solutions on dynamic response of an isotropic poroelastic half-plane. Figure 4.1(a) shows a comparison of vertical profiles of normalized vertical

displacement along the z -axis, u_z^* ($= Gu_z / f_0 a$), of a poroelastic half-plane under the uniform vertical loading applied at $z/a = 1$ between the present solution and the solution reported by Senjuntichai and Rajapakse (1994). The comparison of u_z^* under uniform fluid pressure applied at $z/a = 1$ is also shown in Figure 4.1(b). The normalized parameters used in Fig. 1 are defined as: $E_h^* = E_v^* = 2.6$; $\nu_h = \nu_{vh} = 0.3$; $\alpha_h = \alpha_v = 0.95$; $\rho_f^* = 0.53$; $m_h^* = m_v^* = 1.1$; $M^* = 12.2$ and $b_h^* = b_v^* = 2.3$. It can be observed from Figure 4.1 that the present solution agrees very closely with the existing solution by Senjuntichai and Rajapakse (1994).

The comparisons with existing solutions of a transversely isotropic elastic half-plane are also shown to confirm the accuracy of the present solution. Figure 4.2(a) presents a comparison between the present solution and the existing solution given by Ai and Zhang (2015) for normalized vertical displacements u_z^* and normalized vertical stress σ_{zz}^* ($= \sigma_{zz} / f_0$) of a transversely isotropic half-plane under the uniform vertical loading applied on the surface ($z/a = 0$). The employed normalized parameters are: $E_h^* = 2/3$; $E_v^* = 1/3$; $\nu_h = \nu_{vh} = 0.25$ whereas the other parameters are negligibly small (≈ 0.001). As shown in Figure 4.2(a), very good agreement between the two results is observed.

Rajapakse and Wang (1991) presented normalized horizontal displacements u_x^* ($= Gu_x / f_0 a$) and normalized shear stress σ_{xz}^* ($= \sigma_{xz} / f_0$) of a transversely isotropic half-plane under buried horizontal loading ($z/a = 1$). The properties of the half-plane are defined as: $c_{11}/c_{44} = 4.26$; $c_{33}/c_{44} = 4.57$ and $c_{13}/c_{44} = 1.64$. A comparison shown in Figure 4.2(b) confirms that the obtained solution from the present scheme is in very good agreement with the existing solution provided by Rajapakse and Wang (1991). The accuracy of the present numerical solution is thus verified.

Dynamic response of a transversely isotropic poroelastic half-plane under uniformly distributed loading or fluid pressure of intensity f_0 applied over a width $2a$ is presented next. Three types of transversely isotropic poroelastic materials,

namely, Mat A, Mat B and Mat C are considered in the numerical study. The material properties of Mat A, which is an isotropic poroelastic material, are given as follows: $E_h^* = E_v^* = 3$; $\nu_h = \nu_{vh} = 0.3$; $\alpha_h = \alpha_v = 0.95$; $\rho_f^* = 0.5$; $m_h^* = m_v^* = 1$; $M^* = 12.5$; and $b_h^* = b_v^* = 2$, and Mat A is taken as the reference material in the numerical study. The properties of Mat B and Mat C are also identical to those of Mat A except the parameter b_v^* is equal to 0.2 for Mat B, and the parameter E_v^* is equal to 1.5 for Mat C. These two materials are presented in order to portray the influence of anisotropy properties in Young's modulus and the parameter b on dynamic response of a transversely isotropic poroelastic half-plane.

Figure 4.3(a) shows normalized vertical displacement profiles of u_z^* along the x -axis of all three materials due to vertical distributed loading of uniform intensity f_0 applied at $z/a = 1$. Profiles along the x -axis of u_x^* due to buried horizontal distributed loading ($z/a = 1$) of uniform intensity f_0 are also presented in Figure 4.3(b). Numerical results are presented in Figure 4.3 for all three material types at two frequencies of excitation, i.e. $\delta = 0.5$ and 2.0, and they show that normalized displacements depend significantly on non-dimensional frequency. Both real and imaginary parts of displacements vary rapidly along the x -axis, and they become more oscillatory with higher frequency. The difference in the displacements among the three materials shown in Figure 4.3 is more substantial in the case of the vertical displacement under vertical loading (u_z^*) since the parameters that are varied, i.e. b_v^* and E_v^* , represent the anisotropic properties in the vertical direction. In addition, the influence of anisotropy on both displacements is more evident at a lower frequency ($\delta = 0.5$) when compared to what observed at a higher frequency ($\delta = 2.0$).

Figure 4.4(a) shows profiles along the z -axis of non-dimensional vertical stress σ_{zz}^* due to the vertical distributed loading of uniform intensity f_0 applied at the depth $z/a = 1$. Vertical variation of normalized vertical stress along the z -axis due to the applied pore pressure of uniform intensity f_0 at the depth $z/a = 1$ is also presented in Figure 4.4(b). As expected, a unit discontinuity exists in the real part of

σ_{zz}^* at the depth $z = a$ due to the applied loading at that level whereas, under the applied pore pressure, a discontinuity of magnitude α_v is observed at $z/a = 1$ consistent with Eq. (4.2b). Numerical results shown in Figures 4.4(a) and 4.4(b) indicate that vertical variations of vertical stresses corresponding to different loading types are quite similar. Comparison of stress profiles for different materials reveals that the influence of anisotropic properties on the real part of σ_{zz}^* is less than what observed in the imaginary part. In addition, normalized stresses show oscillatory variations along the z -axis at $\delta = 2.0$ whereas at a lower frequency ($\delta = 0.5$) smooth variations of vertical stress profiles with depth are observed.

Profiles of normalized pore pressure $p^* (= p/f_0)$ along the z -axis due to applied vertical loading and applied fluid pressure are respectively presented in Figures 4.5(a) and 4.5(b). Both applied loading and fluid pressure are distributed over a width $2a$ with uniform intensity f_0 at the depth $z = a$. Both real and imaginary parts of normalized pore pressure under both loading cases are zero at the surface due to the imposed hydraulic boundary condition [see Eq. (4.1b)]. However, the real parts of normalized pore pressure profiles in Figure 4.5(b) show a unit discontinuity at the depth $z = a$ due to the fluid pressure applied at this level [see Eq. (4.2a)]. In Fig. 5(a), both real and imaginary parts of pore pressure profiles under applied vertical loading display a significant influence on anisotropic material properties and the frequency, in which the pore pressure shows oscillatory variations along the z -axis at $\delta = 2.0$ while at a lower frequency ($\delta = 0.5$) the variation of p^* with depth is smooth. On the other hand, pore pressure profiles under the applied fluid pressure presented in Figure 4.5(b) reveal that the influence of anisotropic material properties on the real part is almost negligible, whereas for the imaginary part, significant dependence on both anisotropic material properties and the frequency of excitation is observed.

4.2 Fundamental Solutions for Multi-Layered Half-Plane

4.2.1 Exact Stiffness Matrix Method

Consider a multi-layered transversely isotropic poroelastic half-plane consisting of N layers with different properties and thicknesses overlying a homogenous transversely isotropic poroelastic half-plane as shown in Figure 4.6. A superscript n is used to denote quantities associated with an n th layer ($n = 1, 2, \dots, N$), where the top and bottom levels are denoted by z_n and z_{n+1} respectively. The relationship for the n th layer can be established by using Eq. (3.16) as follows:

$$\begin{bmatrix} i\bar{u}_x(\xi, z_n) \\ \bar{u}_z(\xi, z_n) \\ \bar{p}(\xi, z_n) \\ i\bar{u}_x(\xi, z_{n+1}) \\ \bar{u}_z(\xi, z_{n+1}) \\ \bar{p}(\xi, z_{n+1}) \end{bmatrix} = \begin{bmatrix} i\chi_1 e^{\lambda_1 z_n} & -i\chi_1 e^{-\lambda_1 z_n} & i\chi_2 e^{\lambda_1 z_n} & -i\chi_2 e^{-\lambda_1 z_n} & i\chi_3 e^{\lambda_1 z_n} & -i\chi_3 e^{-\lambda_1 z_n} \\ \psi_1 e^{\lambda_1 z_n} & \psi_1 e^{-\lambda_1 z_n} & \psi_2 e^{\lambda_2 z_n} & \psi_2 e^{-\lambda_2 z_n} & \psi_3 e^{\lambda_3 z_n} & \psi_3 e^{-\lambda_3 z_n} \\ \zeta_1 e^{\lambda_1 z_n} & -\zeta_1 e^{-\lambda_1 z_n} & \zeta_2 e^{\lambda_2 z_n} & -\zeta_2 e^{-\lambda_2 z_n} & \zeta_3 e^{\lambda_3 z_n} & -\zeta_3 e^{-\lambda_3 z_n} \\ i\chi_1 e^{\lambda_1 z_{n+1}} & -i\chi_1 e^{-\lambda_1 z_{n+1}} & i\chi_2 e^{\lambda_1 z_{n+1}} & -i\chi_2 e^{-\lambda_1 z_{n+1}} & i\chi_3 e^{\lambda_1 z_{n+1}} & -i\chi_3 e^{-\lambda_1 z_{n+1}} \\ \psi_1 e^{\lambda_1 z_{n+1}} & \psi_1 e^{-\lambda_1 z_{n+1}} & \psi_2 e^{\lambda_2 z_{n+1}} & \psi_2 e^{-\lambda_2 z_{n+1}} & \psi_3 e^{\lambda_3 z_{n+1}} & \psi_3 e^{-\lambda_3 z_{n+1}} \\ \zeta_1 e^{\lambda_1 z_{n+1}} & -\zeta_1 e^{-\lambda_1 z_{n+1}} & \zeta_2 e^{\lambda_2 z_{n+1}} & -\zeta_2 e^{-\lambda_2 z_{n+1}} & \zeta_3 e^{\lambda_3 z_{n+1}} & -\zeta_3 e^{-\lambda_3 z_{n+1}} \end{bmatrix} \begin{bmatrix} A_1 \\ B_1 \\ A_2 \\ B_2 \\ A_3 \\ B_3 \end{bmatrix} \quad (4.9)$$

$$\begin{bmatrix} -i\bar{\sigma}_{xz}(\xi, z_n) \\ -\bar{\sigma}_{zz}(\xi, z_n) \\ -\bar{w}_z(\xi, z_n) \\ i\bar{\sigma}_{xz}(\xi, z_{n+1}) \\ \bar{\sigma}_{zz}(\xi, z_{n+1}) \\ \bar{w}_z(\xi, z_{n+1}) \end{bmatrix} = \begin{bmatrix} -i\varphi_1 e^{\lambda_1 z_n} & -i\varphi_1 e^{-\lambda_1 z_n} & -i\varphi_2 e^{\lambda_1 z_n} & -i\varphi_2 e^{-\lambda_1 z_n} & -i\varphi_3 e^{\lambda_1 z_n} & -i\varphi_3 e^{-\lambda_1 z_n} \\ -\eta_1 e^{\lambda_1 z_n} & \eta_1 e^{-\lambda_1 z_n} & -\eta_2 e^{\lambda_2 z_n} & \eta_2 e^{-\lambda_2 z_n} & -\eta_3 e^{\lambda_3 z_n} & \eta_3 e^{-\lambda_3 z_n} \\ -\varpi_1 e^{\lambda_1 z_n} & -\varpi_1 e^{-\lambda_1 z_n} & -\varpi_2 e^{\lambda_2 z_n} & -\varpi_2 e^{-\lambda_2 z_n} & -\varpi_3 e^{\lambda_3 z_n} & -\varpi_3 e^{-\lambda_3 z_n} \\ i\varphi_1 e^{\lambda_1 z_{n+1}} & i\varphi_1 e^{-\lambda_1 z_{n+1}} & i\varphi_2 e^{\lambda_1 z_{n+1}} & i\varphi_2 e^{-\lambda_1 z_{n+1}} & i\varphi_3 e^{\lambda_1 z_{n+1}} & i\varphi_3 e^{-\lambda_1 z_{n+1}} \\ \eta_1 e^{\lambda_1 z_{n+1}} & -\eta_1 e^{-\lambda_1 z_{n+1}} & \eta_2 e^{\lambda_2 z_{n+1}} & -\eta_2 e^{-\lambda_2 z_{n+1}} & \eta_3 e^{\lambda_3 z_{n+1}} & -\eta_3 e^{-\lambda_3 z_{n+1}} \\ \varpi_1 e^{\lambda_1 z_{n+1}} & \varpi_1 e^{-\lambda_1 z_{n+1}} & \varpi_2 e^{\lambda_2 z_{n+1}} & \varpi_2 e^{-\lambda_2 z_{n+1}} & \varpi_3 e^{\lambda_3 z_{n+1}} & \varpi_3 e^{-\lambda_3 z_{n+1}} \end{bmatrix} \begin{bmatrix} A_1 \\ B_1 \\ A_2 \\ B_2 \\ A_3 \\ B_3 \end{bmatrix} \quad (4.10)$$

In above equations, the elements in Eq. (4.9) are the Fourier transforms of displacements and pore pressure at the top and bottom surfaces of the n th layer while the elements in Eq. (4.10) are the Fourier transforms of traction and fluid displacements at the top and bottom surfaces of the n th. The matrices of displacements and pore pressure as well as traction and fluid displacements in Eqs. (4.9) and (4.10) can be expressed in the following forms.

$$\mathbf{u}^{(n)} = [i\bar{u}_x(\xi, z_n) \quad \bar{u}_z(\xi, z_n) \quad \bar{p}(\xi, z_n) \quad i\bar{u}_x(\xi, z_{n+1}) \quad \bar{u}_z(\xi, z_{n+1}) \quad \bar{p}(\xi, z_{n+1})]^T \quad (4.11)$$

$$\boldsymbol{\sigma}^{(n)} = [-i\bar{\sigma}_{xz}(\xi, z_n) \quad -\bar{\sigma}_{zz}(\xi, z_n) \quad -\bar{w}_z(\xi, z_n) \quad i\bar{\sigma}_{xz}(\xi, z_{n+1}) \quad \bar{\sigma}_{zz}(\xi, z_{n+1}) \quad \bar{w}_z(\xi, z_{n+1})]^T \quad (4.12)$$

Then, the relationship between $\mathbf{u}^{(n)}$ and $\boldsymbol{\sigma}^{(n)}$ for the n th layer can be established as follows:

$$\boldsymbol{\sigma}^{(n)} = \mathbf{K}^{(n)} \mathbf{u}^{(n)}, \quad n=1, 2, 3, \dots, N, \quad (4.13)$$

where $\mathbf{K}^{(n)}$ is an exact stiffness matrix in the frequency-wave number domain. It is found that the matrix $\mathbf{K}^{(n)}$ is symmetric and its elements are functions of the layer thickness, the layer material properties, the frequency of excitation ω , and the horizontal wave numbers ξ . The elements of $\mathbf{K}^{(n)}$ are given explicitly in **Appendix A**.

Similarly, the stiffness matrix $\mathbf{K}^{(N+1)}$ for the underlying half-space can be established from the relationship between $\mathbf{u}^{(N+1)}$ and $\boldsymbol{\sigma}^{(N+1)}$. Note that the matrices $\mathbf{u}^{(N+1)}$ and $\boldsymbol{\sigma}^{(N+1)}$ are the columns matrices that represents the generalized displacement and force at the level z_{N+1} . The elements of $\mathbf{K}^{(N+1)}$ do not contain the exponential term, and depend only on the half-plane material properties. Note that the matrix $\mathbf{K}^{(n+1)}$ is also symmetric and its elements are also given explicitly in **Appendix B**.

The global stiffness matrix of a multi-layered transversely isotropic poroelastic half-plane as shown in Figure 4.6 can be assembled by using the layer and half-plane stiffness matrices together with the continuity conditions of traction and fluid flow at the layer interfaces. The global equation system can be expressed as

$$\mathbf{K}^* \mathbf{U}^* = \mathbf{F}^* \quad (4.14)$$

where \mathbf{K}^* is the global stiffness matrix and \mathbf{U}^* is the global vector of generalized displacements. In addition, \mathbf{F}^* is the global vector of generalized forces defined as

$$\mathbf{F}^* = [\mathbf{T}^{(1)} \quad \mathbf{T}^{(2)} \quad \dots \quad \mathbf{T}^{(n)} \quad \dots \quad \mathbf{T}^{(N+1)}]^T \quad (4.15)$$

In Eq. (4.15), the sub-matrix $\mathbf{T}^{(n)} = [i\bar{T}_x^{(n)} \quad \bar{T}_z^{(n)} \quad \frac{\bar{Q}^{(n)}}{i\omega}]$. In addition, $\bar{T}_j^{(n)}$ and $\bar{Q}^{(n)}$ denote the Fourier transforms of applied traction in the j -direction ($j = x, z$) and

applied fluid source at the n th interface, respectively. For example, if a multi-layered half-plane is subjected to normal traction of uniform intensity f_0 applied over a strip of width $2a$ at the top surface of n layer, all elements of \mathbf{F}^* are zero except that

$$\bar{T}_z^{(n)}(\xi) = \sqrt{\frac{2}{\pi}} \frac{\sin(a\xi)}{\xi} f_0 \quad (4.16)$$

In the case of a multi-layered transversely isotropic poroelastic half-plane subjected to applied pore fluid pressure f_p at a depth $z = h$, the boundary and continuity conditions similar to what given by Eqs. (4.1a) to (4.1c) and (4.2) for a homogeneous half-plane have to be employed. A slight modification to the global equation, Eq. (4.14), has to be made to satisfy the continuity condition of pore pressure at that level since the pore pressure is typically an unknown of the equation. At the layer interface with a depth $z = h$, the pore pressure variable in the matrix \mathbf{U}^* is now given and it is moved to the right hand side of Eq. (4.14). A global stiffness matrix \mathbf{K}^* is altered accordingly and the modified global equation is then solved for the solution corresponding to the applied fluid pressure case. The obtained fundamental solution is the influence function required in the formulation of dynamic interaction problems between impermeable strip foundations and multi-layered transversely isotropic poroelastic soils.

4.2.2 Numerical solutions and discussion

A computer code based on the solution procedure presented in the previous section has been developed. The major computational effort in the analysis involves the computation of influence functions solved the global equation in Eq. (4.14) based on exact stiffness method. The parameters in Eq. (4.14) are expressed in terms of semi-infinite integrals of the Fourier transform parameter. It should be noted that the integrand has no singularities along the ξ -axis due to material damping associated with fluid friction of poroelastic materials. To numerically evaluate the semi-infinite integrals, a globally adaptive numerical quadrature scheme proposed by Piessens (1983) has been implemented in the computer code. In this work, a non-dimensional

frequency is defined as $\delta = \omega a \sqrt{\rho^{(1)} / G^{(1)}}$, where $\rho^{(l)}$ and $G^{(l)}$ are the parameters of the first layer. In addition, a set of normalized material parameters for all layers are defined as: $E_h^* = E_h / G^{(1)}$, $E_v^* = E_v / G^{(1)}$, $G^* = G / G^{(1)}$, $M^* = M / G^{(1)}$, $\rho^* = \rho / \rho^{(1)}$, $\rho_f^* = \rho_f / \rho^{(1)}$, $m_h^* = m_h / \rho^{(1)}$, $m_v^* = m_v / \rho^{(1)}$, $b_h^* = b_h a / \sqrt{\rho^{(1)} G^{(1)}}$ and $b_v^* = b_v a / \sqrt{\rho^{(1)} G^{(1)}}$.

The accuracy of the present solution scheme is first verified by comparing with existing solutions on dynamic response of a multi-layered transversely isotropic half-plane under the uniform vertical loading of magnitude f_0 with width $2a$ applied on the surface. Figure 4.7(a) presents a comparison between the present solution and the existing solution given by Ai and Zhang (2015) for normalized vertical displacement profile u_z^* ($= G^{(1)} u_z / f_0 a$) along z -axis, where $\delta = 1$. The multi-layered considered by Ai and Zhang (2015) consists of two layers, with the thickness of $4a$ and $3a$ respectively, and an underlying half-plane. The normalized parameters are: $E_h^* = 6$; $E_v^* = 3$ and $G^* = 1$ for first layer; $E_h^* = 3$; $E_v^* = 1.5$ and $G^* = 0.5$ for second layer; $E_h^* = 2$; $E_v^* = 1$ and $G^* = 0.3$ for underlying half-plane. In addition, ν_h and ν_v are equal to 0.25 for all layers. It should be noted that the other parameters are negligibly small (≈ 0.001). It can be seen that a very good agreement between the two results is obtained as shown in Figure 4.7(a). The comparison with existing solutions Rajapakse and Senjuntichai (1995) for dynamic response of a multi-layered isotropic poroelastic half-plane is shown in Figure 4.7(b). The multi-layered medium consists of two layers with the thickness of a and underlying half-plane, and is subjected to the uniform vertical loading applied at $h/a = 1$, where h denotes depth of loading. The results from this present solution scheme and that of Rajapakse and Senjuntichai (1995) are compared throughout the non-dimensional frequency range of $\delta = 0.2$ -2.6. It can be observed from Fig. Figure 4.7(b) that the present solution agrees very closely with the existing solution.

To investigate the dynamic response of a multi-layered transversely isotropic poroelastic soil, the selected material properties for two layers with a thickness a

and underlying half-plane are expressed in Table 4.1, and it is called System A. Another system considered in the numerical study is called System B, which represents a multi-layered isotropic poroelastic half-plane. The properties of System B are the same as those given in in Table 4.1, except that the properties in the direction normal to the isotropic plane ($i = v$) are set to be equal to those in the plane of isotropy ($i = h$), in the two layers and the underlying half-plane. For example, $E_v^* = E_h^* = 2.5$, $b_v^* = b_h^* = 2$ in the first layer of System B.

Figures 4.8(a) and 4.8(b) respectively show non-dimensional vertical displacement $u_z^* (= G^{(1)}u_z / f_0a)$ due to a uniformly distributed vertical load of magnitude f_0 and non-dimensional horizontal displacement $u_x^* (= G^{(1)}u_x / q_0a)$ due to a uniformly distributed horizontal load of magnitude q_0 . Both vertical and horizontal loads are applied on the surface ($h = 0$) and at the level $h/a = 1$. In Figures 4.8(a) and 4.8(b), System A and System B are considered in the numerical study over the non-dimensional frequency range of $0.2 < \delta \leq 2.6$. It is found from Figures 4.8(a) and 4.8(b) that the influence of anisotropy is more evident for both real and imaginary parts of the vertical displacement while the influence on horizontal displacement is almost negligible. This is due to the fact that the variations of the parameters representing the anisotropic properties of transversely isotropic poroelastic materials in the vertical direction (e.g., E_v^* and b_v^*) between System A and System B are different. Thus, the variations of the parameters E_h and b_h are suggested to be considered in the parametric studies in order to portray the influence of anisotropy effect on the horizontal displacement. In addition, the vertical displacements of System A are higher than that of System B due to the fact that E_v^* of System A is higher than that of System B in all layers. From Figures 4.8(a) and 4.8(b), both real and imaginary parts of non-dimensional displacements due to surface loading are larger than those under buried loading. Thus, the layered medium becomes less stiff and less damped under surface loading than buried loading.

4.3 Conclusion

In this chapter, the fundamental solutions of a homogeneous transversely isotropic poroelastic half-plane subjected to time-harmonic buried loads and fluid sources are presented by employing the general solutions for the case of plane strain derived in Chapter 3. Those general solutions are employed in the exact stiffness matrix scheme to determine the fundamental solutions of a multi-layered transversely isotropic poroelastic half-plane under time-harmonic loading. A computer program based on an accurate numerical integration scheme is developed, and the accuracy of present solution is verified by comparing with existing solutions. Selected numerical results under low and high frequencies are presented to demonstrate the anisotropy effects in the vertical direction of Young's modulus (E_v) and the parameter b (b_v) on dynamic response of homogenous and multi-layered half-planes, and it is found that normalized displacements, stresses and pore pressure depend significantly on the anisotropic parameters and the frequency of excitation. The present fundamental solutions are employed as the influence functions required in the analysis of dynamic interaction between strip foundations and transversely isotropic poroelastic soils presented in Chapter 6.

Table 4.1 Material properties of System A

	E_h^*	E_v^*	ν_h^*	ν_{vh}^*	G^*	α_h^*	α_v^*
First layer	2.5	4	0.3	0.3	1	0.95	0.5
Second layer	1.3	2.5	0.3	0.3	0.5	0.98	0.98
Half-plane	10	15	0.25	0.25	4	0.9	0.9
	ρ^*	ρ_f^*	m_h^*	m_v^*	b_h^*	b_v^*	M^*
First layer	1	0.5	1.5	1.5	2	3	10
Second layer	0.5	0.5	0.9	0.9	1	1.5	7.5
Half-plane	4	0.5	2.4	2.4	6	9	8



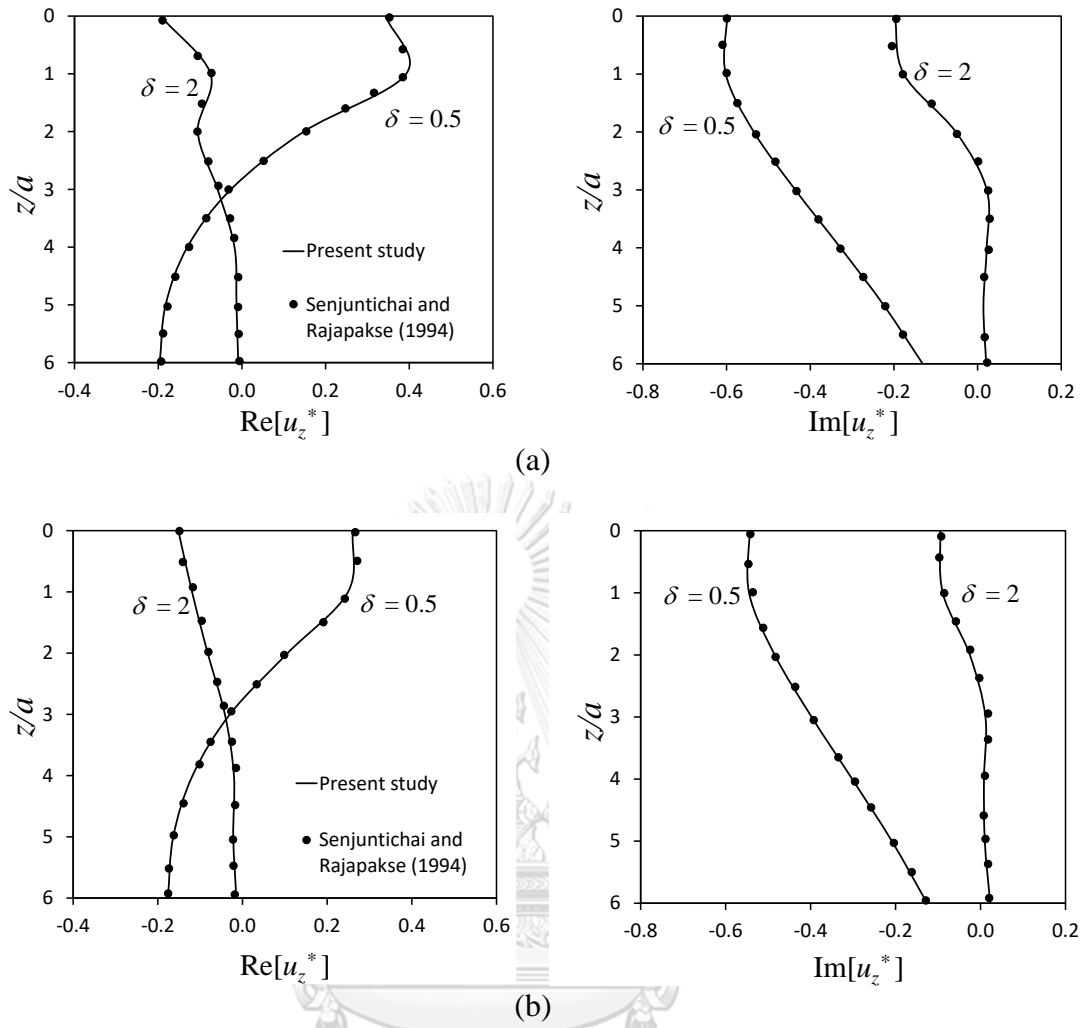


Figure 4.1 Comparisons of normalized vertical displacement profiles of an isotropic poroelastic half-plane under buried loading ($z/a = 1$): (a) applied vertical load; (b) applied fluid pressure

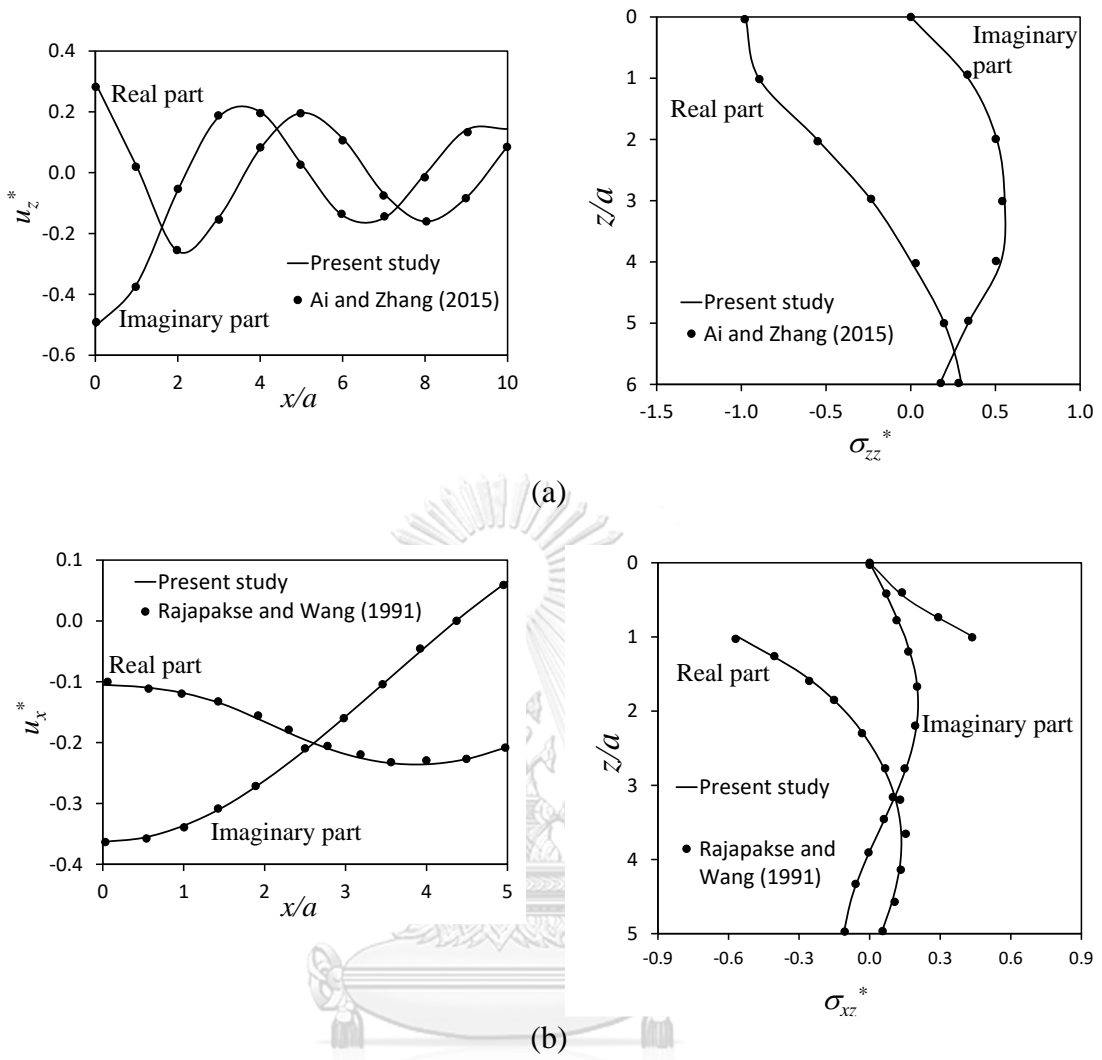


Figure 4.2 Comparisons of normalized elastic fields of transversely isotropic elastic half-planes: (a) vertical displacements and vertical stress under surface vertical loading; (b) horizontal displacement and horizontal stress under buried horizontal loading ($z/a = 1$)

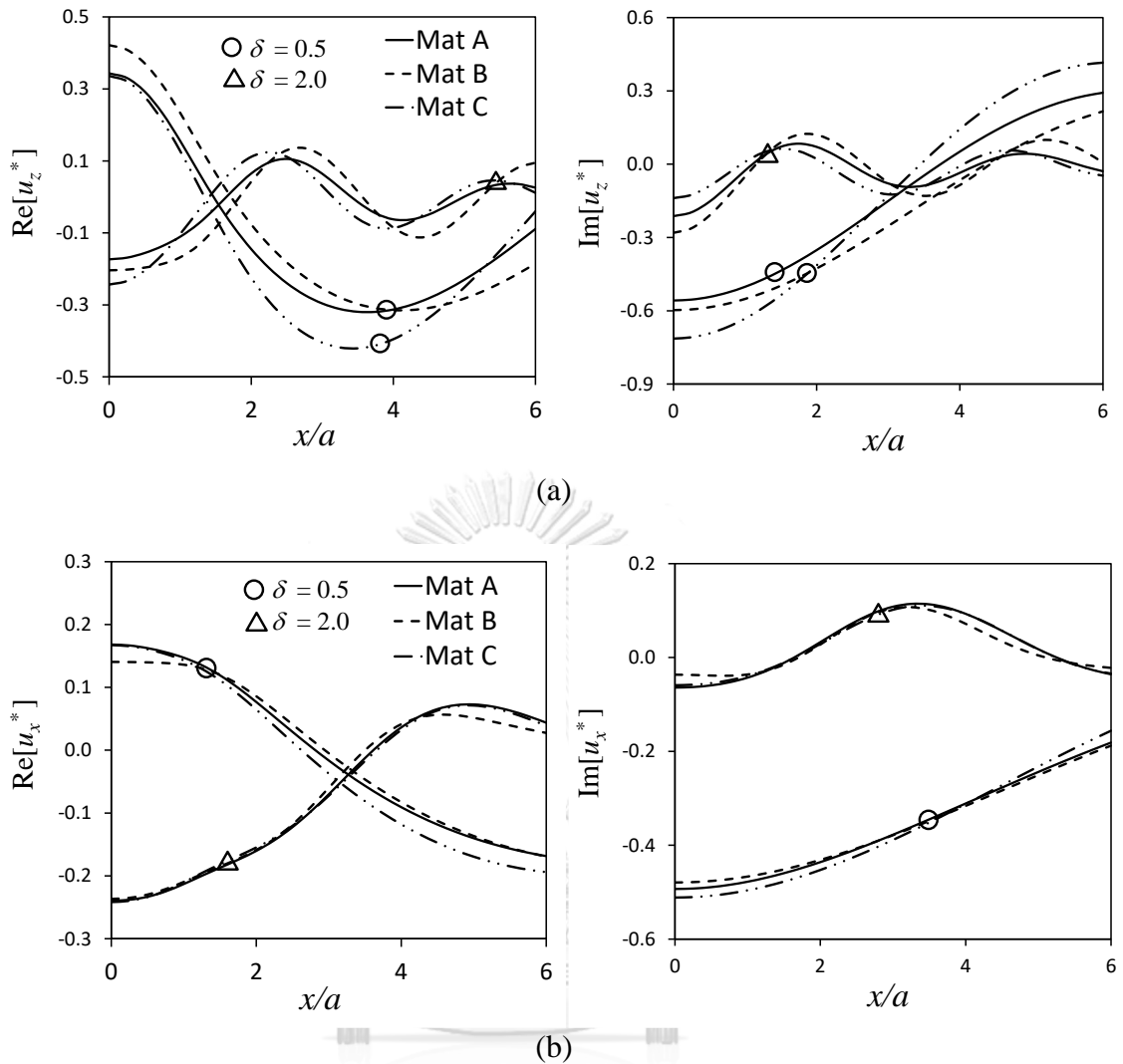


Figure 4.3 Normalized displacement profiles along the x -axis under buried loading ($z/a = 1$): (a) vertical displacements under vertical loading; (b) horizontal displacement under horizontal loading

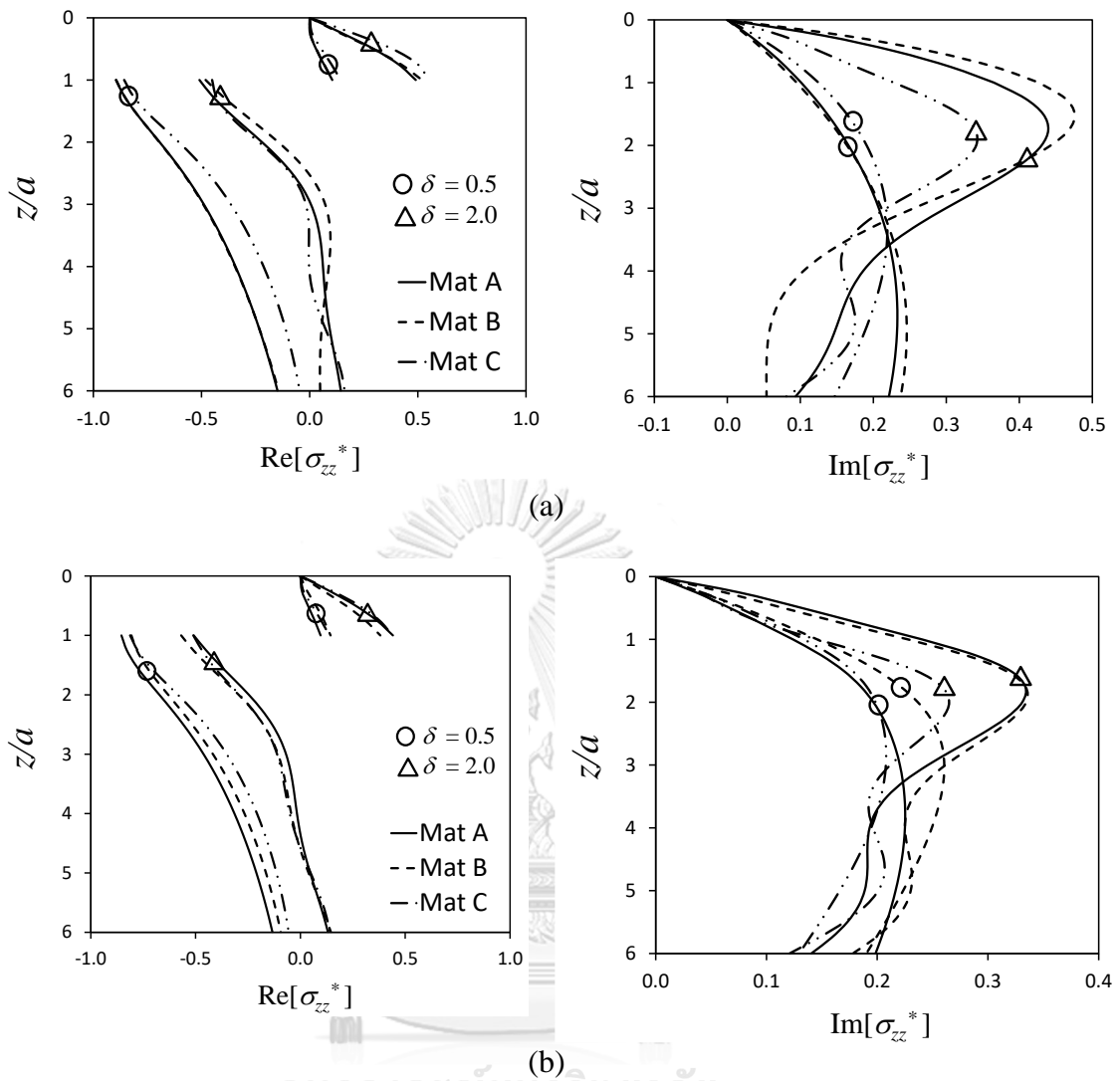


Figure 4.4 Normalized vertical stress profiles along the z -axis under buried loading ($z/a = 1$): (a) applied vertical load; and (b) applied fluid pressure

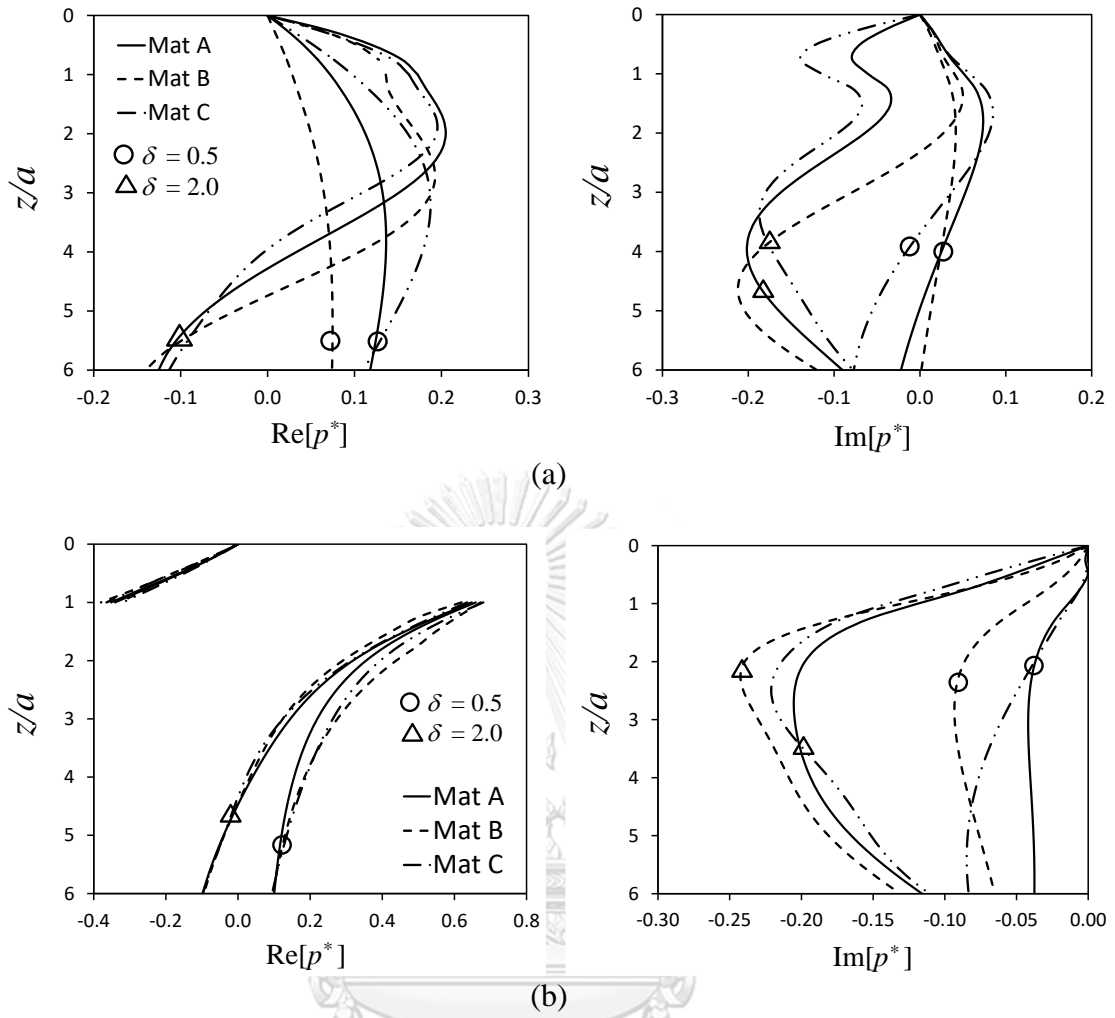


Figure 4.5 Normalized pore pressure profiles along the z-axis under buried loading ($z/a = 1$): (a) applied vertical load and (b) applied fluid pressure

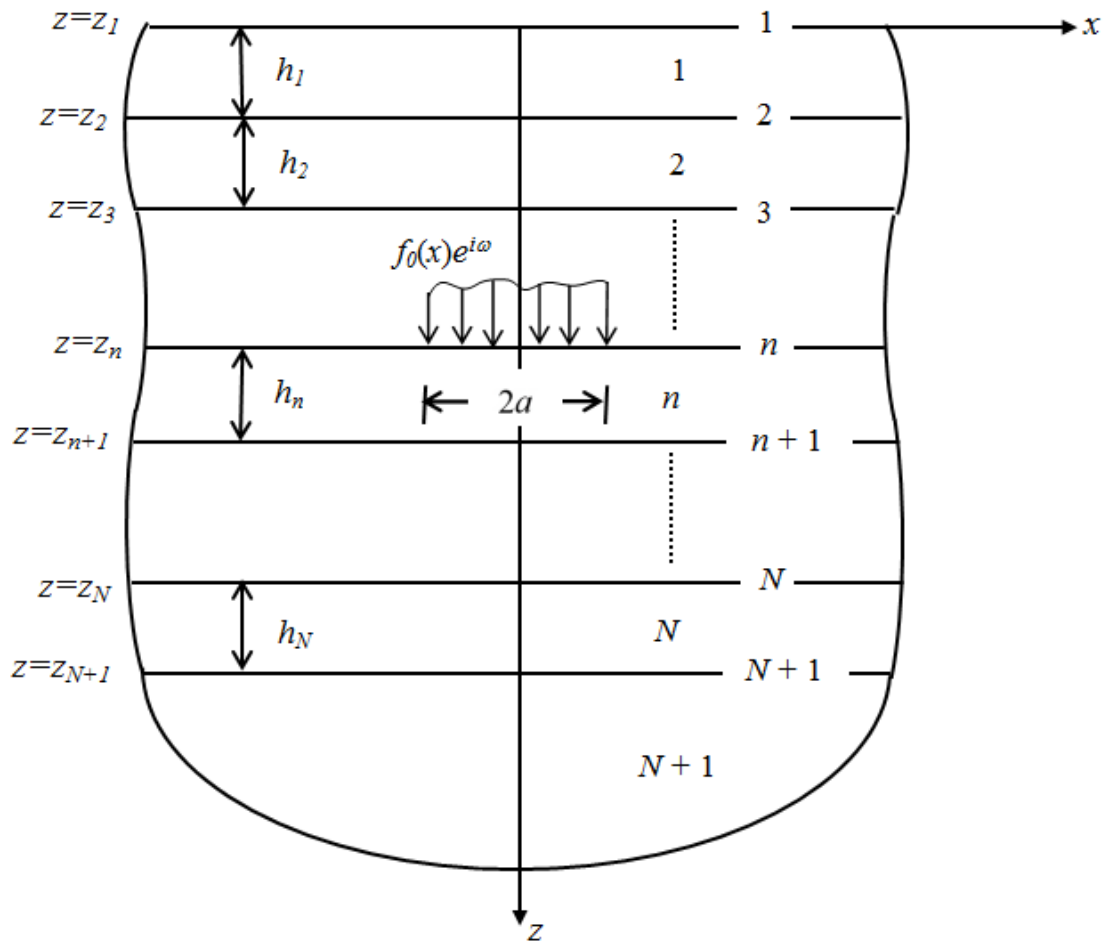


Figure 4.6 Geometry of a multi-layered transversely isotropic poroelastic half-plane under time-harmonic loading

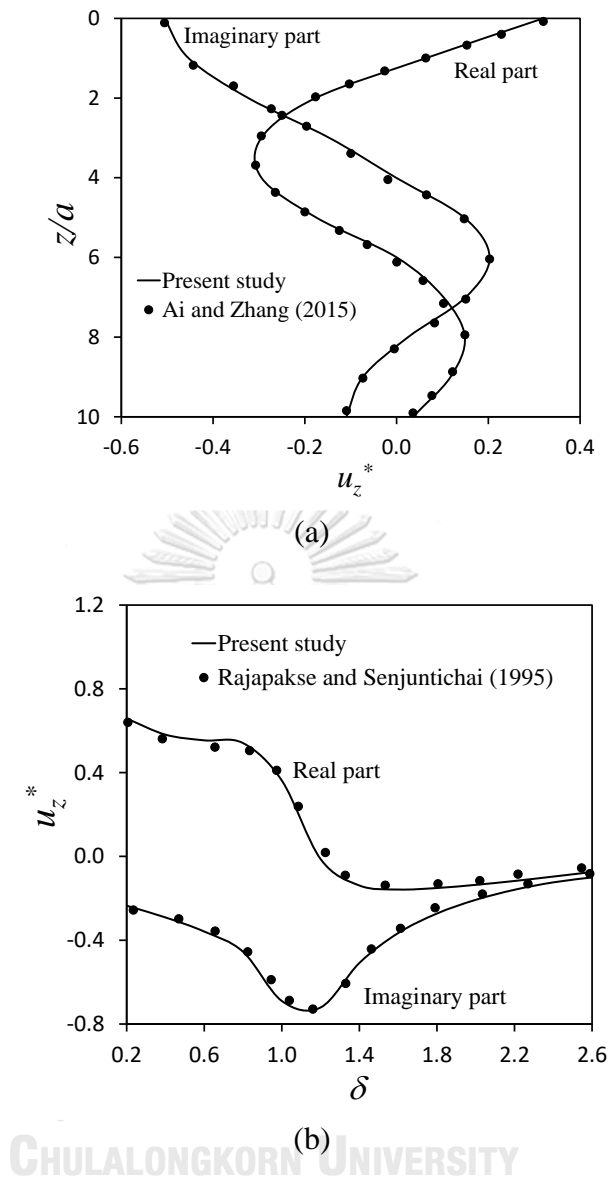


Figure 4.7 Comparison of: (a) normalized vertical displacement profiles of a multi-layered transversely isotropic half-plane under surface vertical loading ($h/a = 0$); (b) normalized vertical displacement of a multi-layered poroelastic half-plane under buried loading ($h/a = 1$)

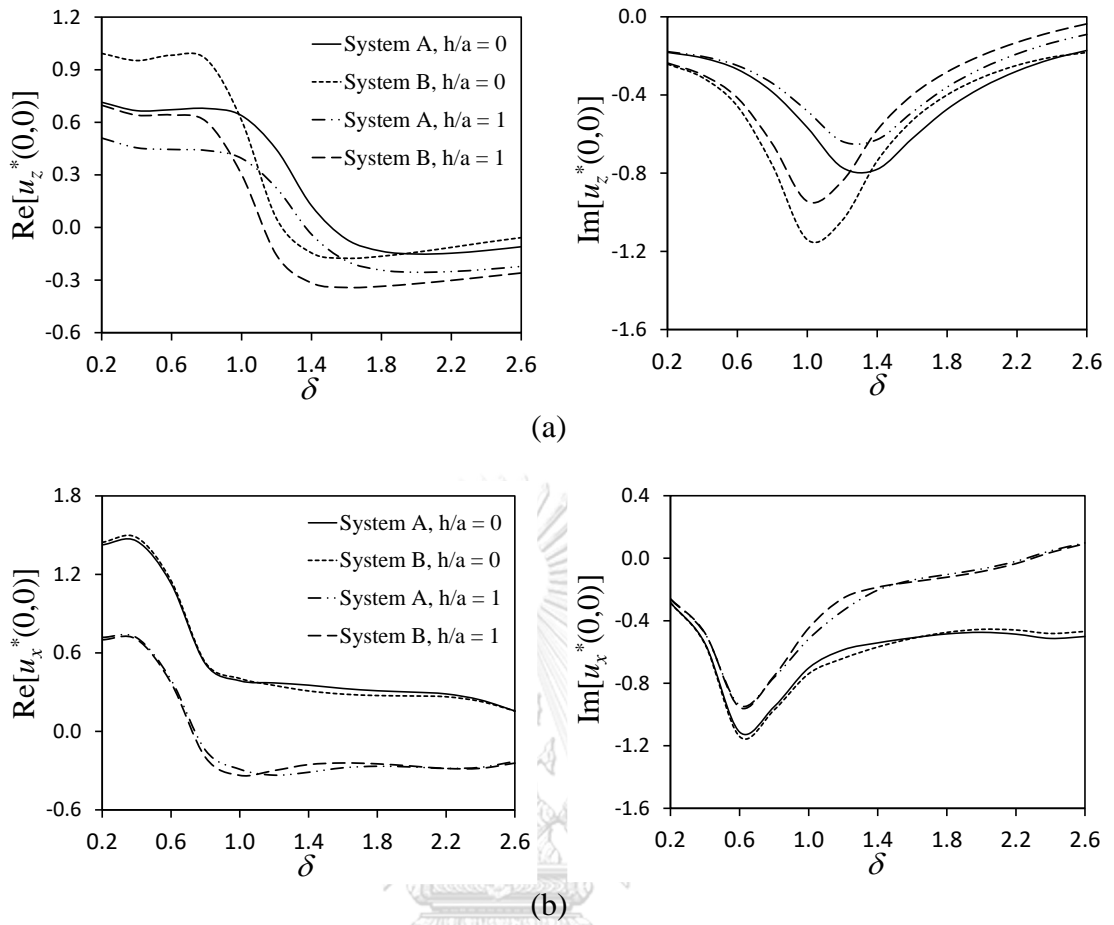


Figure 4.8 Non-dimensional displacements due to surface ($h/a = 0$) and buried loading ($h/a = 1$): (a) vertical displacement due to vertical loading; (b) horizontal displacement due to horizontal loading

CHAPTER 5

AXISYMMETRIC FUNDAMENTAL SOLUTIONS OF TRANSVERSELY ISOTROPIC POROELASTIC MEDIA

The general solutions derived in Chapter 3 are used to obtain the fundamental solutions of a homogeneous half-space and multi-layered medium under axisymmetric deformations. For a homogeneous half-space, the boundary-value problems corresponding to axisymmetric deformations of a transversely isotropic poroelastic half-space subjected to time-harmonic buried loading are presented. For a multi-layered medium, an exact stiffness matrix method is employed to determine the fundamental solutions of a multi-layered transversely isotropic poroelastic half-space under axisymmetric loading. Selected numerical results are presented to portray the influence of anisotropic and poroelastic effects on dynamic response of transversely isotropic poroelastic media.

5.1 Fundamental Solutions for Homogeneous Half-Space

5.1.1 Boundary-value problems

The fundamental solutions for axisymmetric problems can be obtained by solving boundary value problems for a transversely isotropic poroelastic half-space subjected to time-harmonic buried loading. Four loading types, i.e. a vertical load f_z , a tangential load f_r , a fluid source f_q and applied fluid pressure f_p , applied at the depth $z = h$ below surface are considered. Similar to the case of homogeneous half-plane under buried loading presented in Section 4.1, the boundary value problems are solved by treating it as two-domain boundary-value problem. The domain "1" is bounded by $0 \leq z \leq h$, and the domain "2" by $h \leq z \leq \infty$. The boundary and continuity conditions corresponding to a transversely isotropic poroelastic half-space subjected to buried axisymmetric a vertical load, a tangential load, a fluid source can be expressed as,

$$\sigma_{nz}^{(1)}(r, 0) = 0 \quad (n = r, z) \quad (5.1a)$$

$$p^{(1)}(r,0) = 0 \quad (5.1b)$$

$$u_n^{(1)}(r,h) - u_n^{(2)}(r,h) = 0 \quad (n = r, z) \quad (5.1c)$$

$$p^{(2)}(r,h) - p^{(1)}(r,h) = 0 \quad (5.1d)$$

$$\sigma_{nz}^{(1)}(r,h) - \sigma_{nz}^{(2)}(r,h) = f_n(r) \quad (n = r, z) \quad (5.1e)$$

$$w_z^{(1)}(r,h) - w_z^{(2)}(r,h) = \frac{if_q(r)}{\omega} \quad (5.1f)$$

For the case of a transversely isotropic poroelastic half-space subjected to applied pore fluid pressure, the boundary and continuity conditions are given by Eqs. (5.1a) to (5.1c) together with the following continuity conditions:

$$p^{(2)}(r,h) - p^{(1)}(r,h) = f_p(r) \quad (5.1g)$$

$$\sigma_{zz}^{(1)}(r,h) - \sigma_{zz}^{(2)}(r,h) = \alpha_v f_p(r) \quad (5.1h)$$

$$\sigma_{rz}^{(1)}(r,h) - \sigma_{rz}^{(2)}(r,h) = 0 \quad (5.1i)$$

$$w_z^{(1)}(r,h) - w_z^{(2)}(r,h) = 0 \quad (5.1j)$$

where

$$f_n(r) = H(a-r) \quad (n = z, r, q, p) \quad (5.2)$$

and a denotes the radii of the circular loading respectively.

The boundary value problem corresponding to four types of loading cases are considered separately, i.e. $f_r = f_q = f_p = 0$ for the applied vertical loading case. The application of the Hankel integral transform, Eqs. (3.20a) to (3.2f), together with the substitution of the general solutions, Eq. (3.27), for each loading case yields the solutions to the four boundary value problems. The general solutions for the domain "1" are given by Eq. (3.27), whereas for the domain "2", the general solutions are also given by Eq. (3.27) with the arbitrary functions A_j and B_j ($j = 1, 2, 3$) being replaced by the arbitrary functions C_j and D_j ($j = 1, 2, 3$) respectively. Note that $C_j \equiv 0$ to ensure the regularity of the solutions at infinity. The substitution of the general solutions for

the two domains into the boundary and continuity conditions, Eq. (5.1), yields a set of linear simultaneous equations to determine the arbitrary functions A_j , B_j and D_j ($j=1,2,3$). The arbitrary functions for each loading case are similar to those presented in Eq. (4.4) for the applied vertical loading case, Eq. (4.5) for the applied tangential loading case (by substituting f_x by f_r), Eq. (4.6) for the fluid source case and Eq. (4.7) for the applied fluid pressure case. Note that all variables in Eqs. (4.5) to (4.7) are given by Eq. (3.28) for a transversely isotropic poroelastic half-space under axisymmetric deformation.

5.1.2 Numerical solutions and discussions

The solution procedure outlined in the previous section is implemented into a computer program to compute the dynamic response of transversely isotropic poroelastic half-space under circular loading. The major computational effort required in the analysis involves the computation of influence functions which are expressed in terms of semi-infinite integrals of the Hankel transform parameter ζ by using a globally adaptive numerical quadrature scheme (Piessens 1983) as described in Chapter 4.

As the influence functions have a direct effect on the accuracy of the current solution scheme, their accuracy is verified first by considering the case of an isotropic poroelastic half-space subjected to uniformly distributed vertical loading of intensity f_0 applied over a circular area of radius a at a depth $h/a = 1$. The solution to this problem was given by Zeng and Rajapakse (1999) who presented numerical solutions for the isotropic case with $E_h^* = E_v^* = 2.6$, $\nu_h = \nu_v = 0.3$, $\alpha_h = \alpha_v = 0.95$, $\rho_f^* = 0.53$, $m_h^* = m_v^* = 1.1$, $M^* = 12.2$, and $b_h^* = b_v^* = 2.3$. Comparison of the profiles of normalized vertical displacement u_z^* ($= Gu_z^* / f_0 a$) shown in Figure 5.1 confirms excellent agreement with the solution of Zeng and Rajapakse (1999) for different frequencies ($\delta = 0.5$ and 2).

To demonstrate the basic features of dynamic response of an anisotropic poroelastic soil, we consider the case of Berea sandstone (Rice and Cleary 1976)

which is isotropic with the properties, $E_h^* = E_v^* = 2.6$, $\nu_h = \nu_v = 0.3$, $\alpha_h = \alpha_v = 0.95$, $\rho_f^* = 0.53$, $m_h^* = m_v^* = 1.1$, $M^* = 12.2$, and $b_h^* = b_v^* = 2.3$. In the absence of experimental results for properties of anisotropic poroelastic materials, we consider a hypothetical Berea sandstone with $n = 0.5, 1$ and 2 and other material properties unchanged to illustrate the coupled influence of anisotropy and poroelasticity.

Figures 5.2(a), 5.2(b) and 5.2(c) show the profiles of non-dimensionalized vertical displacement u_z^* ($= Gu_z / f_0 a$), pore pressure p^* ($= p / f_0$) and vertical stress σ_{zz}^* ($= \sigma_{zz} / f_0$) along the z -axis of a soil under uniformly distributed time-harmonic circular load of radius a and magnitude f_0 applied on the surface ($h/a = 0$). The variation of displacement, pore pressure and stress along the depth is generally smooth at lower frequencies ($\delta = 0.5$) but show a higher degree of oscillations at higher frequencies ($\delta = 2$). The influence of anisotropy (i.e., n) is also more significant at higher frequencies and displacements decrease as n increases. The profiles of displacements and stress confirm that poroelastic effects are also significant at higher frequencies. The pore pressure profiles show substantial influence of anisotropy. The peak values of pore pressure occur within $z/a \leq 2$ and it is less than 20% of the peak total stress values.

5.2 Fundamental Solutions for Multi-Layered Half-Space

5.2.1 Exact Stiffness Matrices

Consider a multi-layered transversely isotropic poroelastic half-space under axisymmetric deformations consisting of N layers with different properties and thicknesses overlying a homogenous transversely isotropic poroelastic half-space as shown in Figure 5.3. A superscript n is used to denote quantities associated with an n th layer ($n = 1, 2, \dots, N$), where the top and bottom levels are denoted by z_n and z_{n+1} respectively. The relationship for the n th layer can be established by using Eq. (3.27) as follow,

$$\begin{bmatrix} \bar{u}_r(\xi, z_n) \\ \bar{u}_z(\xi, z_n) \\ \bar{p}(\xi, z_n) \\ \bar{u}_r(\xi, z_{n+1}) \\ \bar{u}_z(\xi, z_{n+1}) \\ \bar{p}(\xi, z_{n+1}) \end{bmatrix} = \begin{bmatrix} \chi_1 e^{\lambda_1 z_n} & -\chi_1 e^{-\lambda_1 z_n} & \chi_2 e^{\lambda_2 z_n} & -\chi_2 e^{-\lambda_2 z_n} & \chi_3 e^{\lambda_3 z_n} & -\chi_3 e^{-\lambda_3 z_n} \\ \psi_1 e^{\lambda_1 z_n} & \psi_1 e^{-\lambda_1 z_n} & \psi_2 e^{\lambda_2 z_n} & \psi_2 e^{-\lambda_2 z_n} & \psi_3 e^{\lambda_3 z_n} & \psi_3 e^{-\lambda_3 z_n} \\ \zeta_1 e^{\lambda_1 z_n} & -\zeta_1 e^{-\lambda_1 z_n} & \zeta_2 e^{\lambda_2 z_n} & -\zeta_2 e^{-\lambda_2 z_n} & \zeta_3 e^{\lambda_3 z_n} & -\zeta_3 e^{-\lambda_3 z_n} \\ \chi_1 e^{\lambda_1 z_{n+1}} & -\chi_1 e^{-\lambda_1 z_{n+1}} & \chi_2 e^{\lambda_2 z_{n+1}} & -\chi_2 e^{-\lambda_2 z_{n+1}} & \chi_3 e^{\lambda_3 z_{n+1}} & -\chi_3 e^{-\lambda_3 z_{n+1}} \\ \psi_1 e^{\lambda_1 z_{n+1}} & \psi_1 e^{-\lambda_1 z_{n+1}} & \psi_2 e^{\lambda_2 z_{n+1}} & \psi_2 e^{-\lambda_2 z_{n+1}} & \psi_3 e^{\lambda_3 z_{n+1}} & \psi_3 e^{-\lambda_3 z_{n+1}} \\ \zeta_1 e^{\lambda_1 z_{n+1}} & -\zeta_1 e^{-\lambda_1 z_{n+1}} & \zeta_2 e^{\lambda_2 z_{n+1}} & -\zeta_2 e^{-\lambda_2 z_{n+1}} & \zeta_3 e^{\lambda_3 z_{n+1}} & -\zeta_3 e^{-\lambda_3 z_{n+1}} \end{bmatrix} \begin{bmatrix} A_1 \\ B_1 \\ A_2 \\ B_2 \\ A_3 \\ B_3 \end{bmatrix} \quad (5.3)$$

$$\begin{bmatrix} -\bar{\sigma}_{rz}(\xi, z_n) \\ -\bar{\sigma}_{zz}(\xi, z_n) \\ -\bar{w}_z(\xi, z_n) \\ \bar{\sigma}_{rz}(\xi, z_{n+1}) \\ \bar{\sigma}_{zz}(\xi, z_{n+1}) \\ \bar{w}_z(\xi, z_{n+1}) \end{bmatrix} = \begin{bmatrix} -\varphi_1 e^{\lambda_1 z_n} & -\varphi_1 e^{-\lambda_1 z_n} & -\varphi_2 e^{\lambda_2 z_n} & -\varphi_2 e^{-\lambda_2 z_n} & -\varphi_3 e^{\lambda_3 z_n} & -\varphi_3 e^{-\lambda_3 z_n} \\ -\eta_1 e^{\lambda_1 z_n} & \eta_1 e^{-\lambda_1 z_n} & -\eta_2 e^{\lambda_2 z_n} & \eta_2 e^{-\lambda_2 z_n} & -\eta_3 e^{\lambda_3 z_n} & \eta_3 e^{-\lambda_3 z_n} \\ -\varpi_1 e^{\lambda_1 z_n} & -\varpi_1 e^{-\lambda_1 z_n} & -\varpi_2 e^{\lambda_2 z_n} & -\varpi_2 e^{-\lambda_2 z_n} & -\varpi_3 e^{\lambda_3 z_n} & -\varpi_3 e^{-\lambda_3 z_n} \\ \varphi_1 e^{\lambda_1 z_{n+1}} & \varphi_1 e^{-\lambda_1 z_{n+1}} & \varphi_2 e^{\lambda_2 z_{n+1}} & \varphi_2 e^{-\lambda_2 z_{n+1}} & \varphi_3 e^{\lambda_3 z_{n+1}} & \varphi_3 e^{-\lambda_3 z_{n+1}} \\ \eta_1 e^{\lambda_1 z_{n+1}} & -\eta_1 e^{-\lambda_1 z_{n+1}} & \eta_2 e^{\lambda_2 z_{n+1}} & -\eta_2 e^{-\lambda_2 z_{n+1}} & \eta_3 e^{\lambda_3 z_{n+1}} & -\eta_3 e^{-\lambda_3 z_{n+1}} \\ \varpi_1 e^{\lambda_1 z_{n+1}} & \varpi_1 e^{-\lambda_1 z_{n+1}} & \varpi_2 e^{\lambda_2 z_{n+1}} & \varpi_2 e^{-\lambda_2 z_{n+1}} & \varpi_3 e^{\lambda_3 z_{n+1}} & \varpi_3 e^{-\lambda_3 z_{n+1}} \end{bmatrix} \begin{bmatrix} A_1 \\ B_1 \\ A_2 \\ B_2 \\ A_3 \\ B_3 \end{bmatrix} \quad (5.4)$$

In above equations, the elements in Eq. (5.4a) are the Hankel transforms of displacements and pore pressure at the top and bottom surfaces of the n th layer while the elements in Eq. (5.4b) are the Hankel transforms of traction and fluid displacements at the top and bottom surfaces of the n th. The matrices of displacements and pore pressure as well as traction and fluid displacements in Eqs. (5.4a) and (5.4b) can be expressed in the following forms.

$$\mathbf{u}^{(n)} = [\bar{u}_r(\xi, z_n) \quad \bar{u}_z(\xi, z_n) \quad \bar{p}(\xi, z_n) \quad \bar{u}_r(\xi, z_{n+1}) \quad \bar{u}_z(\xi, z_{n+1}) \quad \bar{p}(\xi, z_{n+1})]^T \quad (5.5)$$

$$\boldsymbol{\sigma}^{(n)} = [-\bar{\sigma}_{rz}(\xi, z_n) \quad -\bar{\sigma}_{zz}(\xi, z_n) \quad -\bar{w}_z(\xi, z_n) \quad \bar{\sigma}_{rz}(\xi, z_{n+1}) \quad \bar{\sigma}_{zz}(\xi, z_{n+1}) \quad \bar{w}_z(\xi, z_{n+1})]^T \quad (5.6)$$

Then, the relationship between vectors $\mathbf{u}^{(n)}$ and $\boldsymbol{\sigma}^{(n)}$ for the n th layer can be established as follow,

$$\boldsymbol{\sigma}^{(n)} = \mathbf{K}^{(n)} \mathbf{u}^{(n)}, \quad n=1, 2, 3, \dots, N, \quad (5.7)$$

where $\mathbf{K}^{(n)}$ is an exact stiffness matrix in the frequency-wave number domain. It is found that the elements in matrices $\mathbf{K}^{(n)}$ and $\mathbf{K}^{(N+1)}$ are similar to that shown in

Appendix A and **Appendix B** respectively except K_{12} , K_{13} , K_{15} , K_{16} , \bar{K}_{12} and \bar{K}_{13} that have to multiply with $-i$ (imaginary number).

The global stiffness matrix of a multi-layered transversely isotropic poroelastic half-space under axisymmetric deformations as shown in Figure 5.3 can be assembled by using the layer and half-space stiffness matrices together with the continuity conditions of traction and fluid flow at the layer interfaces. The global equation system can be expressed as

$$\mathbf{K}^* \mathbf{U}^* = \mathbf{F}^* \quad (5.8)$$

where \mathbf{K}^* is the global stiffness matrix and \mathbf{U}^* is the global vector of generalized displacements. In addition, \mathbf{F}^* is the global vector of generalized forces defined as

$$\mathbf{F}^* = [\mathbf{T}^{(1)} \quad \mathbf{T}^{(2)} \quad \dots \quad \mathbf{T}^{(n)} \quad \dots \quad \mathbf{T}^{(N+1)}]^T \quad (5.9)$$

In Eq. (5.9), the sub-matrix $\mathbf{T}^{(n)} = [i\bar{T}_r^{(n)} \quad \bar{T}_z^{(n)} \quad \frac{\bar{Q}^{(n)}}{i\omega}]$. In addition, $\bar{T}_j^{(n)}$ and $\bar{Q}^{(n)}$ denote the Hankel transforms of applied traction in the j -direction ($j = r, z$) and applied fluid source at the n th interface, respectively. For example, if a multi-layered half-space is subjected to normal traction of uniform intensity f_0 applied over a circular area with a radius a at the top surface of n layer, all elements of \mathbf{F}^* are zero except that

$$\bar{T}_z^{(n)}(\xi) = \frac{1}{\pi} a J_1(\xi a) f_0 \quad (5.10)$$

Note that normal traction of a unit vertical point load applied at top surface of n layer can be expressed as,

$$\bar{T}_z^{(n)}(\xi) = 1 \quad (5.11)$$

For the case of a multi-layered transversely isotropic poroelastic half-space subjected to applied pore fluid pressure f_p at a depth $z = h$, the boundary and continuity conditions similar to what given by Eqs. (5.1a) to (5.1c) and (5.1g) to (5.1j) for a homogeneous half-space have to be employed. The global equation, Eq. (5.8), has to be slightly modified in order to satisfy the continuity condition of pore pressure at that

level since the pore pressure is typically an unknown of the equation. The pore pressure variable at the layer interface with a depth $z = h$ is now given in the matrix \mathbf{U}^* . It is then moved to the right hand side of Eq. (5.8). A global stiffness matrix \mathbf{K}^* is altered accordingly and the modified global equation is then solved for the solution corresponding to the applied fluid pressure case. As a results, the fundamental solution is obtained, and can be used as a required influence function in the formulation of dynamic interaction problems between an impermeable circular foundation and a multi-layered transversely isotropic poroelastic half-space.

5.2.2 Numerical solutions and discussions

A computer code based on the solution procedure presented above has been developed. The major computational effort in the analysis involves the computation of influence functions from exact stiffness matrix method that are expressed in terms of semi-infinite integrals of the Hankel transform parameter ζ by using a globally adaptive numerical quadrature scheme described in Chapter 4. The accuracy of the present solution scheme is verified by comparing with existing solutions. Zheng et al. (2013) presented vertical profiles of vertical displacements in a multi-layered poroelastic half-space under a time-harmonic vertical point load. The layered half-space consists of two poroelastic layers overlying a homogeneous poroelastic half-space, in which the normalized thicknesses of the first and the second layers are one and two respectively. The normalized properties are $\alpha_i = 0.9$, $M = 2$, $\rho = 1$, $\rho_f = 0.5$, $m_i = 2$ and $b_i = 1$ ($i = v, h$) for the two layers and the half-space. In addition, the normalized Lamé' constants λ and μ are equal to 1.5, 2, and 3, respectively, for the first layer, the second layer, and the half-space. The comparison in the case of homogeneous poroelastic half-space was also presented, in which the parameters λ and μ are equal to one in the two layers and the half-space. The vertical point load is applied at the depth of $h = 2$. Note that only real parts are given in the works by Zheng et al. (2013). It is evident from Figure 5.4 that the numerical solutions from the present study agree very closely with those presented by Zheng et al. (2013).

The two layer systems, System A and System B identical to that presented in Chapter 4, are considered in the numerical study. Figures 5.5(a) and 5.5(b) respectively show non-dimensional vertical displacement $u_z^* (= G^{(1)} u_z / f_0 a)$ and non-dimensional radial displacement $u_r^* (= G^{(1)} u_r / f_0 a)$ due to a uniformly distributed vertical load of magnitude f_0 applied on the surface ($h = 0$) and at the level $h/a = 1$. Figures 5.5(a) and 5.5(b) present the vertical and radial displacements respectively of System A and System B under vertical loading over the non-dimensional frequency range of $0.2 < \delta \leq 2.6$. It can be seen that the difference in transversely isotropic poroelastic materials in the vertical direction (e.g., E_v^* and b_v^*) between System A and System B has a significant influence on both vertical and radial displacements. It is found that System A is basically stiffer than System B. In addition, the multi-layered medium under surface loading is less stiff and less damped than that under buried loading as illustrated in Figures 5.5(a) and 5.5(b).

5.3 Conclusion

The fundamental solutions of homogeneous and multi-layered transversely isotropic poroelastic half-spaces subjected to time-harmonic axisymmetric loading are presented in this chapter. The fundamental solutions for the homogeneous half-space are explicitly derived by solving the boundary value-problems based on the axisymmetric general solutions, whereas the exact stiffness matrix method is employed to obtain the fundamental solutions of the multi-layered half-space under axisymmetric deformations. Note that the arbitrary functions obtained for the axisymmetric fundamental solutions are akin to what obtained for the plane strain solutions presented in Chapter 4, except that all parameters involved in the expressions are given by Eq. (3.28) for a transversely isotropic poroelastic half-space under axisymmetric deformation. The accuracy of fundamental solutions for both homogeneous and multi-layered half-spaces are confirmed by comparing with their isotropic poroelastic counterparts. Selected numerical results indicate that anisotropic properties has a significant influence on vertical displacement, vertical stress and pore pressure in a transversely isotropic poroelastic half-space under vertical loading. In

addition, it is also the multi-layered half-space under surface loading is less stiff and less damped than that under buried loading. The axisymmetric fundamental solutions presented in this chapter are the required influence functions in the formulation of dynamic interaction between circular foundations and transversely isotropic poroelastic soils presented in Chapter 7.



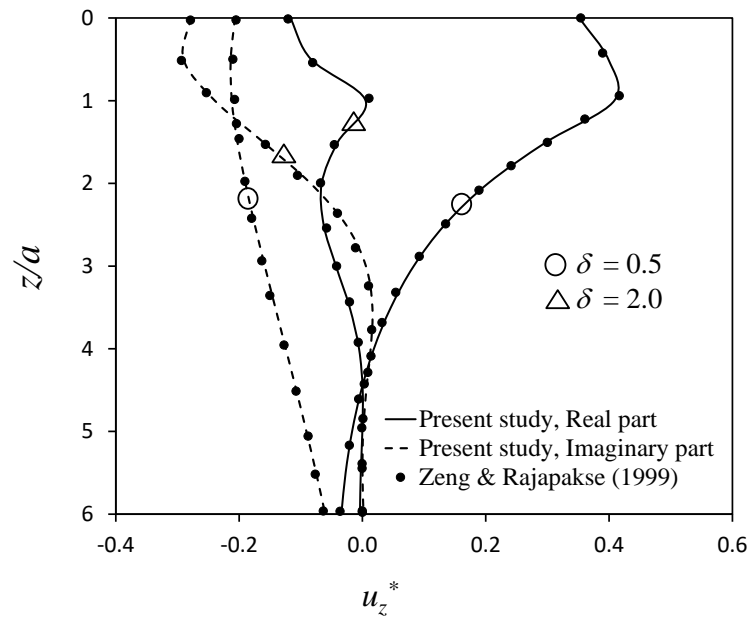


Figure 5.1 Comparison of non-dimensional vertical displacements of isotropic poroelastic half-space under applied vertical load

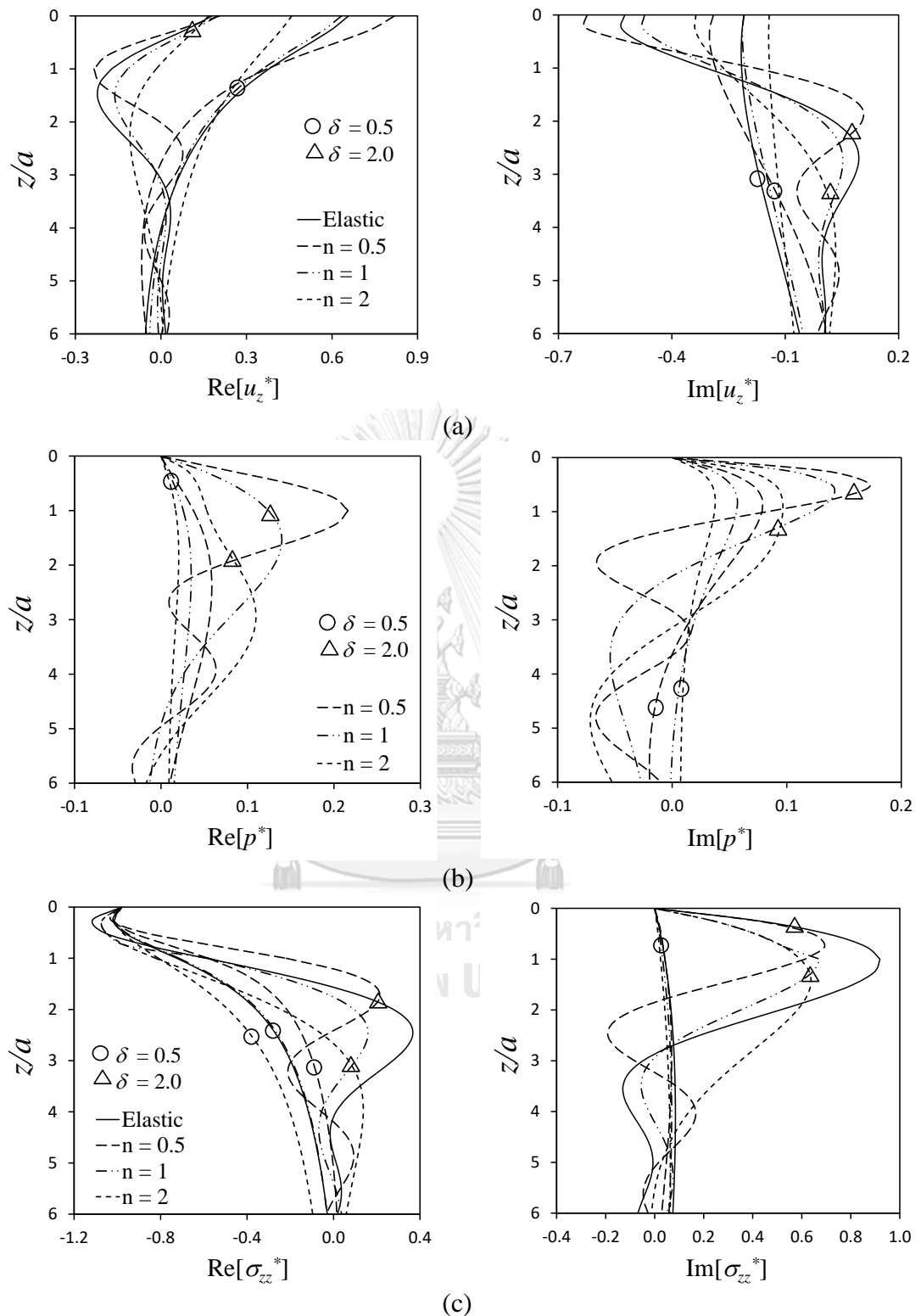


Figure 5.2 (a) Vertical displacement; (b) pore pressure and (c) vertical stress along z -axis under a surface vertical load

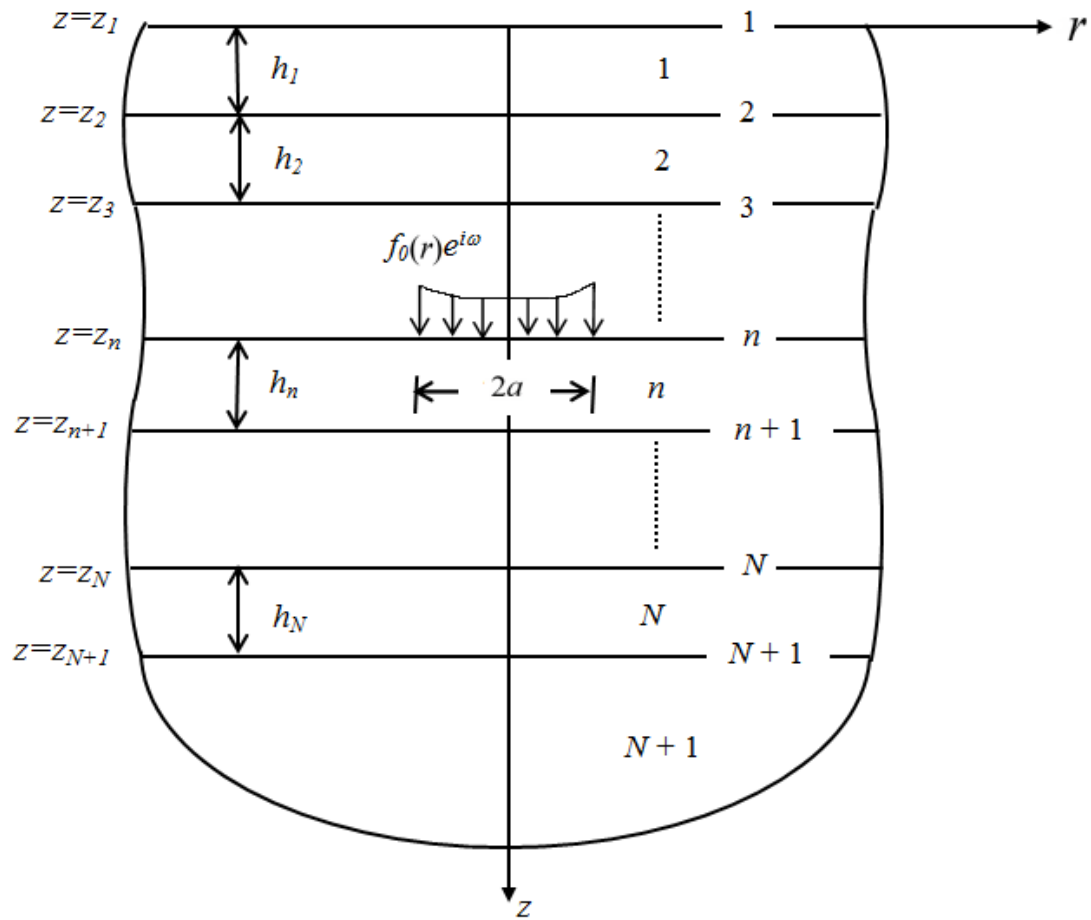


Figure 5.3 Geometry of a multi-layered transversely isotropic poroelastic half-space under time-harmonic loading

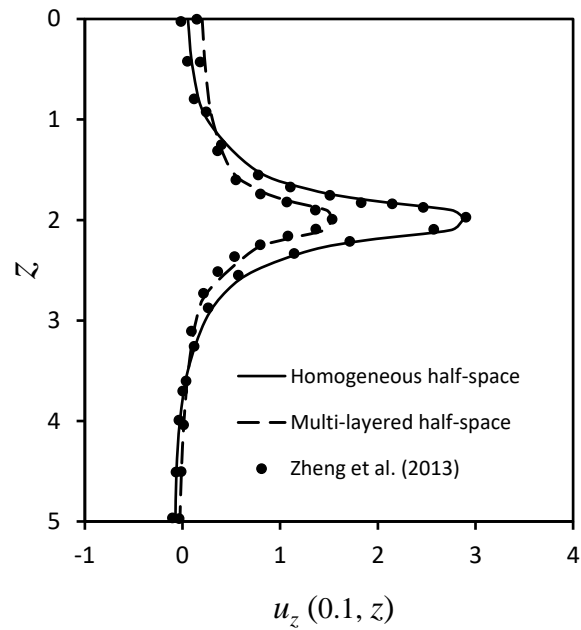


Figure 5.4 Comparison of normalized vertical displacement profiles of a multi-layered isotropic poroelastic half-plane under buried loading at $h = 2$



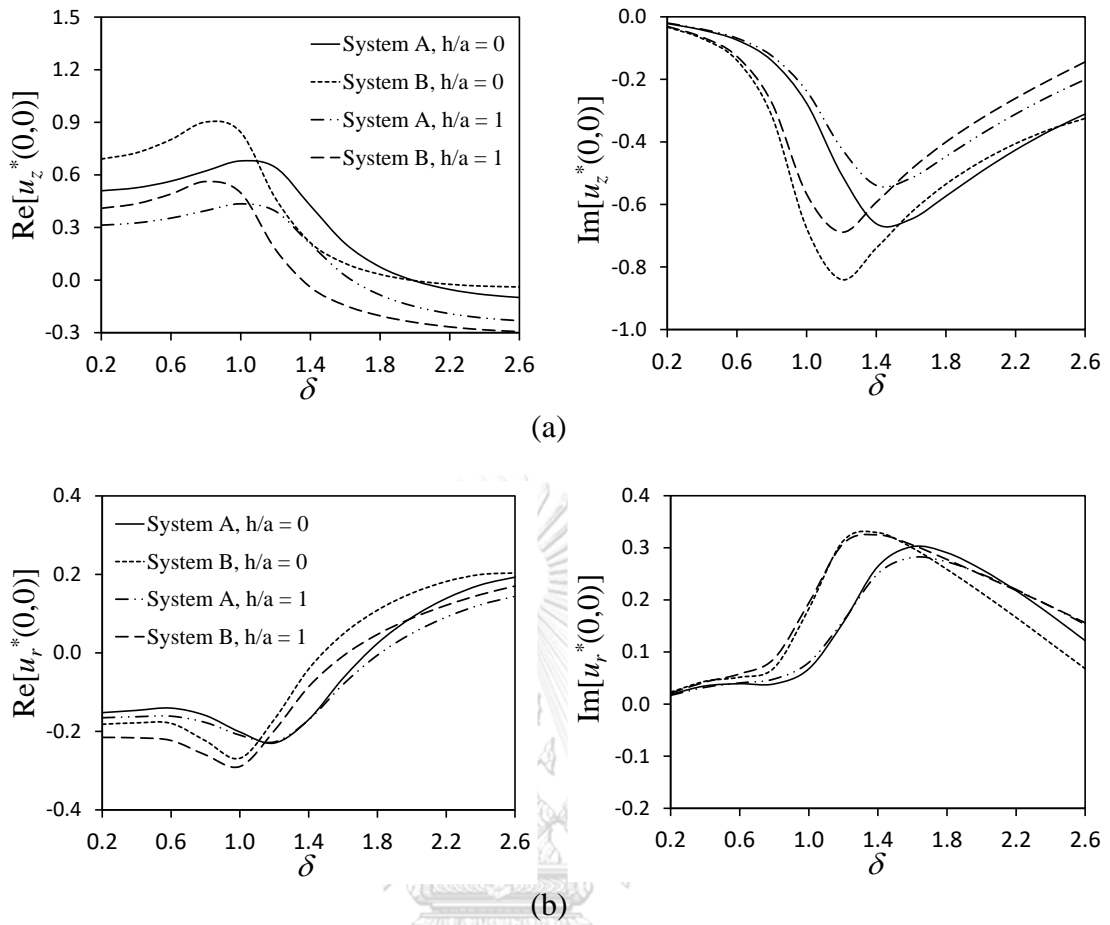


Figure 5.5 Non-dimensional displacements due to surface ($h/a = 0$) and buried loading ($h/a = 1$): (a) vertical displacement due to vertical loading; (b) radial displacement due to vertical loading

CHAPTER 6

INTERACTION BETWEEN STRIP FOUNDATIONS AND TRANSVERSELY ISOTROPIC PORORELASTIC SOILS

In this chapter, the fundamental solutions of homogeneous and multi-layered transversely isotropic poroelastic half-plane derived in Chapter 4 are employed to solve soil-structure interaction problems involving strip foundations and transversely isotropic poroelastic soils. Three problems, namely a rigid strip foundation embedded in a homogeneous half-plane, multiple rigid strip foundations on a homogeneous layer with rigid base and multiple flexible strip foundations on a multi-layered medium, are presented. Selected numerical results are presented to portray the influence of anisotropic and poroelastic properties on dynamic response of strip foundations.

6.1 Rigid Strip Foundation in Homogeneous Half-Plane

6.1.1 Formulation of interaction problem

The analysis of soil-structure interaction problems involving a rigid strip foundation and a transversely isotropic poroelastic half-plane is presented in this section. Consider a rigid strip foundation with a width of $2a$ embedded in a transversely isotropic poroelastic half-plane with a depth h below the surface as shown in Figure 6.1(a). The strip foundation is assumed to be rigid, massless and subjected to time-harmonic line loading [see Figure 6.1(a)]. In addition, the foundation is assumed to be perfectly bonded to the supporting soil with either fully permeable or impermeable contact surface. The displacements at an arbitrary point on the contact surface ($|x| \leq a$ and $z = h$) can be expressed as,

$$u_x(x, h) = \Delta_x \quad (6.1a)$$

$$u_z(x, h) = \Delta_z + x\phi \quad (6.1b)$$

where $\Delta_i (i = x, z)$ represents the displacement amplitude in the i -direction at the center of the foundation; and ϕ denotes the amplitude of the rotation about the y -axis.

The traction and the pore pressure jump generated at the contact surface between an impermeable foundation and the supporting soil in the i -direction are denoted by T_i ($i = x, z$) and T_p respectively. To determine the unknowns T_x , T_z and T_p , the contact surface is discretized into N equally spaced nodes as shown in Figure 6(b). It is assumed that the contact stresses and pore pressure are distributed uniformly over the tributary length of each node. The displacement u_i ($i = x, z$) at the node with the coordinate (x_k, h) can be expressed as,

$$u_x(x_k, h) = \sum_{l=1}^N U_{xx}(x_k; x_l) T_x(x_l) + \sum_{l=1}^N U_{xz}(x_k; x_l) T_z(x_l) + \sum_{l=1}^N U_{xp}(x_k; x_l) T_p(x_l) \quad (6.2a)$$

$$= \Delta_x$$

$$u_z(x_k, h) + x\phi = \sum_{l=1}^N U_{zx}(x_k; x_l) T_x(x_l) + \sum_{l=1}^N U_{zz}(x_k; x_l) T_z(x_l) + \sum_{l=1}^N U_{zp}(x_k; x_l) T_p(x_l) \quad (6.2b)$$

$$= \Delta_z$$

In addition, the zero flow condition under the impermeable foundation is given by,

$$w_z(x_k, h) = \sum_{l=1}^N U_{px}(x_k; x_l) T_x(x_l) + \sum_{l=1}^N U_{pz}(x_k; x_l) T_z(x_l) + \sum_{l=1}^N U_{pp}(x_k; x_l) T_p(x_l) \quad (6.2c)$$

$$= 0$$

where $U_{ij}(x_k; x_l)$ ($i = j = z, x, p$) denotes the influence function, which is the vertical ($i = z$) or horizontal ($i = x$) displacement or the relative fluid displacement ($i = p$) at the nodal location (x_k, h) due to a unit vertical ($j = z$) or horizontal ($j = x$) line load or a line fluid source ($j = p$) applied at the nodal location (x_l, h) . The influence functions $U_{ij}(x_k; x_l)$ are obtained from the fundamental solutions presented in Section 4.1.

For vertical vibrations, a rigid foundation is only subjected to vertical loading, and the contact surface between the foundation and the supporting soil is assumed to be smooth. The following relationship can be established from Eqs. (6.2b) and (6.2c):

$$\begin{Bmatrix} \Delta_z \\ \mathbf{0} \end{Bmatrix} = \begin{bmatrix} \mathbf{U}_{zz} & \mathbf{U}_{zp} \\ \mathbf{U}_{pz} & \mathbf{U}_{pp} \end{bmatrix} \begin{Bmatrix} \mathbf{T}_z \\ \mathbf{T}_p \end{Bmatrix} \quad (6.3)$$

where $\Delta_z = \{\Delta_z \ \Delta_z \ \dots \ \Delta_z\}^T$ is a column vector of size $N \times 1$ containing the amplitude of the vertical displacement, and $\mathbf{0}$ is a zero vector of size $N \times 1$. In addition, \mathbf{T}_z and \mathbf{T}_p are column vectors of size $N \times 1$ whose elements are the contact traction $T_z(x_l)$ and the pore pressure jump $T_p(x_l)$ respectively, and \mathbf{U}_{ij} ($i = j = z, p$) is a matrix of size $N \times N$ whose elements are the influence functions $U_{ij}(x_k; x_l)$.

Once the contact traction (T_z) and pore pressure jump (T_p) are obtained, the equation of equilibrium of vertical forces applied to the rigid strip foundation can then be expressed as,

$$F_z = - \int_{-a}^a (T_z + \alpha_v T_p) dx \quad (6.4)$$

where α_v is Biot's parameter defined in Eq. (3.1).

For a rigid foundation with fully permeable contact area, Eq. (6.3) is reduced to:

$$\Delta_z = \mathbf{U}_{zz} \mathbf{T}_z \quad (6.5)$$

and the equation of equilibrium of vertical forces in Eq. (6.4) involves only the normal contact traction (T_z).

For the analysis of a rigid foundation under horizontal and moment loading, the influence of hydraulic boundary conditions on dynamic response of the foundation is negligible, and the fully permeable condition is usually assumed. The following relationship can be established from Eqs. (6.2a) and (6.2b) for a rigid foundation under horizontal and moment loading and fully bonded to a poroelastic half-plane with fully permeable contact surface:

$$\begin{Bmatrix} \Delta_x \\ \Phi \end{Bmatrix} = \begin{bmatrix} \mathbf{U}_{xx} & \mathbf{U}_{xz} \\ \mathbf{U}_{zx} & \mathbf{U}_{zz} \end{bmatrix} \begin{Bmatrix} \mathbf{T}_x \\ \mathbf{T}_z \end{Bmatrix} \quad (6.6)$$

where $\Delta_{\mathbf{x}} = \{\Delta_x \quad \Delta_x \quad \dots \quad \Delta_x\}^T$ and $\Phi = \{x_1\phi \quad x_2\phi \quad \dots \quad x_N\phi\}^T$ are column vectors of size $N \times 1$, and (x_k, h) is the location of the nodal point of the k^{th} element ($k = 1, 2, \dots, N$). In addition, the elements of the matrices \mathbf{U}_{ij} and \mathbf{T}_i ($i = j = x, z$) are defined similarly to what given for the two matrices \mathbf{U}_{ij} and \mathbf{T}_i ($i = j = z, p$) respectively in Eq. (6.3).

After the normal traction T_z and the shear traction T_x are obtained, the equations of equilibrium for horizontal forces and moment can then be computed as,

$$F_x = - \int_{-a}^a (T_x) dx \quad (6.7a)$$

$$M = - \int_{-a}^a (T_z) x dx \quad (6.7b)$$

Thereafter, the relationship between applied loading F_z , F_x and M , and the displacement amplitudes Δ_z , Δ_x and ϕ can be expressed in the following matrix form:

$$\begin{Bmatrix} \Delta_z \\ \Delta_x \\ x\phi \end{Bmatrix} = \begin{bmatrix} C_V & 0 & 0 \\ 0 & C_H & C_{HM} \\ 0 & C_{HM} & C_M \end{bmatrix} \begin{Bmatrix} F_z \\ F_x \\ M \end{Bmatrix} \quad (6.8)$$

where C_V , C_H , C_M and C_{HM} represent vertical, horizontal, coupling and rocking compliances of rigid strip foundation respectively.

6.1.2 Numerical solutions and discussions

A computer code based on the formulations presented above has been developed in order to investigate dynamic response of a rigid strip foundation. Figure 6.2(a) shows the comparison of non-dimensional vertical compliance C_v^* ($= Ga\Delta_z / \pi F_z$) of a rigid strip foundation resting on the surface of a transversely isotropic poroelastic half-plane between the present solutions and the solutions given by Ai and Zhang (2016). The material properties of the half-plane are $E_h^* = 2/3$; E_v^*

$= 1/3$; $\nu_h = \nu_{vh} = 0.25$. In addition, the contact surface is divided into a number of N elements, where $N = 4, 8, 16, \text{ and } 32$. It can be seen that the present solution converges to the solution by Ai and Zhang (2016) with increasing number of N , and accurate numerical results can be obtained when $N \geq 32$. In Figure 6.2(b), the impedances, which are obtained from the inversion of the compliances, of a fully permeable strip foundation resting on a surface of a homogeneous poroelastic half-plane are presented for a comparison between the present solution and the existing solutions given by Senjuntichai and Rajapakse (1996) with $N = 32$. The comparison of vertical, horizontal, rocking and coupling impedances, denoted by K_V^* , K_H^* , K_M^* and K_{HM}^* respectively, presented in Figure 6.2(b) indicates a very good agreement between the two solutions for both real and imaginary parts of all impedances. Thus, all numerical results presented in Figures 6.3 to 6.5 are obtained with the discretized contact area of $N = 32$.

The vertical compliance of a rigid strip foundation resting on a transversely isotropic poroelastic half-plane are presented in Figures 6.3(a) and 6.3(b) for fully permeable or impermeable contact surfaces respectively. In addition, all three types of materials which are similar to those in Section 4.1 are considered in the two figures over the frequency range $0.2 \leq \delta \leq 3$. Numerical results presented in Figure 6.3 reveal that the anisotropic material properties and the hydraulic boundary condition have a significant influence on the vertical compliance, particularly in the imaginary part at low frequency. The vertical compliances vary smoothly over the frequency range $0.2 \leq \delta \leq 3$ for both real and imaginary parts. In addition, the impermeability at the contact surface makes the soil-foundation system stiffer and less damped when compared to the case of fully permeable condition.

The influence of embedded depth “ h ” on non-dimensional vertical compliances of a rigid strip foundation is also investigated. Figures 6.4(a) and 6.4(b) respectively show C_V^* for the cases of fully permeable and impermeable foundations embedded in the half-plane of Mat B at various depths of $h/a = 0, 1, 2, 5$ and 10 . Numerical results indicate that vertical compliance of strip foundations depends significantly on the depth of embedment. Similar to what observed in Figure 6.4, non-dimensional compliances of the impermeable foundation are smaller than those

of the fully permeable one. Numerical results presented in Figure 6.4 also indicate that both real and imaginary parts of C_v^* for surface ($h/a = 0$) and deeply buried ($h/a = 20$) foundations vary smoothly with frequency whereas, for foundations with intermediate embedded depths ($h/a = 1, 2$ and 5), they show oscillatory variation with δ . This is due to the effects of standing waves generated between the free surface and the embedded foundation that virtually diminish as the embedded depth increases. Non-dimensional rocking ($C_M^* = Ga^3\theta_x / \pi M$), horizontal ($C_H^* = Ga\Delta_x / \pi F_x$), and coupling ($C_{HM}^* = Ga^2\Delta_z / \pi M$) compliances of a rigid surface strip foundation ($z/a = 0$) are presented in Figures 6.5(a), 6.5(b) and 6.5(c) respectively over the frequency range $0.2 \leq d \leq 3$ under the condition of fully permeable contact surface. Numerical results presented in Figure 6.5 indicate that both real and imaginary parts of all compliances vary smoothly with the frequency. It is evident that both real and imaginary parts of the moment and coupling compliances depend significantly on the anisotropic material properties. On the other hand, the influence of the anisotropic material parameters E_v and b_v on the horizontal compliances is almost negligible due to the fact that these two parameters represent the anisotropic properties of poroelastic materials in the vertical direction. Thus, the variations of the parameters E_h and b_h would also be considered in the parametric studies to investigate the influence of anisotropic properties on horizontal vibrations of embedded foundations in poroelastic soils.

6.2 Multiple Rigid Strip Foundations on Homogeneous Layer with Rigid Base

6.2.1 Formulation of interaction problem

Consider a system of N strip foundations, subjected to time-harmonic loading resting on a homogeneous transversely isotropic poroelastic layer as shown in Figure 6.6(a). All strips are assumed to be rigid, massless, and undergoing time-harmonic translational and rotational displacements. In addition, they are assumed to be bonded to the underlying layer with fully permeable contact surface. Under this condition, both normal traction and shear traction on the contact area under each

strip are unknown. If the contact area is impermeable, pore pressure jump is also an unknown in addition to the contact traction. The modelling of impermeable contact surface was employed in the past for vertical vibrations of rigid foundations. It was found that the variation of vertical compliances with frequency for fully permeable and impermeable contact surfaces show similar trends with the maximum difference being less than ten percent. Furthermore, the influence of hydraulic conditions at the contact area of rigid foundations under other loading types is typically negligible. In view of this observation, the current assumption of fully permeable contact surface is acceptable for the interaction problem under consideration.

Consider a rigid strip i ($i=1,2,\dots,N$) with a width of $2a^i$ and the center of its contact surface being located at $(x_c^i, 0)$ as shown in Figure 6.6(a). The horizontal and vertical displacements, denoted by u_x^i and u_z^i respectively, at an arbitrary point on the contact surface of the strip i are given by,

$$u_x^i(x, 0) = \Delta_x^i, \quad x_c^i - a^i \leq x \leq x_c^i + a^i \quad (6.9a)$$

$$u_z^i(x, 0) = \Delta_z^i + x\phi^i, \quad x_c^i - a^i \leq x \leq x_c^i + a^i \quad (6.9b)$$

where Δ_j^i ($j = x, z$) represents the displacement amplitude in the j -direction at the center of the strip; and ϕ^i denotes the amplitude of the rotation about the y -axis of the strip. Let define the unknown traction in the j -direction generated at the contact surface between the strip i and the underlying layer as T_j^i ($j = x, z$). To determine the unknowns T_x^i and T_z^i , the contact surface under the strip i is discretized into N_E^i equally spaced nodes with the tributary length $t^i (= a^i/N_E^i)$ as shown in Figure 6.6(b). It is assumed that T_x^i and T_z^i are uniformly distributed over each discretized element. The displacements at the node k , with the coordinate $(x_k, 0)$ on the contact surface under the strip i ($i=1,2,\dots,N$), can be expressed as,

$$u_x^i(x_k^i, 0) = \sum_{j=1}^N \left[\sum_{l=1}^{N_E^j} U_{xx}^{ij}(x_k^i; x_l^j) T_{xl}^j(x_l^j) + \sum_{l=1}^{N_E^j} U_{xz}^{ij}(x_k^i; x_l^j) T_{zl}^j(x_l^j) \right] \quad (6.10a)$$

$$u_z^i(x_k^i, 0) = \sum_{j=1}^N \left[\sum_{l=1}^{N_E^j} U_{zx}^{ij}(x_k^i; x_l^j) T_{xl}^j(x_l^j) + \sum_{l=1}^{N_E^j} U_{zz}^{ij}(x_k^i; x_l^j) T_{zl}^j(x_l^j) \right] \quad (6.10b)$$

where $U_{mn}^{ij}(x_k^i; x_l^j)$ denotes the influence function, which is the horizontal ($m = x$) or vertical ($m = z$) displacement at the nodal location $(x_k^i; 0)$ at the contact surface under the strip i due to a uniform horizontal ($n = x$) or vertical ($n = z$) strip load of unit intensity applied at the nodal location $(x_l^j; 0)$ at the contact surface under the strip j . In addition, T_{xl}^j and T_{zl}^j ($l = 1, 2, \dots, N_E^j$) are the shear and normal contact tractions at the node l of the strip j , which are assumed to be uniformly distributed over the tributary length of the node.

These influence functions U_{mn}^{ij} can be obtained by solving a boundary value problem of a transversely isotropic poroelastic layer subjected to uniformly distributed vertical and horizontal strip loads of unit intensity, and the corresponding boundary conditions can be expressed as,

$$\sigma_{nz}(x, 0) = f_n \quad (n = x, z) \quad (6.11a)$$

$$p(x, 0) = 0 \quad (6.11b)$$

$$u_n(x, h) = 0 \quad (n = x, z) \quad (6.11c)$$

$$w_z(x, h) = 0 \quad (6.11d)$$

where

$$f_n(x) = [H(x + 0.5t) - H(x - 0.5t)]; \quad (n = z, x) \quad (6.11e)$$

and $0.5t$ is the half-width of the applied loads. The arbitrary functions for the applied vertical and horizontal loading cases can be obtained by solving the boundary-value problem for each case separately, i.e. $f_x = 0$ for the applied vertical ring load and $f_z = 0$ for the applied horizontal load. The application of the Fourier integral transform, Eq. (3.8a), together with the substitution of the general solutions, Eq. (3.16), for

each loading case yields the solutions of the six arbitrary functions A_j and B_j ($j = 1, 2, 3$). The influence functions in the Fourier transform domain are then obtained by substituting those arbitrary functions into Eq. (3.16).

The equilibrium equations of applied forces on a rigid strip j ($j = 1, 2, \dots, N$) can then be expressed as,

$$F_x^j = -\sum_{l=1}^{N_E^j} T_{xl}^j t^j \quad (6.12a)$$

$$F_z^j = -\sum_{l=1}^{N_E^j} T_{zl}^j t^j \quad (6.12b)$$

$$M_y^j = -\sum_{l=1}^{N_E^j} T_{zl}^j t^j (x_c^j - x_l^j) \quad (6.12c)$$

Finally, the relationship between the applied loading on the strip j , and the displacement amplitudes of the strip i , can be expressed in the following matrix form:

$$\begin{Bmatrix} \mathbf{D}^1 \\ \mathbf{D}^2 \\ \vdots \\ \mathbf{D}^N \end{Bmatrix} = \begin{bmatrix} \mathbf{C}^{11} & \mathbf{C}^{12} & \dots & \mathbf{C}^{1N} \\ \mathbf{C}^{21} & \mathbf{C}^{22} & \dots & \mathbf{C}^{2N} \\ \vdots & \vdots & \ddots & \vdots \\ \mathbf{C}^{N1} & \mathbf{C}^{N2} & \dots & \mathbf{C}^{NN} \end{bmatrix} \begin{Bmatrix} \mathbf{F}^1 \\ \mathbf{F}^2 \\ \vdots \\ \mathbf{F}^N \end{Bmatrix} \quad (6.13a)$$

where

$$\mathbf{D}^i = \begin{Bmatrix} \Delta_z^i \\ \Delta_x^i \\ a^i \phi^i \end{Bmatrix}; \quad \mathbf{C}^{ij} = \begin{bmatrix} C_V^{ij} & 0 & 0 \\ 0 & C_H^{ij} & C_{HM}^{ij} \\ 0 & C_{HM}^{ij} & C_M^{ij} \end{bmatrix}; \quad \mathbf{F}^j = \begin{Bmatrix} F_z^j \\ F_x^j \\ M_y^j \end{Bmatrix} \quad (i \text{ and } j = 1, 2, \dots, N) \quad (6.13b)$$

In Eq. (6.13), C_V^{ij} , C_H^{ij} , C_M^{ij} and C_{HM}^{ij} respectively represent the vertical, horizontal, coupling and rocking compliances of the strip i due to the loading applied on the strip j (i and $j = 1, 2, \dots, N$).

6.2.2 Numerical solutions and discussions

Note that the expressions for all those the non-dimensional compliances are the same as those defined in Section 6.1.2. Figure 6.7 shows the comparison of non-dimensional vertical, horizontal and rocking compliances of a rigid strip of a width $2a$ bonded to a transversely isotropic layer with a thickness of $h/a = 1$ between the present solution and the solution given by Gazetas (1981). The material properties of the layer are given as follows: $E_h/E_v = 2$; $G/E_v = 0.5$; $\nu_h = \nu_{vh} = 0.45$. In addition, the compliances from the present study are obtained by setting all poroelastic material parameters to be negligibly small with the number of discretized contact area equal to $N_E = 32$. It can be seen from Figure 6.7 that very good agreement between the two solutions is obtained for both real and imaginary parts of all compliances. Senjuntichai and Rajapakse (1996) presented non-dimensional impedances of a rigid strip bonded to an isotropic poroelastic layer with $h/a = 1$. Note that the impedances of a rigid strip can be obtained from the inversion of the compliance matrix \mathbf{C}^{ij} given by Eq. (6.13). The material properties of the layer are defined as, $E_h^* = E_v^* = 2.6$; $\nu_h = \nu_{vh} = 0.3$; $\alpha_h = \alpha_v = 0.95$; $\rho_f^* = 0.53$; $m_h^* = m_v^* = 1.5$; $M^* = 12.5$; and $b_h^* = b_v^* = 3.16$. It is evident that non-dimensional vertical, horizontal, rocking and coupling impedances, denoted by K_V^* , K_H^* , K_M^* and K_{HM}^* respectively between the present solution with $N_E = 32$ and the solution reported by Senjuntichai and Rajapakse (1996) agree very closely for both real and imaginary parts as shown in Figure 6.8.

Consider a system of two rigid strip foundations with the same width of $2a$ on a transversely isotropic poroelastic layer with the thickness h overlying an impermeable rigid base as shown in Figure 6.9. The distance between the two strips is represented by d , and the contact surface between the strips and the layer is fully permeable. Strip 1 is subjected to the time-harmonic vertical, horizontal and moment loads with its displacements being given by Eq. (6.9). On the other hand, Strip 2 is free of any external loading. In addition, Strip 2 is also restrained such that their vertical and horizontal displacements are zero. It should be noted that the solution to this case where the loading is applied only to one strip can be superimposed to investigate the dynamic interaction problem where both strips are loaded. Numerical solution corresponding to the non-dimensional compliances of Strip 1 of the double-strip system bonded to a transversely isotropic poroelastic

layer, as shown in Figure 6.9, is presented for the rest of the paper. Three types of transversely isotropic poroelastic layers are considered in the numerical study, namely, Layer A, Layer B and Layer C. The material properties of the three layers are given as follows: $E_h^* = 3$; $\nu_h = \nu_{vh} = 0.3$; $\alpha_h = \alpha_v = 0.95$; $\rho_f^* = 0.5$; $m_h^* = m_v^* = 1$; $M^* = 12.5$; and $b_h^* = 2$. In addition, Layer A is chosen as an isotropic poroelastic layer, thus $E_v^* = 3$ and $b_v^* = 2$, whereas $E_v^* = 3$ and $b_v^* = 1$ for Layer B and $E_v^* = 1.5$ and $b_v^* = 2$ for Layer C respectively to portray the anisotropic effects in Young's modulus and the parameter b on the this dynamic structure-soil-structure interaction problem.

Figure 6.10 shows the non-dimensional compliances of Strip 1 of the double-strip system on the three transversely isotropic poroelastic layers of the same thickness $h/a = 1$ over the frequency range $0 < \delta \leq 5$ and the distance between the two strips is $d/a = 0.5$. Numerical results presented in Figure 6.10 indicate that similar variations of the compliances with the frequency are observed in Strip 1 on the three layers. It is evident that the variations in E_v and b_v have a significant influence on the vertical, rocking and coupling compliances. However, a negligible dependence of the real and imaginary parts of C_H^* on E_v and b_v is observed as these two parameters represent the anisotropic properties of poroelastic materials in the vertical direction. In addition, it can be seen from the non-dimensional compliances shown in Figure 6.10 that the consideration of anisotropic properties yields the strip-poroelastic soil system that is less stiff and less damped under vertical and rocking motions.

The influence of the distance between the two strips, d/a , on the non-dimensional compliances of Strip 1 is presented in Figure 6.11 for the frequency range $0 < \delta \leq 3$. Two rigid strips, as shown in Figure 6.9, resting on the transversely isotropic poroelastic Layer C with a thickness of $h/a = 1$ is considered for different values of $d/a = 0.25, 0.5, 1, \text{ and } 4$. The case of single strip foundation is also shown in Figure 6.11 for comparison. It can be observed that the influence of d/a on the compliances is less significant when the distance between the two strips is larger. It is found that the compliances of Strip 1 for the cases of $d/a = 4$ and those of single strip are virtually identical implying that the influence of adjacent foundations could

be ignored if the distance between the two strips are at least four times greater than their width. It should be noted that the case of three-strip system has also been investigated by preparing similar plots of all compliances of the Strip 1 to those presented in Figure 6.11 with the distances between Strip 1 and Strip 2 and between Strip 2 and Strip 3 being $d/a = 0.25$. It is found that the compliances of Strip 1 corresponding to the three-strip system are practically the same as those of the two-strip system. Thus, only the case of the double-strip system is considered to investigate the interaction between adjacent foundations.

The numerical results corresponds to the compliances of Strip 1 on the Layer C with $d/a = 0.5$ for various thicknesses h/a are presented in Figure 6.12 over the non-dimensional frequency range $0 < \delta \leq 3$. The numerical results of all compliances of Strip 1 on a relatively thin layer ($h/a \leq 5$) show oscillatory variations with the frequency due to the standing waves generated within the layer, which practically vanish for the thick layer ($h/a > 15$). In addition, it is found that the compliances of Strip 1 on transversely isotropic saturated layers with $h/a = 15$ and 20 are practically identical, and they vary smoothly over the frequency range under consideration. The analysis of the dynamic interaction between a multiple strip system and a transversely isotropic poroelastic layer with $h/a > 15$ could then be carried out by treating the layer as a half-space.

จุฬาลงกรณ์มหาวิทยาลัย
CHULALONGKORN UNIVERSITY

6.3 Multiple Flexible Strip Foundations on Multi-Layered Half-Plane

6.3.1 Formulation of interaction problem

Consider a system of N_s flexible strip foundations resting on a multilayered transversely isotropic poroelastic half-plane as shown in Figure 6.13. The i^{th} strip foundation has a width of $2a^i$, and a local coordinate μ as $\mu = (x - x^i)/a^i$, where x^i is the x -coordinate at the center of the i^{th} foundation ($i = 1, 2, 3, \dots, N_s$). The contact area between the flexible strip foundations and the half-space is assumed to be smooth, and either fully permeable or impermeable. The vertical displacement of the i^{th} foundation is denoted by $w^i(\mu)$, and can be expressed in the following form.

$$w^i(\mu) = \sum_{n=0}^{N_T} \Delta_n^i \mu^n, \quad i = 1, 2, 3, \dots, N_s \quad (6.14)$$

where Δ_n^i ($n = 0, 1, \dots, N_T$) denotes a set of generalized coordinates. Hence, the bending moment per unit length acting on the i^{th} foundation is in the following form.

$$M^i(\mu) = -D^i \sum_{n=0}^{N_T} n(n-1) \Delta_n^i \mu^{n-2}, \quad i = 1, 2, 3, \dots, N_s \quad (6.15)$$

where

$$D^i = \frac{E_{st}^i (h_{st}^i)^3}{12 \left[1 - (\nu_{st}^i)^2 \right]} \quad (6.16)$$

where h_{st}^i denotes thickness of the i^{th} foundation, and E_{st}^i and ν_{st}^i represent Young's modulus, and Poisson's ratio of the i^{th} foundation material respectively.

For an i^{th} impermeable foundation, there are two unknowns, which are normal traction $T_z^i(\mu)$ and $T_p^i(\mu)$ pore pressure jump. In order to solve for these unknowns, the contact surface between i^{th} foundation is then discretized into a total number of N_E^i strip elements with equally spaced nodes, where the tributary length l^i is equal to a^i/N_E^i as shown in Figure 6.6(b). The vertical displacement compatibility and the impermeable condition are then imposed at the contact surface between the strip foundation and the half-plane. This is done by taking each term of the deflection approximation of the i^{th} foundation with $\Delta_n^i = 1$ ($n = 0, 1, \dots, N_T$ and $i = 0, 1, \dots, N_s$). Thereafter, the resulting deflection variation and zero flow condition are imposed on the nodal locations at the contact surface of the half-plane by applying contact traction T_{znk}^i and pore pressure T_{pnk}^i at the k^{th} node of i^{th} foundation, where $n = 0, 1, \dots, N_T$ and $k = 0, 1, \dots, N_E^i$. The following relationship between the normal traction, pore pressure jump and the generalized displacement can be established on the contact surface of all impermeable foundations.

$$\begin{bmatrix} G_{zz}^{11} & G_{zp}^{11} & \cdots & G_{zr}^{1j} & \cdots & G_{zz}^{1N_s} & G_{zp}^{1N_s} \\ G_{pz}^{11} & G_{pp}^{11} & \cdots & G_{pr}^{1j} & \cdots & G_{pz}^{1N_s} & G_{pp}^{1N_s} \\ \vdots & \vdots & \ddots & \vdots & \ddots & \vdots & \vdots \\ G_{qz}^{i1} & G_{qp}^{i1} & \cdots & G_{qr}^{ij} & \cdots & G_{qz}^{iN_s} & G_{qp}^{iN_s} \\ \vdots & \vdots & \ddots & \vdots & \ddots & \vdots & \vdots \\ G_{zz}^{N_s 1} & G_{zp}^{N_s 1} & \cdots & G_{zr}^{N_s j} & \cdots & G_{zz}^{N_s N_s} & G_{zp}^{N_s N_s} \\ G_{pz}^{N_s 1} & G_{pp}^{N_s 1} & \cdots & G_{pr}^{N_s j} & \cdots & G_{pz}^{N_s N_s} & G_{pp}^{N_s N_s} \end{bmatrix} \begin{Bmatrix} T_{zn}^1 \\ T_{pn}^1 \\ \vdots \\ T_{qn}^i \\ \vdots \\ T_{zn}^{N_s} \\ T_{pn}^{N_s} \end{Bmatrix} = \begin{Bmatrix} u_{zn}^1 \\ u_{pn}^1 \\ \vdots \\ u_{qn}^i \\ \vdots \\ u_{zn}^{N_s} \\ u_{pn}^{N_s} \end{Bmatrix}, \quad (6.17)$$

where

$$G_{qr}^{ij} = \begin{bmatrix} G_{qr,11}^{ij} & G_{qr,12}^{ij} & \cdots & G_{qr,1N_E}^{ij} \\ G_{qr,21}^{ij} & G_{qr,22}^{ij} & \cdots & G_{qr,2N_E}^{ij} \\ \vdots & \vdots & G_{qr,kl}^{ij} & \vdots \\ G_{qr,N_E 1}^{ij} & G_{qr,N_E 1}^{ij} & \cdots & G_{qr,N_E N_E}^{ij} \end{bmatrix} \quad (6.18)$$

where the elements $G_{qr,kl}^{ij}$ ($i, j = 1, 2, \dots, N_s$; $k, l = 1, 2, \dots, N_E$) denote the influence functions, which are the vertical displacement ($q = z$) and the relative fluid displacement ($q = p$) at any point of the k^{th} strip element on contact surface of i^{th} foundation due to a unit vertical load ($r = z$) and applied pore fluid pressure ($r = p$) of unit intensity, which are uniformly distributed over the l^{th} strip element of j^{th} foundation. The influence functions G_{kl}^{ij} can be obtained from the exact stiffness matrix method under plane strain deformations presented in Section 4.2. In addition, the elements of displacement and traction are expressed below.

$$T_{zn}^i = [T_{zn1}^i \quad T_{zn2}^i \quad \cdots \quad T_{znk}^i \quad \cdots \quad T_{znN_E}^i]^T, \quad T_{pn}^i = [T_{pn1}^i \quad T_{pn2}^i \quad \cdots \quad T_{pnk}^i \quad \cdots \quad T_{pnN_E}^i]^T \quad (6.19)$$

$$u_{zn}^i = [u_{zn1}^i \quad u_{zn2}^i \quad \cdots \quad u_{znk}^i \quad \cdots \quad u_{znN_E}^i]^T, \quad u_{pn}^i = [u_{pn1}^i \quad u_{pn2}^i \quad \cdots \quad u_{pnk}^i \quad \cdots \quad u_{pnN_E}^i]^T \quad (6.20)$$

For a fully permeable contact surface on which no pore pressure is generated, Eq. (6.17) is then reduced to,

$$\begin{bmatrix} G_{zz}^{11} & G_{zz}^{12} & \cdots & G_{zz}^{1N_s} \\ G_{zz}^{21} & G_{zz}^{22} & \cdots & G_{zz}^{2N_s} \\ \vdots & \vdots & G_{zz}^{ij} & \vdots \\ G_{zz}^{N_s 1} & G_{zz}^{N_s 2} & \cdots & G_{zz}^{N_s N_s} \end{bmatrix} \begin{Bmatrix} T_{zn}^1 \\ T_{zn}^2 \\ \vdots \\ T_{zn}^{N_s} \end{Bmatrix} = \begin{Bmatrix} u_{zn}^1 \\ u_{zn}^2 \\ \vdots \\ u_{zn}^{N_s} \end{Bmatrix} \quad (6.21)$$

The Lagrangian function Π of the system of N_s flexible strip foundations as shown in Figure 6.13 can be expressed as,

$$\Pi = \sum_{i=1}^{N_s} \left\{ V^i - U^i - \int_{-a}^a \left[\frac{1}{2} \{ T_z^i(\mu) + \alpha_v T_p(\mu) \} - f^i(\mu) \right] w_{st}^i(\mu) d\mu \right\} \quad (6.22)$$

In the above equation, V^i and U^i denote the kinetic and strain energies of the i^{th} strip foundation respectively which can be expressed in term of the generalized coordinates, Δ_n^i ($n = 0, 1, \dots, N_T$; $i = 0, 1, \dots, N_s$), in the following matrix form:

$$V^i = \dot{\Delta}^i \mathbf{M}_{st}^i (\dot{\Delta}^i)^T, \quad U^i = \Delta^i \mathbf{H}_{st}^i (\Delta^i)^T, \quad i = 1, 2, 3, \dots, N_s \quad (6.23)$$

The elements \mathbf{H}_{st}^i and \mathbf{M}_{st}^i can be expressed respectively as,

$$M_{mn}^i = \frac{h_{st}^i \rho_{st}^i (a^i)^{m+n-1}}{2(m+n-1)} \left[1 - (-1)^{m+n-1} \right], \quad (6.24a)$$

$$H_{mn}^i = \frac{E_{st}^i (h_{st}^i)^2 (a^i)^{m+n-5}}{24 \left[1 - (v_{st}^i)^2 \right]} \frac{(m-1)(m-2)(n-1)(n-2)}{(m+n-5)} \left[1 - (-1)^{m+n-5} \right], \quad (6.24b)$$

where ρ_{st}^i denotes mass density of the i^{th} foundation, and $q^i(\mu)$ denotes the external loading acting on the i^{th} foundation and can be written as,

$$q^i(\mu) = \sum_{m=0}^{N_L} \phi_m^i \mu^m \quad (6.25)$$

In addition, ϕ_m^i ($m = 0, 1, \dots, N_L$) denotes coefficients of loading function.

The Lagrangian's equations of motion for this problem are determined from the following equation.

$$\frac{d}{dt} \left(\frac{\partial \Pi}{\partial \dot{\mathbf{A}}} \right) - \frac{\partial \Pi}{\partial \mathbf{A}} = 0, \quad (6.26)$$

where $\mathbf{A} = \left[\Delta^1 \quad \Delta^2 \quad \dots \quad \Delta^{N_s} \right]^T$. As a results, it leads to the following equations of motion for determination of \mathbf{A} .

$$\mathbf{QA} = \mathbf{B} \quad (6.27)$$

where

$$\mathbf{Q} = -\omega^2 (\mathbf{M}_{st} + \mathbf{M}_{st}^T) + \mathbf{H}_{st} + \mathbf{H}_{st}^T + \mathbf{S} + \mathbf{S}^T \quad (6.28)$$

and

$$\mathbf{M}_{st} = \text{diag}[\mathbf{M}_{st}^i], \quad \mathbf{H}_{st} = \text{diag}[\mathbf{H}_{st}^i], \quad \mathbf{S} = \text{diag}[\mathbf{S}^i], \quad \mathbf{B} = [\mathbf{B}^1 \quad \mathbf{B}^2 \quad \dots \quad \mathbf{B}^{N_s}]^T \quad (6.29)$$

In above equations, the element S_{mn}^i and B_m^i of \mathbf{S}^i and \mathbf{B}^i ($m, n = 0, 1, \dots, N_{T+i}$; $i = 0, 1, \dots, N_s$) can be expressed as,

$$S_{mn}^i = \frac{1}{2} \sum_{k=1}^{N_E} l_k^i (\mu_k)^{m-1} (T_{z(n-1)k}^i + \alpha_v T_{p(n-1)k}^i), \quad (6.30a)$$

$$B_m^i = \sum_{k=1}^{N_L} \frac{\phi_k^i (a^i)^{m+k-1}}{(m+k-1)} \left[1 - (-1)^{m+k-1} \right] \quad (6.30b)$$

where l_k^i denotes the width of the k^{th} strip element of the i^{th} foundation.

The solution of a linear simultaneous equation system given by Eq. (6.27) yields the solution of the generalized coordinates Δ_n^i ($n = 0, 1, \dots, N_T$; $i = 0, 1, \dots, N_s$). By substituting the generalized coordinates of i^{th} foundation into Eq. (6.14), the vertical displacement of the i^{th} is then obtained.

6.3.2 Numerical solutions and discussions

To study a soil-structure interaction problem between multiple flexible strip foundations and multi-layered transversely isotropic poroelastic half-planes, corresponding to System A and System B similar to that in Section 4.2, are selected. The dynamic interaction between a system of strip foundations subjected to a uniform vertical load of intensity q_0 resting on a multi-layered transversely isotropic poroelastic half-plane as shown Figure 6.13 is presented next. A non-dimensional deflection (compliance) and a relative flexibility parameter of the foundation defined as $w^*(x) = G^{(1)} w(x) / a q_0$ and $\gamma = E_{st} h_{st}^3 / 12(1 - \nu_{st}^2) a^3 G^{(1)}$ respectively are presented. Figure 6.14(a) shows a comparison of inverted central deflection $1/w^*(0)$ for two values of $\gamma = 0.5$ and $\gamma = 1$ for a strip footing resting on the surface of homogeneous transversely isotropic half-plane between the present study and the solutions given by Ai et al. (2017). The material properties of the half-plane are $E_h^* = 6$; $E_v^* = 3$ and ν_h

$= \nu_{vh} = 0.25$. The converged solution is attained when $N_E \geq 32$ and $N_S \geq 8$. It can be observed from Figure 6.14(a) that the solution of the current formulation is in good agreement with that given by Ai et al. (2017) for both flexibility values. A system of strip footings on multi-layered poroelastic half-plane by Senjuntichai and Kaewjuea (2008) are also employed to verify the present solution scheme. Note that the comparisons in Figure 6.14(b) consist of single foundation and two foundations with $\gamma = 1$ resting on a multi-layered poroelastic half-space. The multi-layered poroelastic half-plane consists of first and second layers with same thickness of a and underlying half-plane. Note that the distance (d) between two foundation is $d/a = 1$. It is evident from Figure 6.14(b) that very good agreement between both solutions is obtained for both real and imaginary parts. The proposed numerical scheme is thus verified through these independent comparisons.

The effect of footing flexibility and permeability on the dynamic response of multiple flexible strips is investigated next. Numerical results in Figures 6.15(a) and 6.15(b) respectively present the vertical displacement $w^*(0)$ and bending moment $M^*(0)$ at the center of a flexible impermeable strip on the multi-layered transversely isotropic poroelastic half-plane identified as System A with the material properties shown in Table 4.1. In this investigation, a set of footing flexibilities, which are $\gamma = 0.2, 0.5, 1, 10$ and 100 , is considered in Figure 6.15. Strip footings with larger γ are stiffer and less damped compared to more flexible footings for both real and imaginary parts as shown in Figure 6.15(a). In addition, the numerical results of central bending moment $M^*(0)$ show that stiffer footings (higher γ values) experience higher bending moments.

Figure 6.16 shows the profiles of non-dimensional contact traction ($T_z^* = T_z/q_0$) and pore pressure jump ($T_p^* = T_p/q_0$) under an impermeable strip with $\gamma = 100$. The selected examples correspond to the cases of $\delta = 0.5$ and 2 , and traction and pore pressure profiles are plotted along the x -axis. It can be seen from Figure 6.16 that the profiles of contact traction and pore pressure jump depend significantly on the frequency. Both real and imaginary parts of contact traction are singular near the boundary of the strip. The magnitude of pore pressure jump is relatively small

for both real and imaginary parts. In addition, both real and imaginary parts of pore pressure jump converge to zero near the boundary of the strip implying that no singular pore pressure jump takes place at the strip edge.

Figures 6.17(a) and 6.17(b) respectively show $w^*(0)$ and $M^*(0)$ of an impermeable flexible strip footing with $\gamma = 1$ resting on different transversely isotropic poroelastic systems. Four transversely isotropic poroelastic systems, namely a homogenous half plane, a homogenous layer of thickness a with an impermeable rigid base, and multi-layered System A and System B, are considered in the figure to investigate the influence of layering and transversely isotropic poroelastic material parameters. The material properties of the homogeneous half-plane and the homogeneous layer are identical to those of the first layer defined in Table 4.1. The geometries and material properties of the multi-layered System A and System B are identical to those used in Chapter 4. It can be seen from Figures 6.17(a) and 6.17(b) that substantial differences among strip foundations on three poroelastic systems are clearly observed. Both real and imaginary parts of $w^*(0)$ and $M^*(0)$ for the strip on the homogeneous half-plane and layer vary smoothly with δ whereas those of System A and System B show oscillatory variations. The difference in the strip displacements between System A and System B is mainly due to the anisotropy effect, where System A corresponds to a transversely isotropic medium while System B corresponds to an isotropic medium. It is found that central vertical displacement of strip foundation on System B is higher than that on System A since the System A has a stiffer properties in the vertical direction.

Figures 6.18(a) and 6.18(b) respectively present $w^*(0)$ of two flexible impermeable strip footings with $\gamma = 0.2$ and 100 resting on the System A for different distances between two footings, i.e. $d/a = 1, 2, 4$ and 8 . In addition, the case of single-footing is also shown in Figure 6.18 for comparison. It is evident from Figure 6.18 that $w^*(0)$ depend significantly on the distance d . The central vertical displacements of closely spaced strips with $d/a \leq 4$ show oscillatory variations with frequency. The variation of $w^*(0)$ becomes smoother when the distance d is larger. It can be seen that the values of $w^*(0)$ converge to those of single foundation when $d/a >$

8 implying that two strip system could be studied as a single strip when the distance from adjacent foundations is larger than two time of their width.

6.4 Conclusion

In this chapter, three problems, namely a rigid strip foundation embedded in a homogeneous half-plane, multiple rigid strip foundations on a homogeneous layer with rigid base and multiple flexible strip foundations on a multi-layered medium, are presented. For rigid strip foundations, vertical, horizontal, rocking, and coupling compliances are presented, whereas for the case of multiple flexible strips only the case of vertical loading is considered. The interaction problem is investigated by employing a semi-analytical discretization technique together with the fundamental solutions obtained in Chapter 4. Accuracy of the present solution scheme is confirmed by comparing with existing solutions. Selected numerical solution on non-dimensional compliance is presented to show the influence of the two anisotropic parameters E_v and b_v on the compliances. Numerical results indicate that all compliances except the horizontal compliance show a strong dependence on the two parameters. It is also found that the impermeable hydraulic boundary condition at the contact area makes a strip foundation under vertical loading stiffer and less damped than the fully permeable one. In addition, the compliances also depend significantly on the distance between adjacent foundations, the layer thickness, the frequency of excitation and the relative rigidity (in the case of flexible strips).

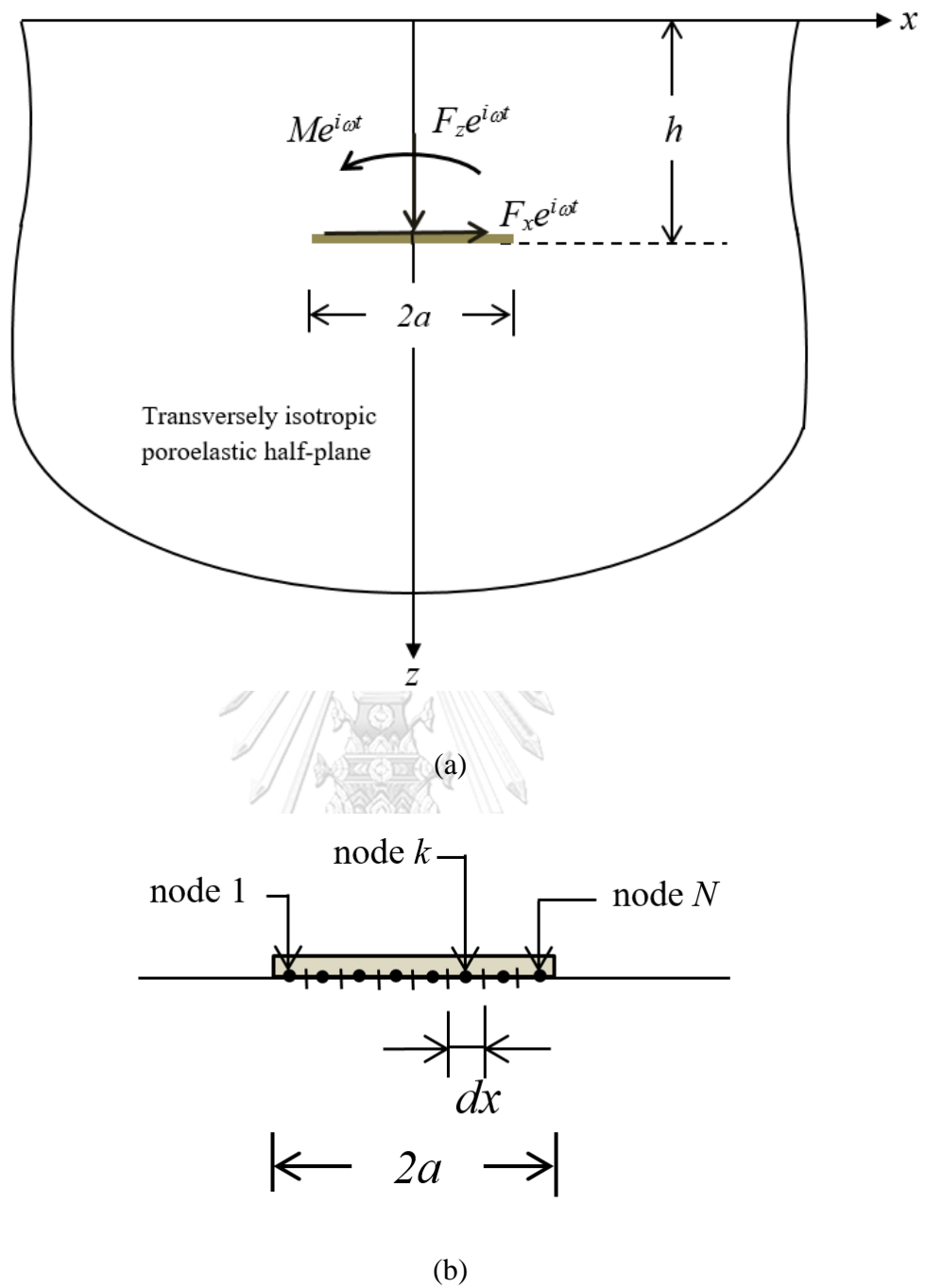


Figure 6.1 (a) Rigid strip foundation embedded in a transversely isotropic poroelastic half-plane under time-harmonic loading; (b) Discretization of contact area

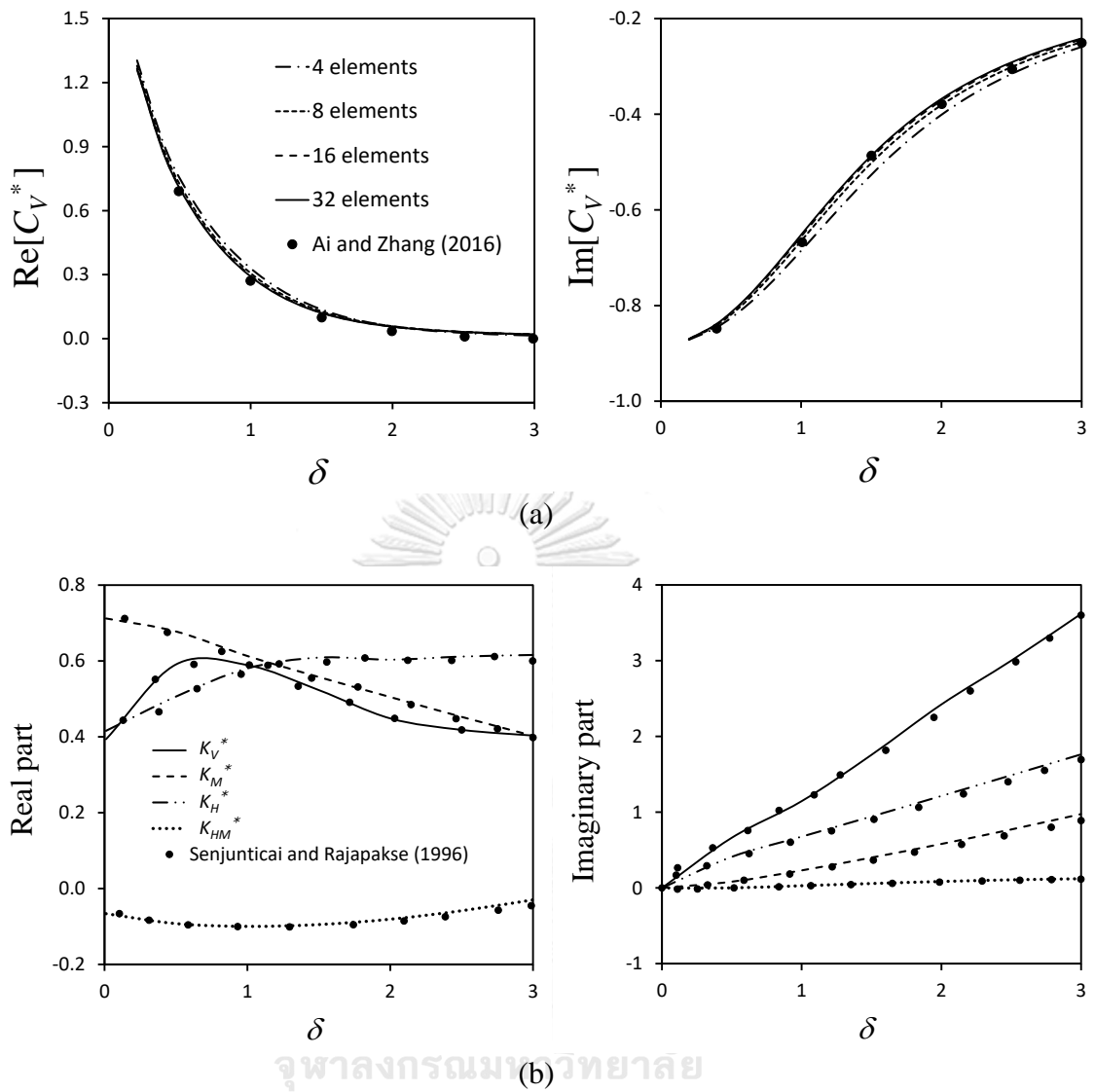


Figure 6.2 Comparison of (a) non-dimensional vertical compliances of a rigid strip resting on a transversely isotropic half-plane; and (b) non-dimensional impedances of a rigid strip resting on an isotropic poroelastic half-plane

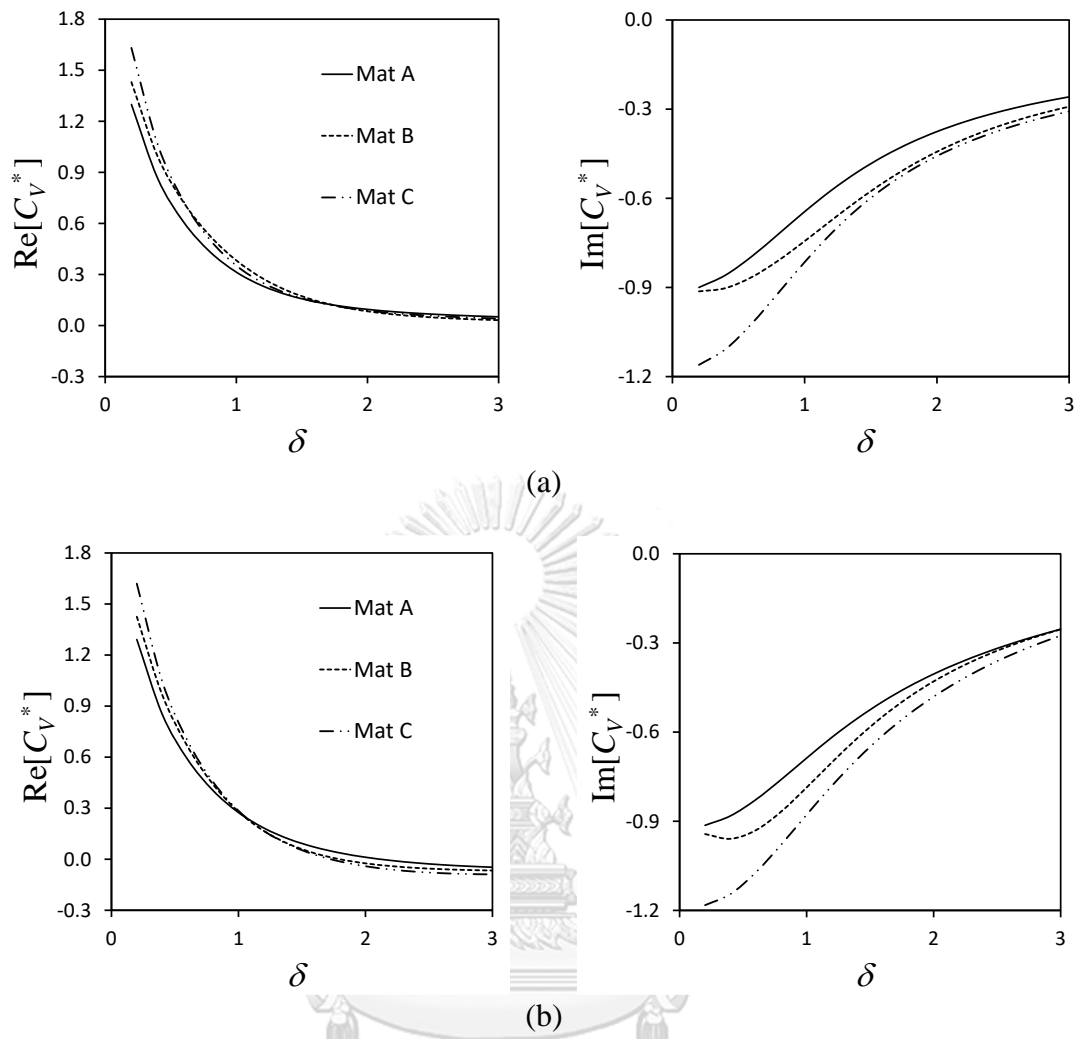


Figure 6.3 Non-dimensional vertical compliances of surface strip foundation ($h/a = 0$): (a) permeable foundation; (b) impermeable foundation

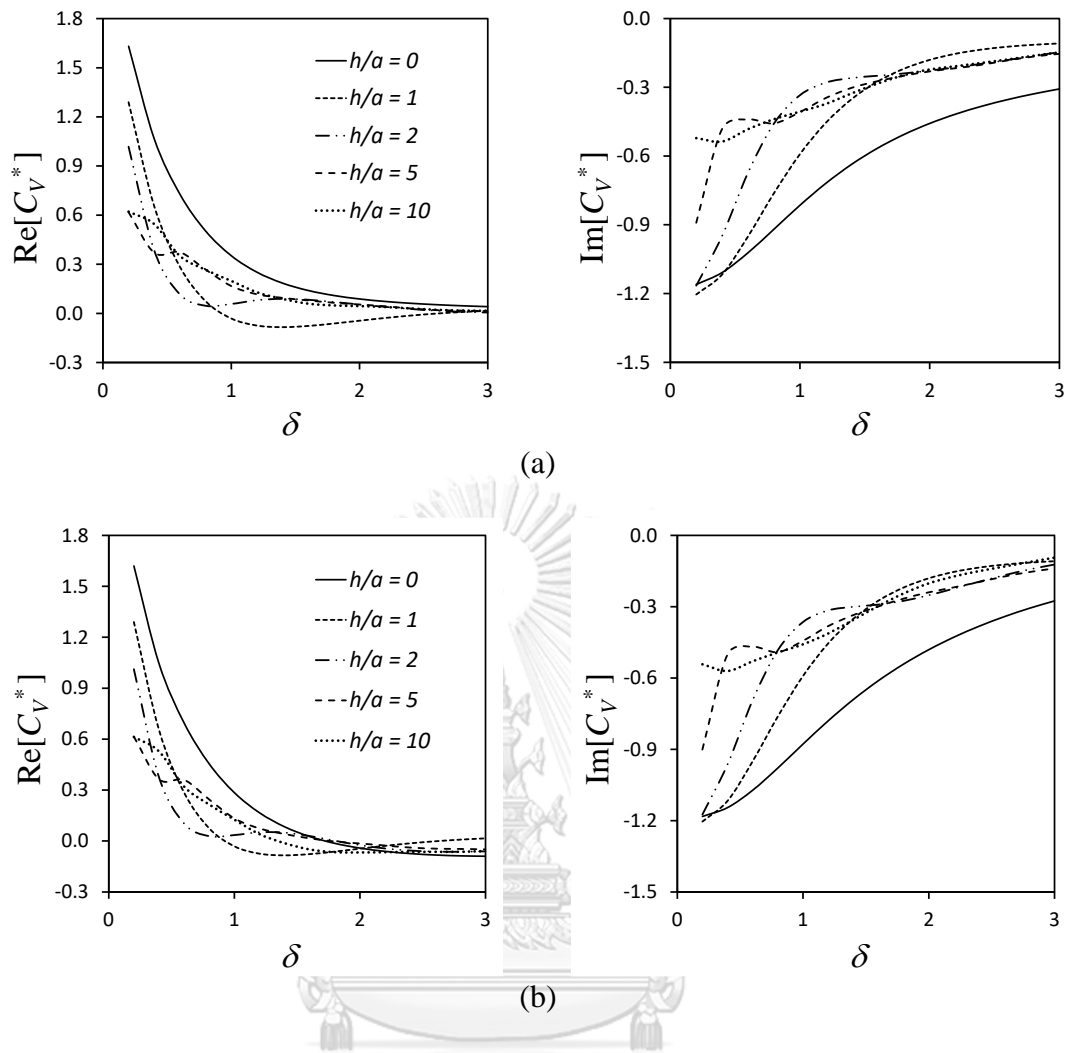


Figure 6.4 Non-dimensional vertical compliances of strip foundation embedded in Mat B with various embedded depths: (a) permeable foundation; (b) impermeable foundation

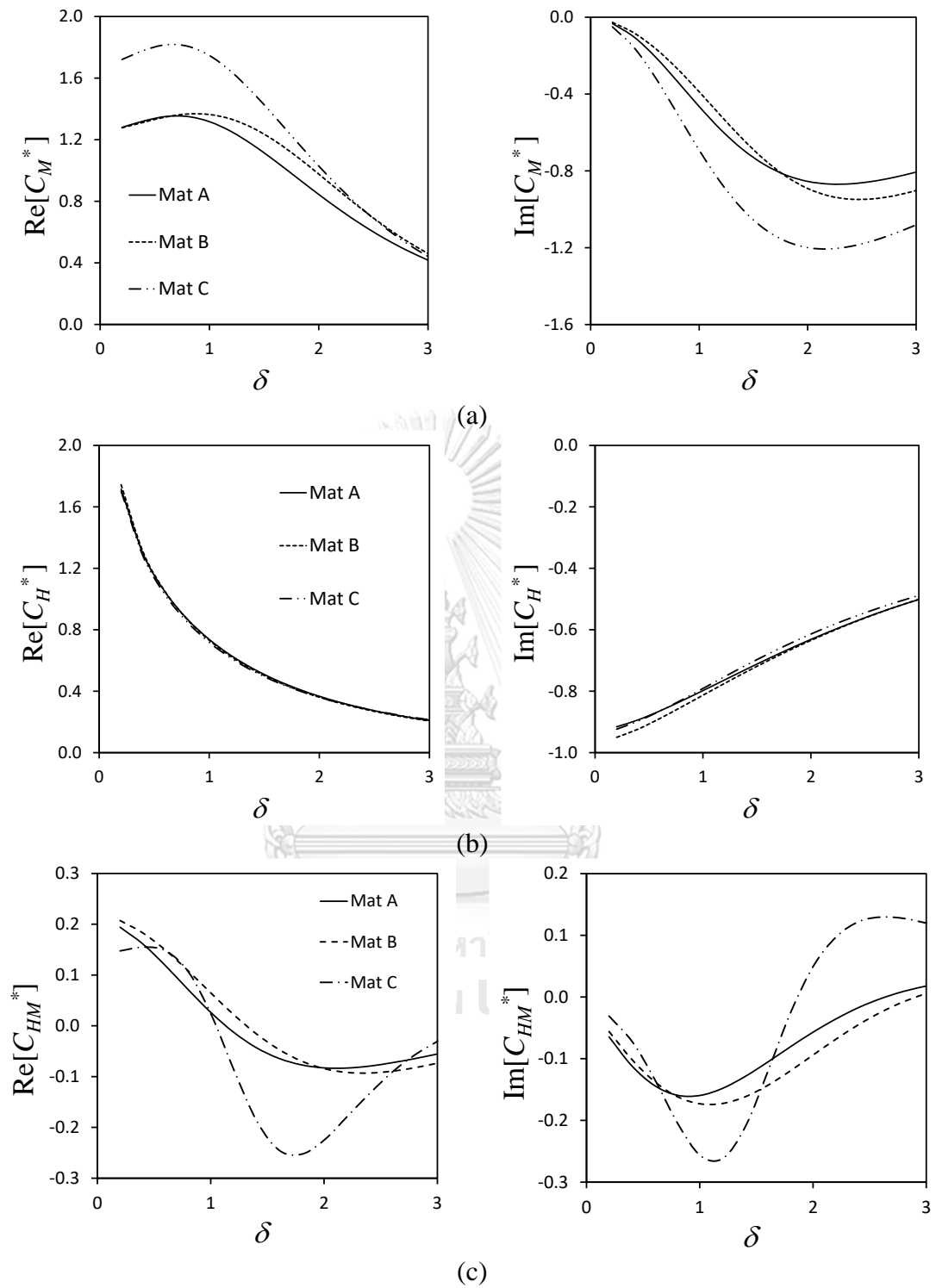
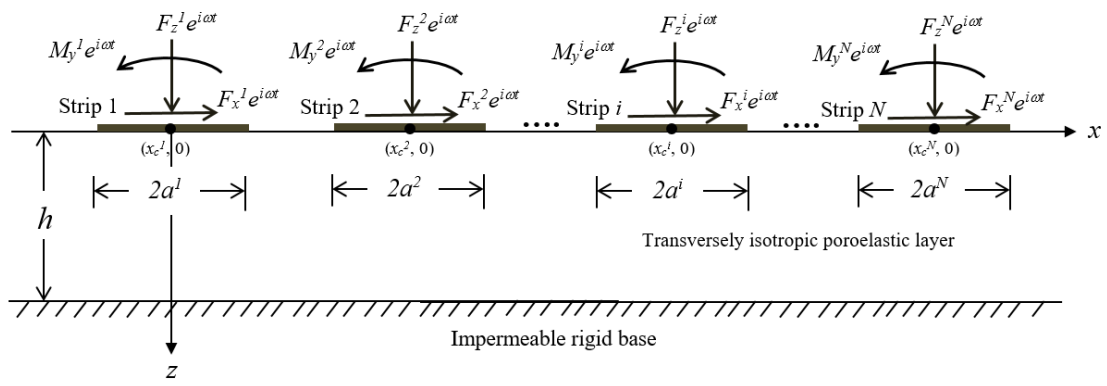
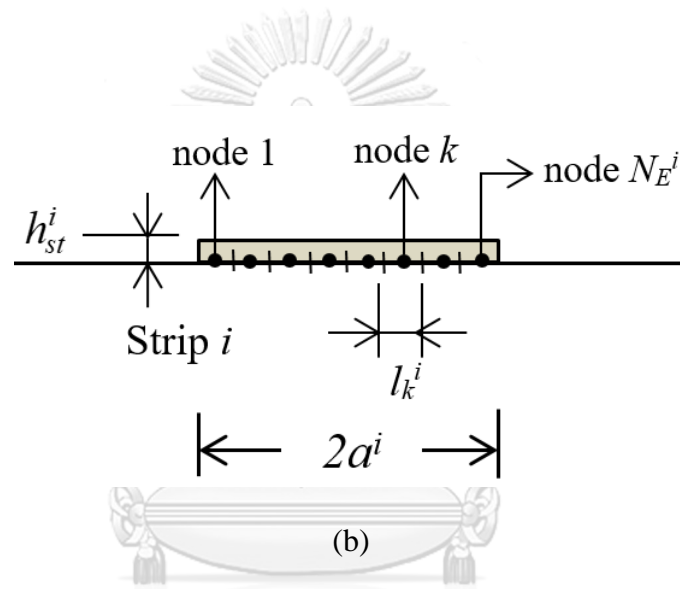


Figure 6.5 Non-dimensional compliances of surface strip foundation ($h/a = 0$): (a) rocking compliance; (b) horizontal compliance; (c) coupling compliance



(a)



(b)

Figure 6.6 (a) A system of N rigid strips on a transversely isotropic poroelastic layer under time-harmonic loading; (b) Discretization of the contact surface under strip i

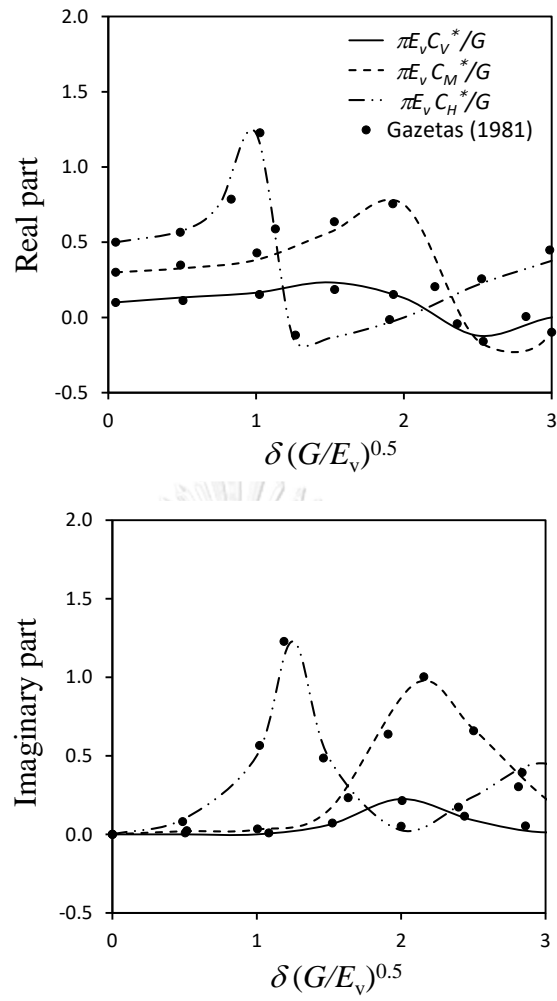


Figure 6.7 Comparison of non-dimensional compliances of a rigid strip on a transversely isotropic elastic layer ($h/a = 1$)

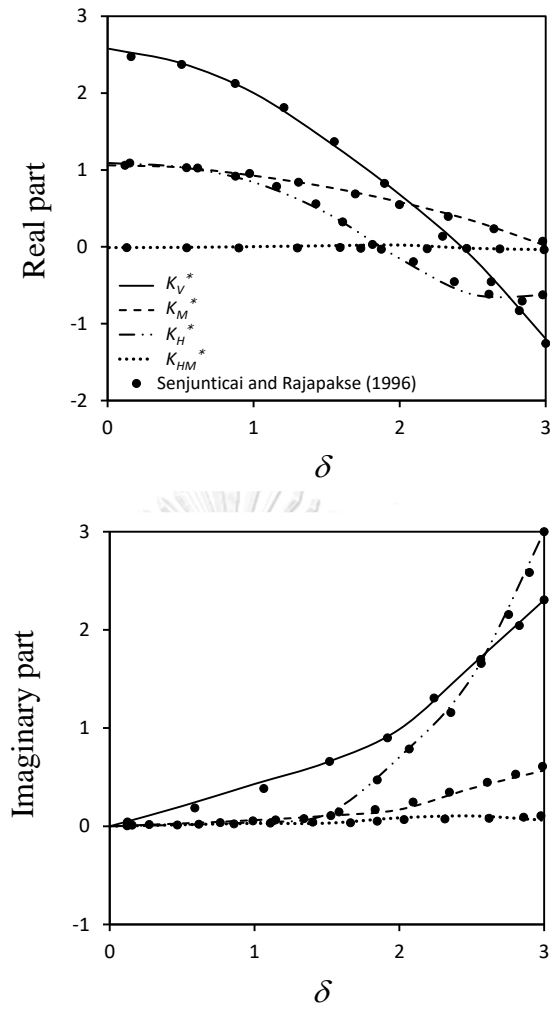


Figure 6.8 Comparison of non-dimensional impedances of a rigid strip on an isotropic poroelastic layer ($h/a = 1$)

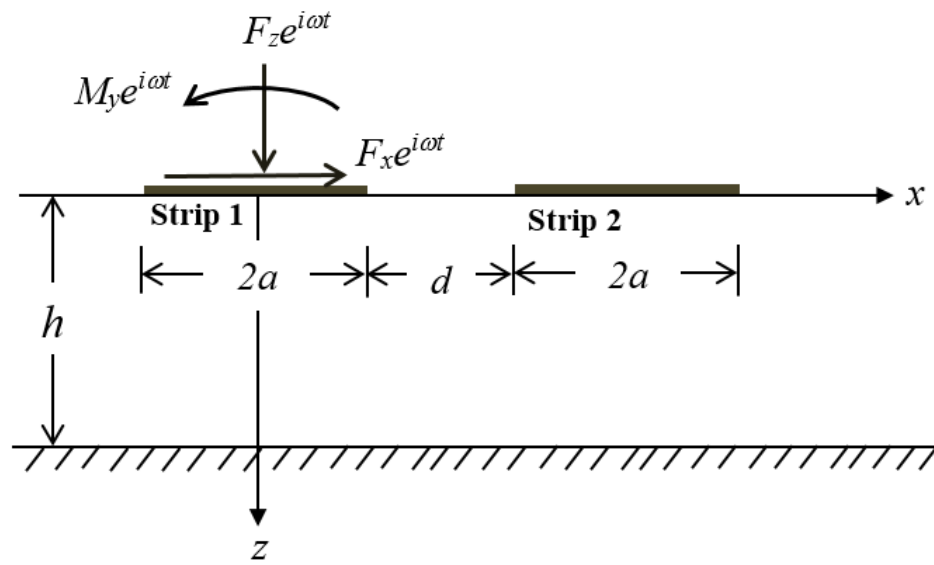
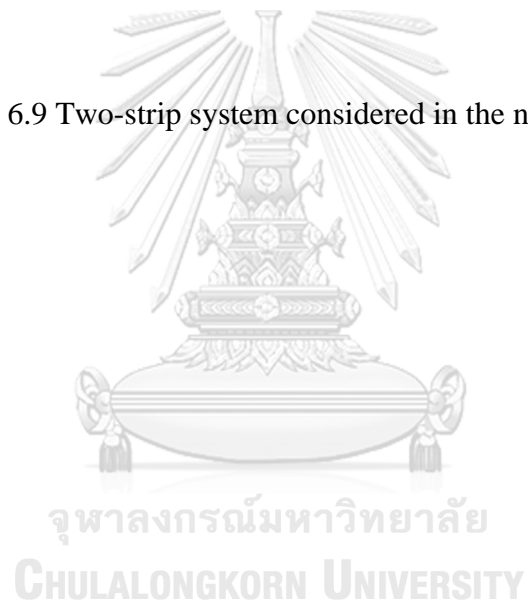


Figure 6.9 Two-strip system considered in the numerical study



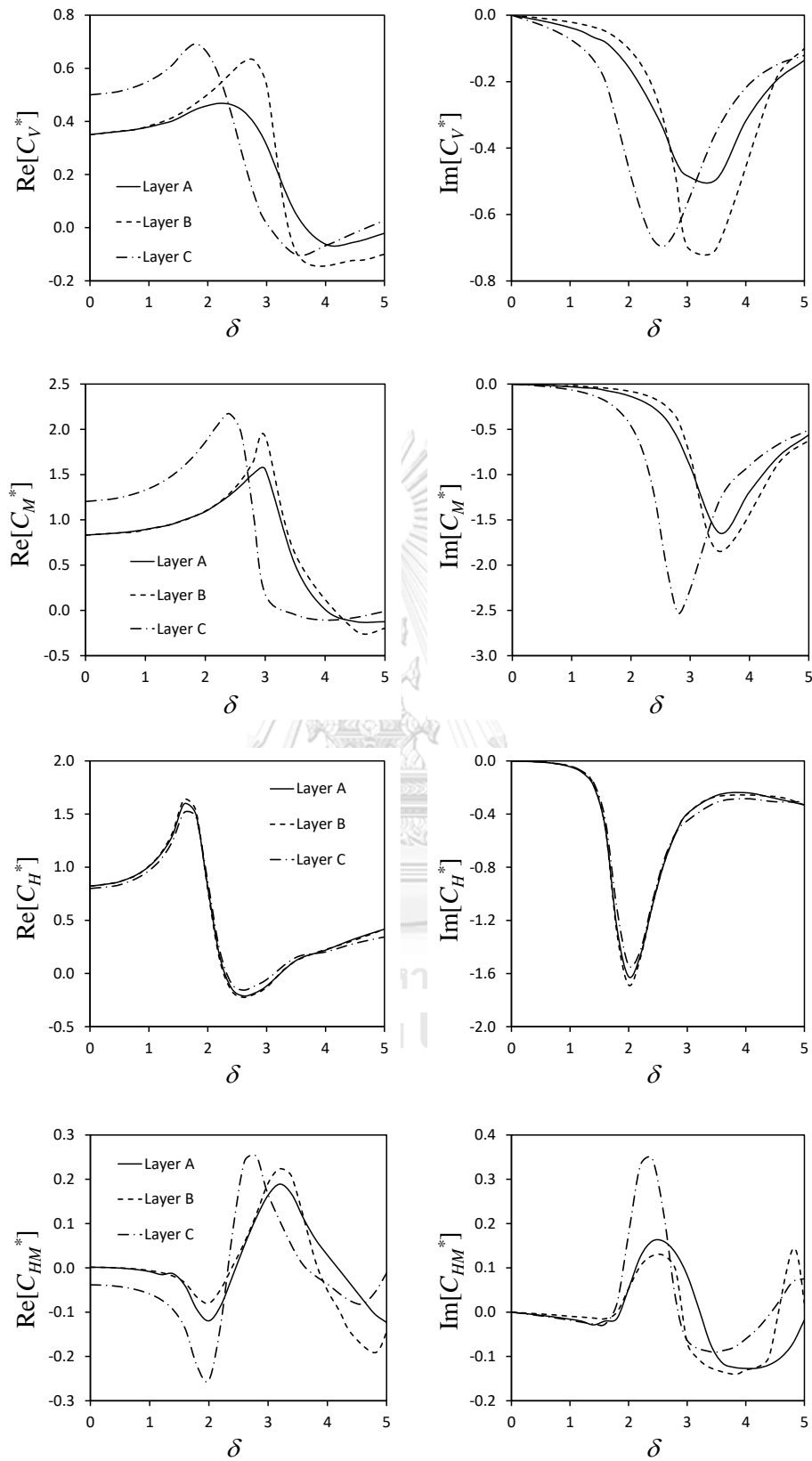


Figure 6.10 Non-dimensional compliances of Strip 1 with $d/a = 0.5$ on different transversely isotropic poroelastic layers with $h/a = 1$

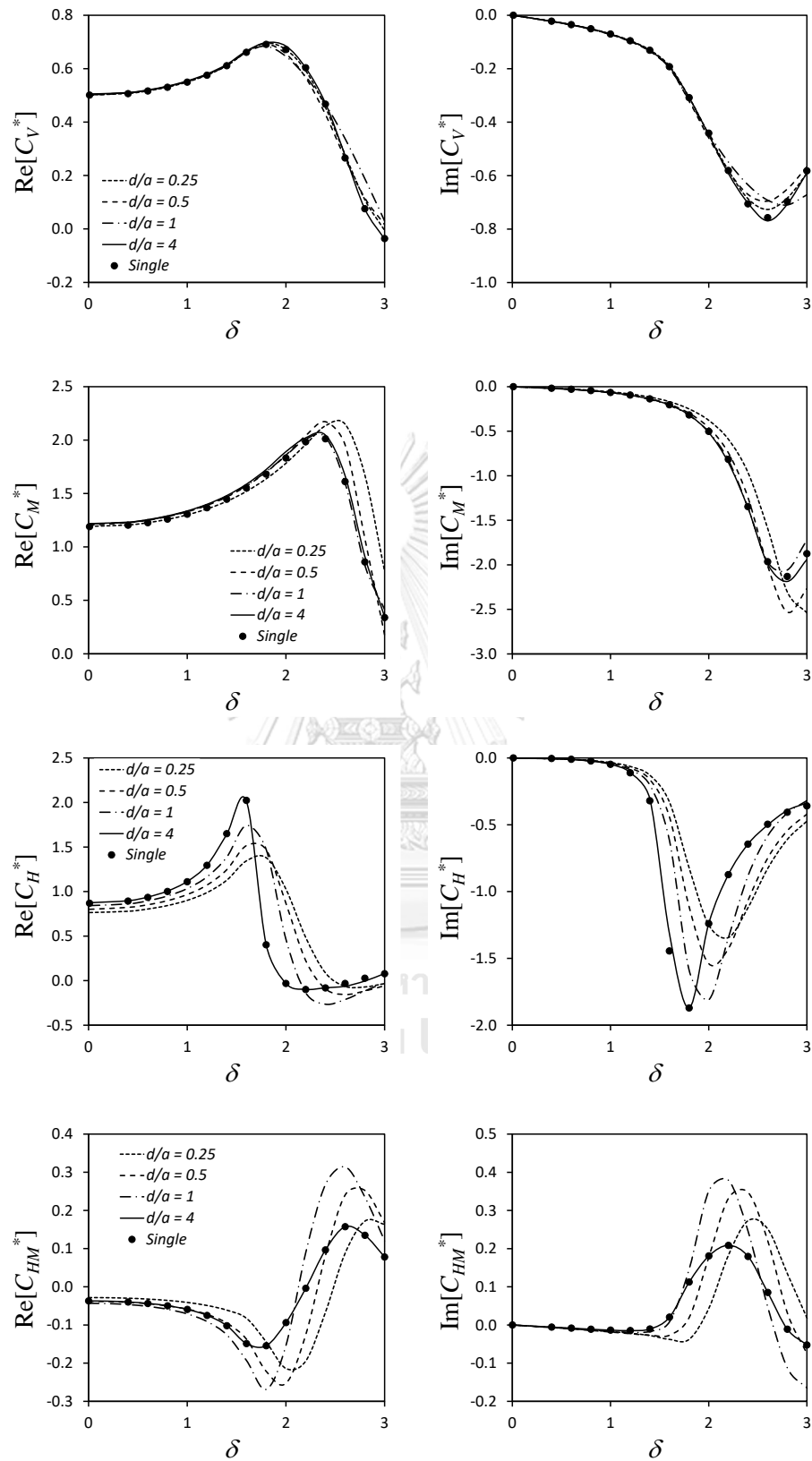


Figure 6.11 Non-dimensional compliances of Strip 1 with various distances (d/a) on transversely Layer C with $h/a = 1$

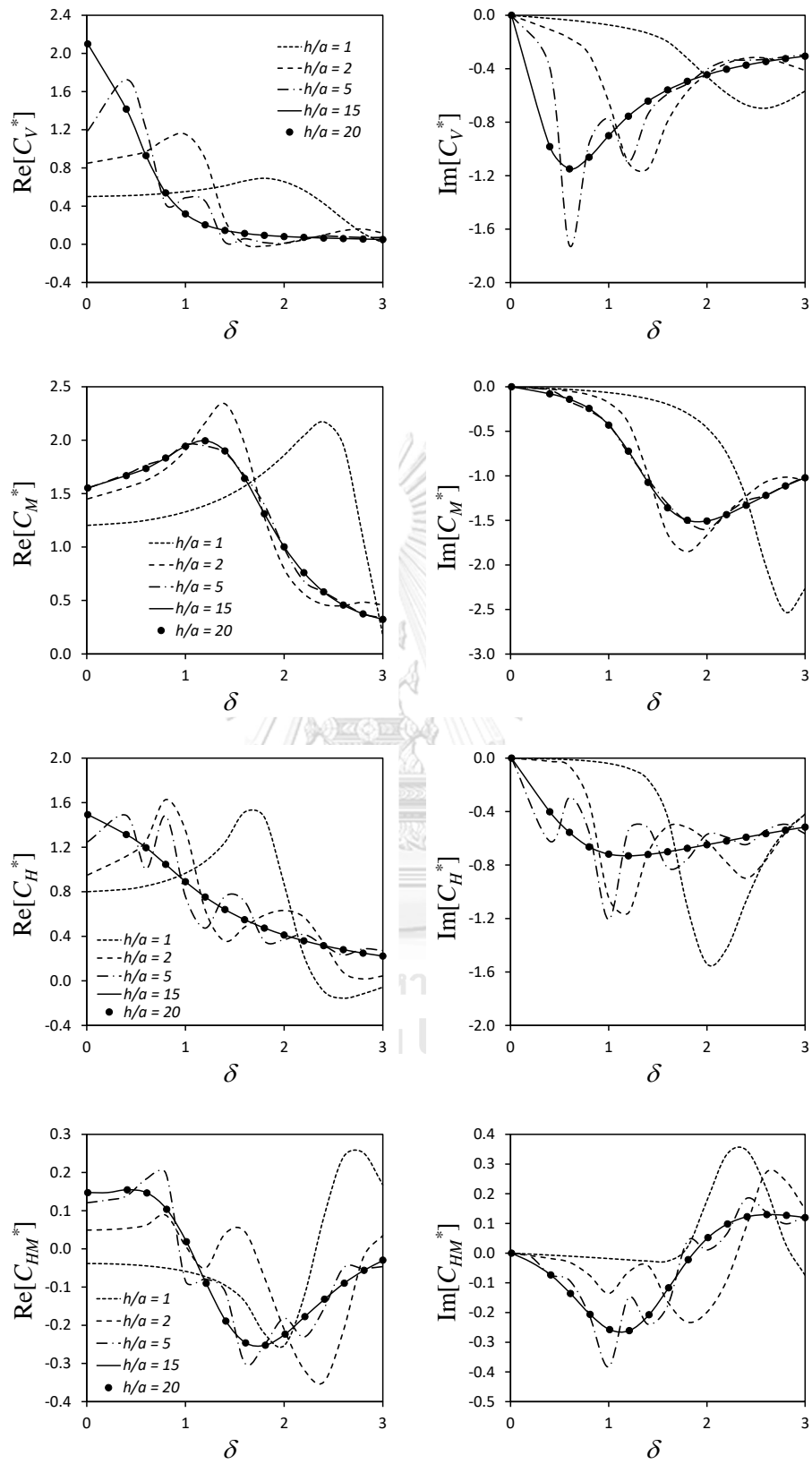


Figure 6.12 Non-dimensional compliances of Strip 1 with $d/a = 0.5$ on Layer C with various thicknesses (h/a)

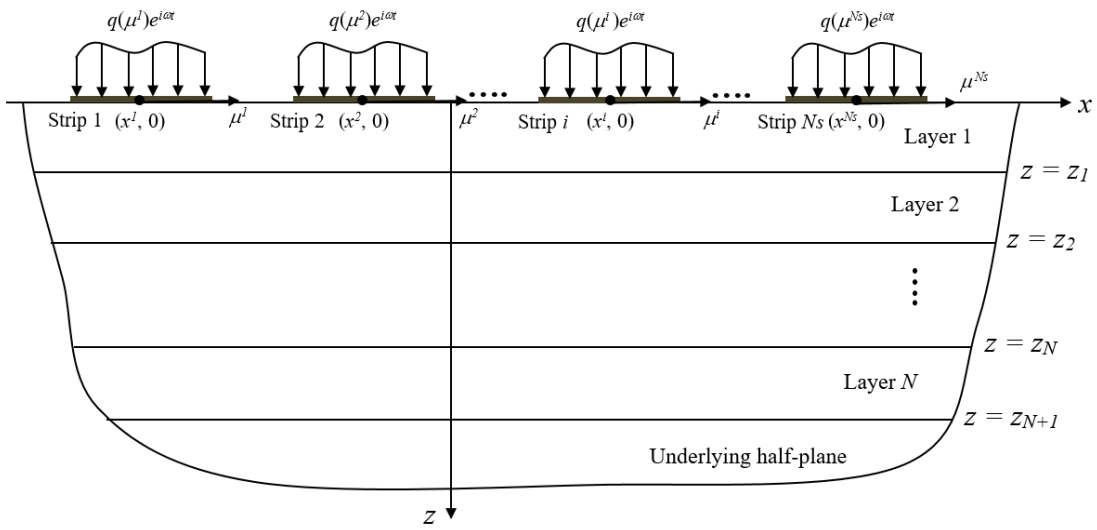
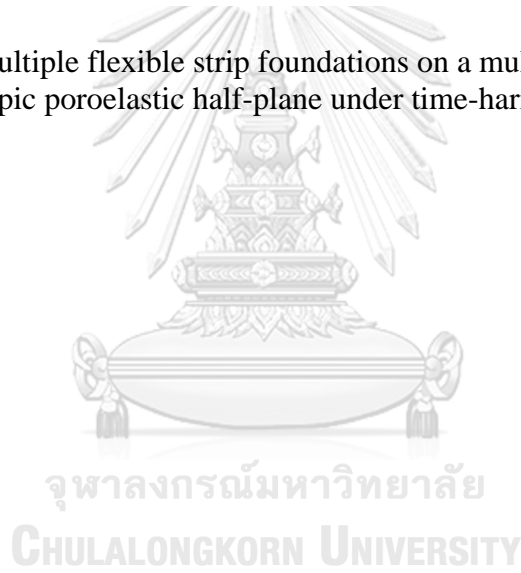


Figure 6.13 Multiple flexible strip foundations on a multi-layered transversely isotropic poroelastic half-plane under time-harmonic loading



จุฬาลงกรณ์มหาวิทยาลัย
CHULALONGKORN UNIVERSITY

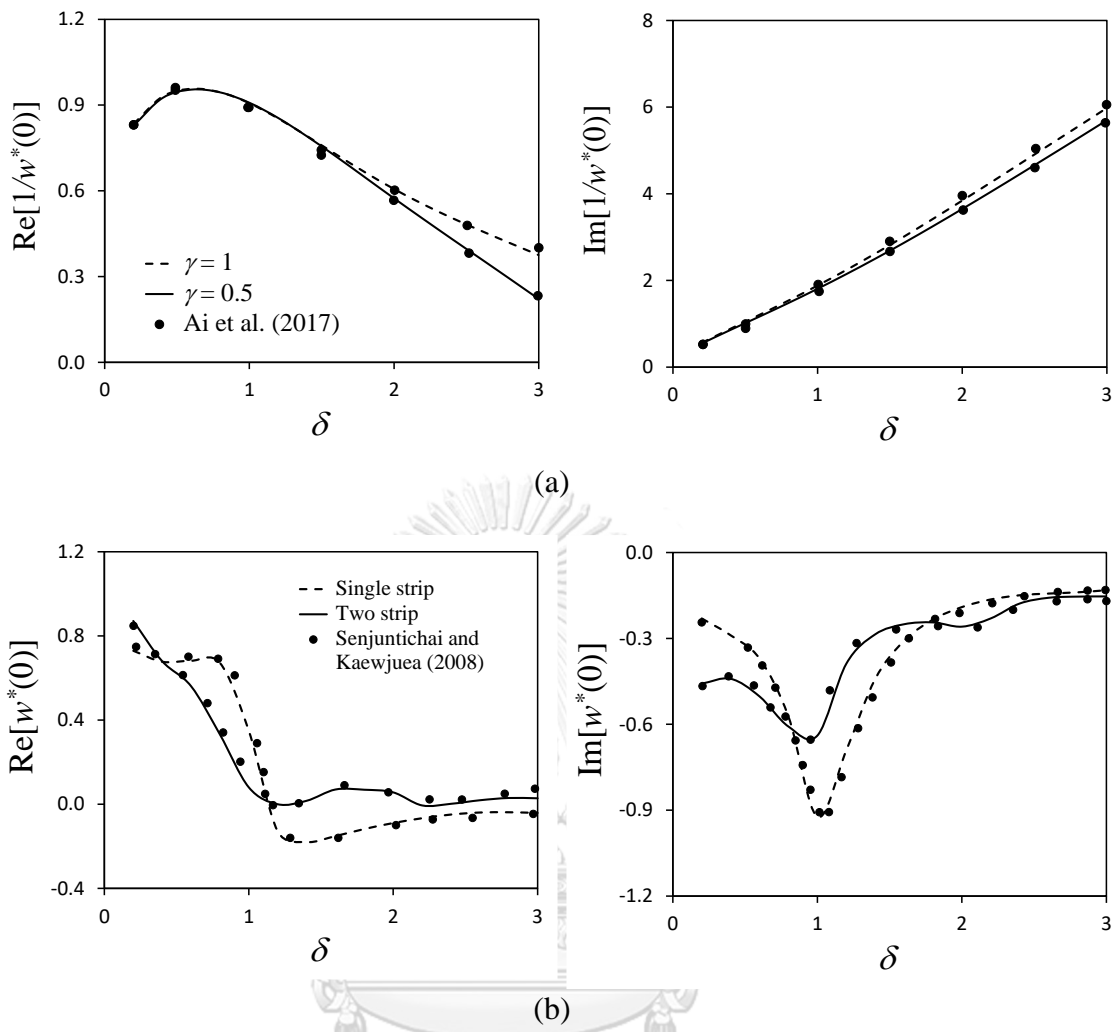


Figure 6.14 Comparison of central displacement of surface strips on: (a) transversely isotropic half-plane; (b) poroelastic half-plane

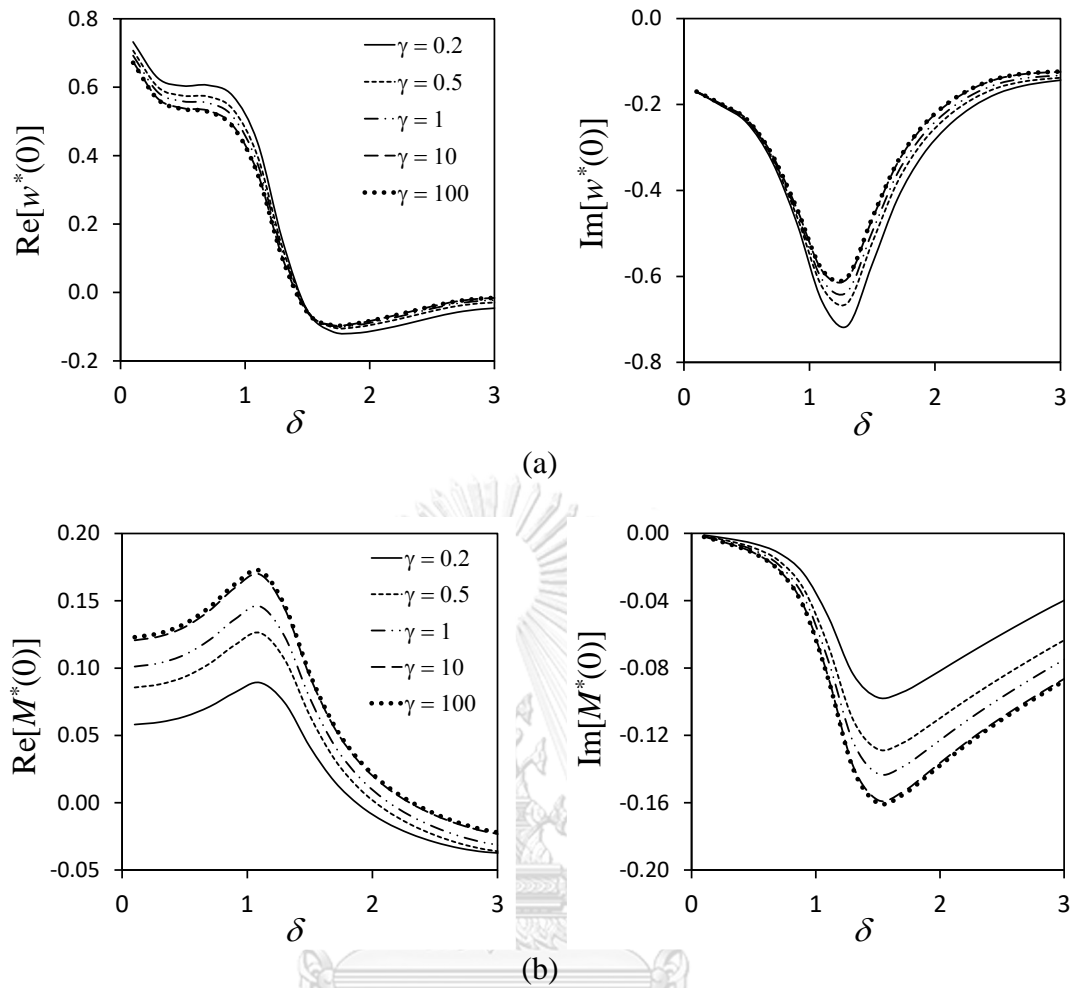


Figure 6.15 (a) Central vertical displacement and (b) Bending moment at the center of a flexible impermeable strip on System A for different foundation flexibilities

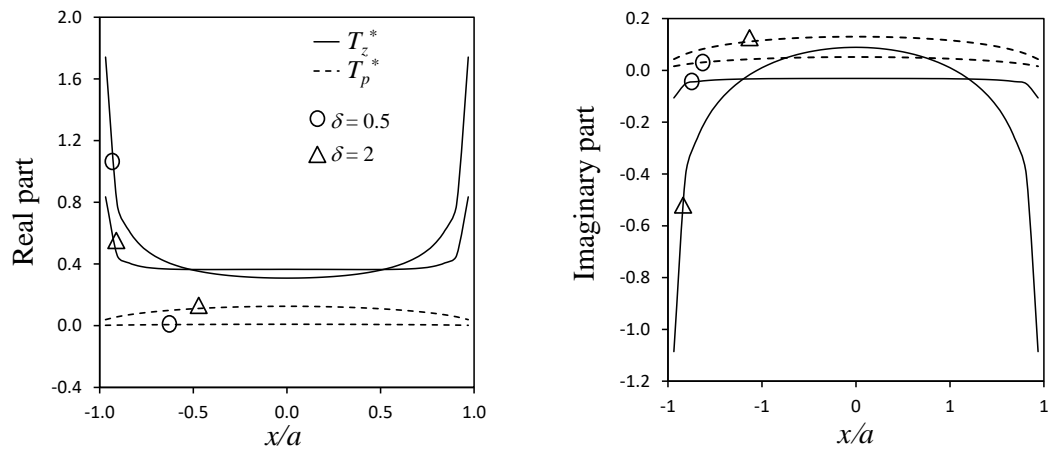


Figure 6.16 Profiles of contact traction and pore pressure jump under flexible impermeable strip with $\gamma = 100$ on System A



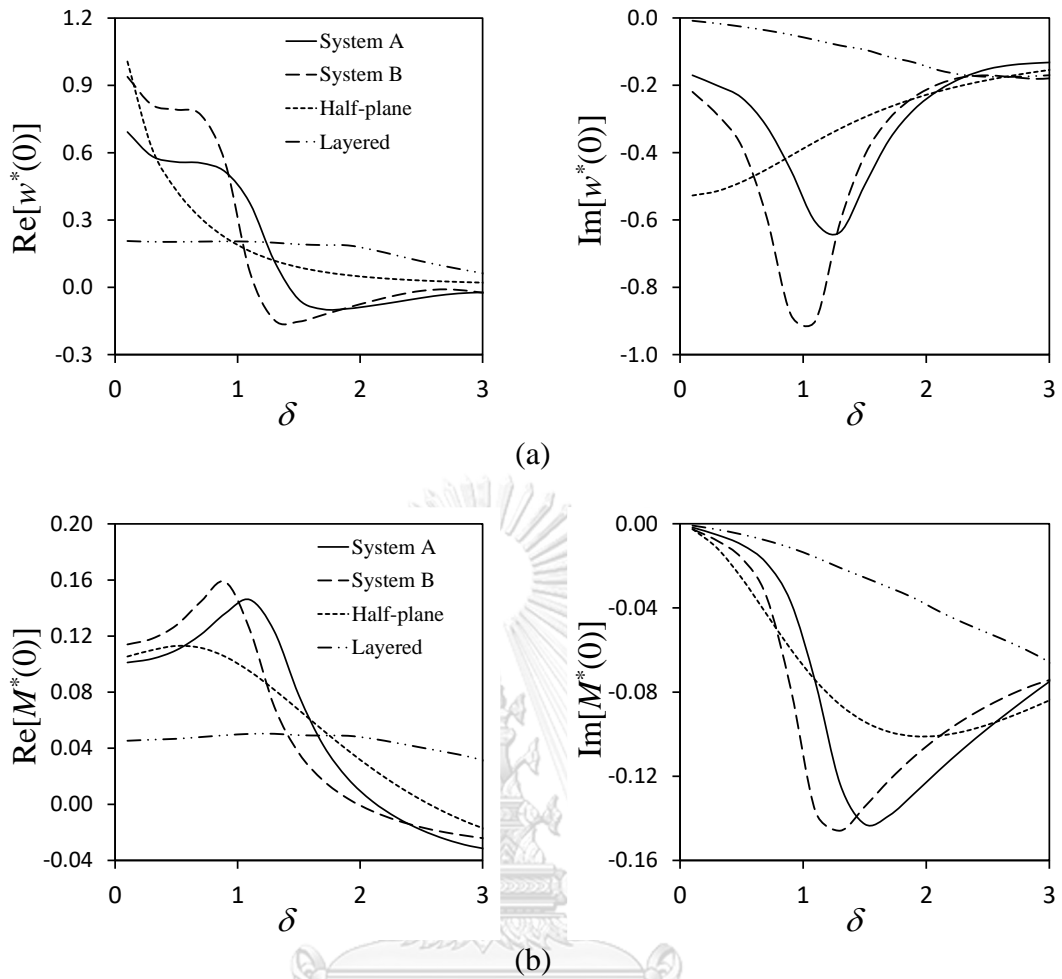


Figure 6.17 Dynamic responses of a flexible impermeable strip with $\gamma = 1$ resting on different system: (a) center vertical displacement; (b) bending moment at the center

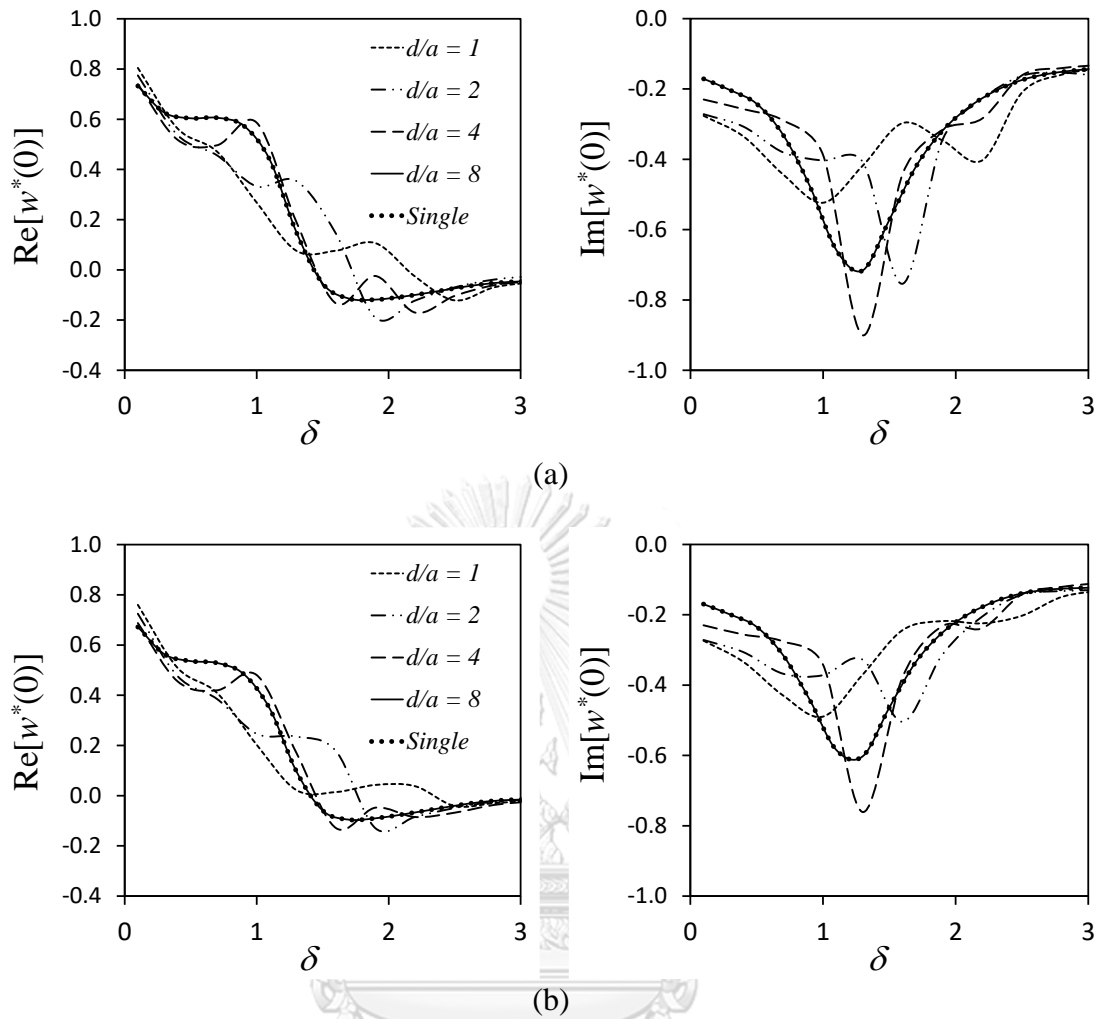


Figure 6.18 Central vertical displacement of two flexible impermeable strips on System A with various distance (d/a): (a) $\gamma = 0.2$; (b) $\gamma = 100$

CHAPTER 7

INTERACTION BETWEEN CIRCULAR FOUNDATION AND TRANSVERSELY ISOTROPIC PORORELASTIC SOILS

In this chapter, the fundamental solutions of homogeneous and multi-layered transversely isotropic poroelastic half-space under axisymmetric deformations derived in Chapter 5 are employed in the analysis of dynamic interaction between a circular foundation and transversely isotropic poroelastic soils. Three problems, namely a rigid circular foundation on a homogeneous layer with rigid base, a flexible circular foundation embedded in a homogeneous half-space and a flexible circular foundation embedded in multi-layered medium, are considered in this chapter. Selected numerical results are presented to portray the influence of relevant parameters on the foundation response.

7.1 Rigid Circular Foundation on Homogeneous Layer with Rigid Base

7.1.1 Formulation of interaction problem

Consider the dynamic interaction between a surface circular foundation of radius a subjected to time-harmonic vertical loading and a transversely isotropic poroelastic layer with rigid base as shown in Figure 7.1. The foundation is assumed to be rigid, massless and undergoing time-harmonic vertical displacement of amplitude Δ_z . The contact surface between the foundation and the layer is assumed to be smooth, and either fully permeable or impermeable. The discretization technique is employed to solve this soil-structure interaction problem. Let S denote the contact surface between the foundation and the saturated layer. The contact area S is then divided into a total number of N_e annular elements, with the width of each element being Δr_l ($l = 1, 2, \dots, N_e$). In addition, the inner and outer radii of the l^{th} annular element are expressed as r_{li} and r_{lo} , respectively (see Figure 7.2). Note that for the first element ($l = 1$) r_{1i} is zero, and the contact area is then a circular area. The

following relationship can be established on the contact surface S under an impermeable foundation:

$$\begin{bmatrix} \mathbf{H}^{zz} & \mathbf{H}^{zp} \\ \mathbf{H}^{pz} & \mathbf{H}^{pp} \end{bmatrix} \begin{Bmatrix} \mathbf{T}_z \\ \mathbf{T}_p \end{Bmatrix} = \begin{Bmatrix} \mathbf{\Delta} \\ \mathbf{0} \end{Bmatrix} \quad (7.1a)$$

In the above equation, the elements H_{kl}^{ij} ($k = l = 1, 2, \dots, N_e$) in \mathbf{H}^{ij} denote the influence functions, which are the vertical displacement ($i = z$), and the relative fluid displacement ($i = p$) at the center of the annular element k on S due to a unit vertical ring load ($j = z$) and ring fluid pressure of unit intensity ($j = p$) applied at the center of the annular element l on S ; each element in the column matrix $\mathbf{\Delta}$ is the displacement amplitude Δ_z ; and $\mathbf{0}$ is a zero column matrix.

These influence functions H_{kl}^{ij} can be obtained by solving a boundary value problem corresponding to a transversely isotropic poroelastic layer overlying a rigid base. Two loading cases are considered to obtain the influence functions, i.e., a unit vertical ring load f_z , and applied ring fluid pressure of unit intensity f_p , which are distributed over an annular area. The boundary conditions for both loading cases are given as follows:

$$\sigma_{rz}(r, 0) = 0 \quad (7.1b)$$

$$\sigma_{zz}(r, 0) = f_z + \alpha_v f_p \quad (7.1c)$$

$$p(r, 0) = f_p \quad (7.1d)$$

$$u_i(r, h) = 0 \quad (i = r, z) \quad (7.1e)$$

$$w_z(r, h) = 0 \quad (7.1f)$$

where

$$f_n = H(r_{lo} - r) - H(r_{li} - r) \quad (n = p, z) \quad (7.1g)$$

and the inner and outer radii of the annular loading are expressed as r_{li} and r_{lo} , respectively (see Figure 7.2). The arbitrary functions for the two loading cases can be obtained by solving the boundary-value problem for each case separately, i.e. $f_p = 0$ for the applied vertical ring load and $f_z = 0$ for the applied ring fluid pressure. The

application of the Hankel integral transform, Eqs. (3.20a) to (3.20f), together with the substitution of the general solutions, Eq. (3.27), for each loading case yields the solutions of the six arbitrary functions A_j and B_j ($j = 1, 2, 3$). The influence functions in the Hankel transform domain are then obtained by substituting those arbitrary functions into Eq. (3.27).

In addition, the elements T_{zl} and T_{pl} in the matrices \mathbf{T}_z and \mathbf{T}_p respectively denote the normal contact traction and pore pressure jump generated at the annular element l on S . Note that T_{zl} and T_{pl} are assumed to be constant within each annular element. The required influence functions, H_{kl}^{ij} , are determined by employing an accurate numerical inversion scheme. Thereafter, the unknown contact traction T_{zl} and pore pressure jump T_{pl} at each annular element can be solved from the discrete version of Eq. (7.1a).

The applied vertical force F can then be calculated from the contact traction and pore pressure jump generated at the contact area S from the following equation:

$$F = \sum_{l=1}^{N_e} \pi(r_{lo}^2 - r_{li}^2)(T_{zl} + \alpha_z T_{pl}) \quad (7.2)$$

where $\pi(r_{lo}^2 - r_{li}^2)$ is the contact area of the l^{th} annular element ($l = 1, 2, \dots, N_e$).

Finally, the vertical vibrations of a rigid circular foundation is characterized by the vertical compliance C_v , in which,

$$C_v = \frac{\Delta_z}{F} \quad (7.3)$$

For a fully permeable foundation, Eq. (7.1a) reduces to

$$\mathbf{H}^{zz} \mathbf{T}^z = \mathbf{\Lambda} \quad (7.4)$$

and Eq. (7.2) involves only T_{zl} in the calculation of vertical load F applied to a fully permeable foundation.

7.1.2 Numerical solutions and discussions

The accuracy of the present numerical scheme is then verified with the existing solutions for rigid circular foundations. Figure 7.3(a) presents the comparison of non-dimensional vertical compliances, defined as $C_v^* = 4GaC_v / (1 - \nu_{vh})$, between the present solution and the solution given by Zeng and Rajapakse (1999). The material properties employed in the present solution are as follows: $E_h^* = E_v^* = 2.6$; $\nu_v = \nu_{vh} = 0.3$; $\alpha_h = \alpha_v = 0.95$; $\rho_f^* = 0.53$; $m_h^* = m_v^* = 1.1$; $M^* = 12.2$; and $b_h^* = b_v^* = 2.3$. Convergence and stability of the proposed solution scheme was studied with respect to the number of annular elements, N_e , employed in the discretization of the contact area. It was found that numerically stable and converged solutions can be obtained when $N_e = 16$. In addition, the half-space can be modeled from the present study by using the layer thickness of $h/a > 15$. It can be clearly seen from Figure 7.3(a) that the present solution, with $N_e = 16$ and $h/a = 20$, agrees very closely with the existing solution for both real and imaginary parts of the compliance.

The accuracy of the present study is also examined by comparing with existing solutions for a transversely isotropic elastic material. Figure 7.3(b) presents the comparison of the non-dimensional vertical impedance, $K_v^* = F / \Delta_z Ga$, of a rigid circular plate resting on a transversely isotropic elastic half-space between the present solution and Ai et al. (2016), where the material properties of the half-space are defined as $E_h^* = 5$; $E_v^* = 2.5$; and $\nu_v = \nu_{vh} = 0.25$. In addition, $N_e = 16$, $h/a = 20$, and all poroelastic material parameters are set to be negligibly small in the present solution. It is evident from Figure 7.3(b) that very good agreement between the two impedances is obtained for both real and imaginary parts. The proposed numerical scheme is thus verified through these independent comparisons.

In this subsection, numerical results for non-dimensional vertical compliance, C_v^* , of a rigid circular foundation on a transversely isotropic poroelastic layer are presented to portray the influence of anisotropic material properties on C_v^* . The following variables are introduced to investigate the anisotropic effects of the saturated layer, i.e., the ratio between the two drained Young's moduli, $n_I = E_v/E_h$, and the ratio between the parameters accounting for the internal friction due to

relative motion between solid and fluid phases, $n_2 = b_v/b_h$. In addition, the following parameters are employed, $E_h^* = 3$; $b_h^* = 2$; $\nu_v = \nu_{vh} = 0.3$; $\alpha_h = \alpha_v = 0.95$; $\rho_f^* = 0.5$; $m_h^* = m_v^* = 1$; $M^* = 12.5$; and $N_e = 16$, for all numerical results presented hereafter. The influence of hydraulic boundary conditions at the contact surface is also investigated with both fully permeable and impermeable foundations being considered in Figures 7.4 to 7.6.

Non-dimensional vertical compliance of a rigid circular foundation resting on a transversely isotropic poroelastic layer with finite thickness $h/a = 1$ are presented in Figures 7.4 and 7.5 for the non-dimensional frequency $0 < \delta < 5$. Figures 7.4(a) and 7.4(b) show the vertical compliances of fully permeable and impermeable foundations, respectively, for different values of n_1 , i.e., $n_1 = 0.5, 1$ and 2 , and $n_2 = 1$ to consider the influence of anisotropy in the Young's moduli. Comparison between the vertical compliances of fully permeable and impermeable foundations, presented in Figures 7.4(a) and 7.4(b) respectively, show similar trend with increasing difference between C_V^* of different hydraulic conditions at the contact surface being observed at high frequencies ($\delta > 2$). It is clearly seen that non-dimensional vertical compliances depend significantly on the ratio of E_v/E_h for both pervious and impervious foundations. The maximum responses of both real and imaginary parts of C_V^* decrease with increasing n_1 since the Young's modulus in the vertical direction E_v increases with increasing n_1 rendering the layer stiffer and more damped. In addition, the peak values of C_V^* are attained at higher frequencies with increasing value of n_1 for both types of foundations.

To study the influence of the parameters b_v and b_h , non-dimensional vertical compliances of rigid circular foundation on a transversely isotropic poroelastic layer with $h/a = 1$ and various values of $n_2 = b_v/b_h$ are presented in Figure 7.5. Figures 7.5(a) and 7.5(b) show the vertical compliances of fully permeable and impermeable foundations respectively on the saturated layer with $n_2 = 0.5, 1$ and 2 , and $n_1 = 1$ for $0 < \delta < 5$. Since the parameter b is inversely proportional to permeability, the layer with $n_2 = 2$ is then the least permeable among all layers considered in Figure 7.5. Numerical results shown in Figure 7.5 indicate that the influence of the parameter n_2 on both real and imaginary parts of the vertical compliance is less significant than

what observed from the effect of n_1 shown in Figure 7.4. In addition, the influence of n_2 becomes almost negligible on C_V^* at low frequency ($\delta < 1.0$). The influence of the hydraulic boundary condition at the contact surface, on the other hand, is more evident on the solutions shown in Figure 7.5 when compared to those in Figure 7.4 as the value of n_2 directly relates to the permeability of the layer. A notable feature observed in Figure 7.5 is the fact that difference between pervious and impervious foundations is decreased with increasing the value of n_2 . This is physically realistic since the layer becomes less permeable with increasing the value of n_2 , the hydraulic boundary condition at the contact surface then becomes less relevant. Therefore, Eq. (7.4) could be employed to study vertical vibrations of rigid foundation, irrespective of its permeable condition, on the layer with a large value of n_2 (or b_v/b_h).

The final set of numerical results corresponds to the case of a rigid circular foundation resting on transversely isotropic poroelastic layers of various thicknesses h/a . Non-dimensional vertical compliances of fully permeable and impermeable foundations are presented in Figures 7.6(a) and 7.6(b) respectively for the layers with $h/a = 1, 2, 5, 15$ and 20 , and $n_1 = n_2 = 0.5$ for the non-dimensional frequency $0 < \delta < 3$. Numerical results presented in Figure 7.6 reveal that both real and imaginary parts of C_V^* for the foundation on the layer with $h/a < 5$ show oscillations with the frequency due to the standing waves generated within the layer, which practically vanish for a deep layer. The difference of C_V^* between pervious and impervious foundations is reduced with increasing the layer thickness h/a . In addition, non-dimensional vertical compliances of the foundation on the layers with $h/a = 15$ and 20 are practically identical implying that the vertical vibrations of a rigid foundation resting on a transversely isotropic poroelastic layer with $h/a > 15$ could be investigated by considering the layer as a transversely isotropic poroelastic half-space.

7.2 Flexible Circular Foundation in Homogeneous Half-Space

7.2.1 Formulation of interaction problem

Consider a flexible embedded circular foundation under time-harmonic vertical loading as shown in Figure 7.7. The contact surface is assumed to be smooth, and either fully permeable or impermeable. The deflection, $w(r)$ of the foundation is expressed in the following form:

$$w(r) = \sum_{n=0}^N \Delta_n r^{2n}, \quad 0 \leq r \leq a \quad (7.5)$$

where Δ_n ($n = 0, 1, \dots, N$) denotes a set of generalized coordinates.

The strain and kinetic energies of the foundation denoted by U_p and V_p respectively can be expressed as (Timoshenko & Woinowsky-Krieger 1959),

$$U_p = \frac{1}{2} \int_0^a 2\pi D \left[\left(\frac{d^2 w}{dr^2} + \frac{1}{r} \frac{dw}{dr} \right)^2 - \frac{2(1-\nu_p)}{r} \frac{dw}{dr} \frac{d^2 w}{dr^2} \right] r dr \quad (7.6a)$$

$$V_p = \frac{1}{2} h_p \int_0^a 2\pi \rho_p [w(r)]^2 r dr \quad (7.6b)$$

where $D = E_p h_p^3 / 12(1-\nu_p^2)$, and h_p denotes thickness of the plate; and E_p , ν_p , and ρ_p denote Young's modulus, Poisson's ratio, and the mass density of the foundation respectively.

In view of Eq. (7.5), the strain and kinetic energies of the foundation can be expressed in terms of Δ_n in the following matrix form.

$$U_p = \{\Delta\}^T [\mathbf{H}^p] \{\Delta\}, \quad V_p = \{\dot{\Delta}\}^T [\mathbf{M}^p] \{\dot{\Delta}\} \quad (7.7)$$

In the above equations, $\{\Delta\} = \{\Delta_0, \Delta_1, \Delta_2, \dots, \Delta_N\}$ is a column vector containing the generalized coordinates, and the elements H_{ij}^p and M_{ij}^p of \mathbf{H}^p and \mathbf{M}^p are given by,

$$H_{ij}^p = \frac{4\pi D(i-1)(j-1)}{2i+2j-6} \left[4(i-1)(j-1) - 2(1-\nu_p)(2i-3) \right] \quad 2 \leq i, j \leq (N+1) \quad (7.8a)$$

$$M_{ij}^p = \frac{h_p \rho_p \pi}{2(i+j-1)} \quad 1 \leq i, j \leq (N+1) \quad (7.8b)$$

Let S denote the contact area between the foundation and the soil. For an impermeable foundation, the applied vertical loading is resisted by the normal contact traction $T_z(r)$ and a pore pressure jump $T_p(r)$ across S . They can be written in terms of the generalized coordinates as follows:

$$T_z(r) = \sum_{n=0}^N \Delta_n T_{nz}(r), \quad T_p(r) = \sum_{n=0}^N \Delta_n T_{np}(r) \quad (7.9)$$

where $T_{nz}(r)$ and $T_{np}(r)$ denote the normal contact traction and the pore pressure jump on S corresponding to the foundation displacement field r^{2n} .

A solution for T_{nz} and T_{np} can be obtained by discretizing S into N_e annular elements. It is assumed that T_{nz} and T_{np} are constant within each annular element. The following relationship can be established.

$$\begin{bmatrix} \mathbf{G}^{zz} & \mathbf{G}^{zp} \\ \mathbf{G}^{pz} & \mathbf{G}^{pp} \end{bmatrix} \begin{Bmatrix} \mathbf{T}_{nz} \\ \mathbf{T}_{np} \end{Bmatrix} = \begin{Bmatrix} \mathbf{u}_{nz} \\ \mathbf{u}_{np} \end{Bmatrix}, \quad n = 0, 1, 2, \dots, N \quad (7.10)$$

where the elements G_{kl}^{ij} ($k = l = 1, 2, \dots, N_e$) in \mathbf{G}^{ij} denote a set of influence functions, which are the vertical displacement ($i = z$) and the relative fluid displacement ($i = p$) at the centre of the k th annular element on S due to uniformly distributed unit vertical pressure and a unit pore pressure jump over the l th annular element. The example of an annular element is shown in Figure 7.8.

The influence functions G_{kl}^{ij} were derived in Section 4.2 and are directly used in Eq. (7.10). The elements T_{nzi} , T_{npi} , u_{nzi} and u_{npi} of \mathbf{T}_{nz} , \mathbf{T}_{np} , \mathbf{u}_{nz} and \mathbf{u}_{np} are given respectively below.

$$T_{nzi} = T_{nz}(r_i), \quad T_{npi} = T_{np}(r_i) \quad (7.11a)$$

$$u_{nzi} = r_i^{2n}, \quad u_{npi} = 0 \quad (7.11b)$$

For a fully permeable foundation no pore pressure jump is generated on S , Eq. (7.10) is then reduced to,

$$[\mathbf{G}^{zz}] \{\mathbf{T}_{nz}\} = \{\mathbf{u}_{nz}\}, \quad n = 0, 1, 2, \dots, N \quad (7.12)$$

The energy corresponding to the tractions on U_h of the soil can be expressed as follows:

$$U_h = 2\pi \int_0^a \frac{1}{2} [T_z(r) + \alpha_v T_p(r)] w(r) r dr \quad (7.13)$$

The potential energy W due to an applied load $q(r)$ on the foundation can be expressed as,

$$W = - \int_0^a 2\pi q(r) w(r) r dr \quad (7.14a)$$

where

$$q(r) = \sum_{m=0}^{M_q} \Psi_m r^m, \quad 0 \leq r \leq a \quad (7.14b)$$

and Ψ_m ($m = 0, 1, \dots, M_q$) denotes coefficients of the loading function.

The Lagrangian L of the foundation is given by (Washizu 1982),

$$L = V_p - U_p - U_h + W \quad (7.15)$$

The equation of motion of the foundation is obtained from,

$$\frac{d}{dt} \left(\frac{\partial L}{\partial \dot{\Delta}_n} \right) - \frac{\partial L}{\partial \Delta_n} = 0, \quad n = 0, 1, \dots, N \quad (7.16)$$

In the view of Eqs. (7.5), (7.7) and (7.9), the Lagrangian L can be expressed in terms of Δ_n . By substituting Eq. (7.15) into Eq. (7.16), the following equations of motion for determination of Δ_n

$$[\mathbf{K}]\{\Delta\} = \{\mathbf{X}\} \quad (7.17)$$

where

$$[\mathbf{K}] = -\omega^2 \left\{ [\mathbf{M}^p] + [\mathbf{M}^p]^T \right\} + \left\{ [\mathbf{H}^p] + [\mathbf{H}^p]^T \right\} + \left\{ [\mathbf{H}^s] + [\mathbf{H}^s]^T \right\} \quad (7.18)$$

In above equations, the elements H_{ij}^s and X_i of \mathbf{H}^s and \mathbf{X} respectively can be expressed as,

$$H_{ij}^s = \pi \sum_{k=1}^{N_e} (T_{jzk} + \alpha_v T_{jpk}) \frac{\left(\frac{r_{ok} + r_k}{2}\right)^{2i} - \left(\frac{r_k - r_{ik}}{2}\right)^{2i}}{2i}, \quad X_i = 2\pi \sum_{m=0}^{M_q} \frac{\Psi_m}{m + 2i} \quad (7.19)$$

where r_{ok} , r_{ik} and r_k denote the outer, inner and center radii of the k th annular element, and T_{jzk} and T_{jpk} are defined in Eq. (7.11a).

The solution of Eq. (7.17) yields the solutions for the generalized coordinates Δ_n ($n = 0, 1, \dots, N$). By substituting the generalized coordinates into Eq. (7.5), the deflection of foundation can be obtained. Normal traction and pore pressure jump on S are obtained from Eq. (7.19). The bending moment $M(r)$ of the foundation is given by:

$$M(r) = -D \sum_{n=0}^N \Delta_n \left[2n(2n-1) + 2nv_p \right] r^{2n-2}, \quad 0 \leq r \leq a \quad (7.20)$$

7.2.2 Numerical solutions and discussions

To demonstrate the basic features of dynamic response of an anisotropic poroelastic soil, we consider the case of Berea sandstone which is similar to that in Section 4.2. Note that that the range of the ratio $n = E_v/E_h$ varies from 0.5 to 2 which are identical to that in Section 4.2. Consider a uniformly loaded circular foundation as shown Figure 7.7. A non-dimensional deflection (compliance) and a relative flexibility parameter of the foundation are defined as $w^*(r) = Gw(r)/aq_0$ and $\gamma = Ga^3/D$, respectively. Note that the foundation mass density is set to a negligible value to eliminate the foundation inertia effects and examine the influence of soil anisotropy, poroelasticity and other relevant parameters on the vertical response. Figure 7.9 shows a comparison of central deflection $w^*(0)$ for two γ values for an embedded impermeable foundation ($h/a = 1$) with the solutions given by Senjuntichai and Sapsathiarn (2003) for an isotropic soil (Berea sandstone). For the foundation, $\nu_p = 0.25$ and $\gamma = 0$ (rigid) and 100 (elastic). The solution scheme is found

to converge for $N_e \geq 32$ and $N \geq 8$. Comparisons shown in Figure 7.9 confirm the accuracy of the current formulation for both flexible and rigid foundations.

Next, we examine the effect of foundation permeability on the dynamic response by considering fully permeable and impermeable rigid surface foundations ($h/a = 0$) in Berea sandstone. The influence of anisotropy is also shown by considering $n = 0.5, 1$ and 2 . Figure 7.10 shows the solutions for foundation compliance $w^*(0)$ in the non-dimensional frequency range, $\delta = 0-4$. The influence of foundation permeability is negligible in the low frequency range ($\delta \leq 1.0$) and become significant as the frequency increases. Impermeable foundations are stiffer and dissipate more energy with increasing frequency. The influence of anisotropy is more visible in the imaginary part of the compliance and generally tend to reduce as frequency increases for the different hydraulic boundary conditions of the foundation. Based on these results, it can be concluded that foundation permeability itself is not a significant factor affecting the dynamic response. In the ensuing sections, only impermeable foundations are considered.

The influence of depth of embedment on the dynamic compliance, $w^*(0)$ is investigated next by considering $h/a = 0, 1, 2, 10$ and 100 for rigid foundations in an isotropic Berea sandstone and an anisotropic Berea sandstone with $n = 2$. Figures 7.11(a) and 7.11(b) show the solutions for the isotropic and anisotropic cases respectively. The foundation in anisotropic Berea sandstone is stiffer and has more damping compared to a foundation on isotropic soil as the modulus in vertical direction is twice the value for the isotropic case. The variation of compliance with frequency is generally smooth for surface ($h/a = 0$) and deeply buried ($h/a = 10$ or 100) foundations whereas shallow foundations ($h/a = 1$ and 2) show oscillatory variations as frequency increases. This behaviour is due to the wave reflection at the free surface for shallow foundations whereas for both deeply buried and surface foundations such wave reflections are minimal. The foundation stiffness and damping increase with the depth of embedment for low frequencies. The influence of frequency decreases as the depth of embedment increase. For $h/a \geq 10$, the foundation can be considered deeply buried.

Figure 7.12 shows the profiles of a non-dimensional contact traction ($T_z^* = T_z/q_0$) and pore pressure jump ($T_p^* = T_p/q_0$) under a rigid impermeable foundation with $\gamma = 0$. The selected examples are the case of $n = 0.5$ and 2, where a rigid foundation is embedded at $h/a = 2$. Traction and pore pressure profiles along the r -axis are presented for different frequencies, i.e., $\delta = 0.5$ and 2. Numerical results presented in Figure 7.12 reveal that the imaginary part of T_z^* shows more dependence on frequency and hydraulic boundary conditions than the real part. Both real and imaginary parts of T_z^* are singular near the boundary of the rigid foundation. For pore pressure jump, the magnitude of T_p^* is relatively small except the imaginary part at higher frequency ($\delta = 2$). This reveals that the applied load is essentially transferred through the solid skeleton, particularly at a low frequency. In addition, both real and imaginary parts of T_p^* converge to zero near the boundary of the foundation indicating no singular pore pressure jump occurred at the foundation edge.

The influence of foundation flexibility on the dynamic response is investigated next by considering foundations with $\gamma = 0.1, 10, 100$ and 1000. Figure 7.13 shows that the central compliance depends significantly on both γ and δ . For a given value of γ , the real part of the compliance decreases with increasing frequency whereas the absolute value of the imaginary part of the compliance initially increases with frequency for $\delta < 2$ and thereafter decreases. Stiffer foundations are more damped compared to softer foundations at higher frequencies but the influence of frequency on the imaginary part of compliance is negligible at very small frequencies. As observed in Figure 7.10, soil anisotropy with $n \geq 1$ makes the response stiffer with higher damping compared to an isotropic case. Central bending moment is an important parameter in the design of foundations. Figure 7.14 shows the influence of the foundation flexibility on the central bending moment $M^*(0)$. Bending moment shows a significant influence of both foundation flexibility and frequency of excitation. Stiffer foundations (smaller γ values) correspond to higher bending

moments and very flexible foundations show negligible bending moment. The soil anisotropy has a small effect on $M^*(0)$.

The force-displacement relationship of a rigid circular foundation of radius a with mass m can be expressed as (Das, 2011),

$$Z = \frac{GaA_z}{Q_0} \quad (7.21)$$

where A_z denotes the amplitude of vertical vibration; Q_0 denotes the amplitude of the time-harmonic force acting on the foundation; and Z denotes the dimensionless amplitude, which is given by,

$$Z = \sqrt{\frac{f_1^2 + f_2^2}{(1 - m^* \delta^2 f_1)^2 + (m^* \delta^2 f_2)^2}} \quad (7.22)$$

In addition, $m^* = m/\rho a^3$; and f_1 and f_2 can be directly obtained from $\text{Re}[w^*/\pi]$ and $\text{Im}[w^*/\pi]$ respectively given in the preceding section.

The amplitude of the force transferred to soil, denoted by P_0 , can be expressed as,

$$P_0 = Q_0 + m^* \delta^2 Z Q_0 \quad (7.23)$$

Richart (1962) presented the solutions for Z for a rigid circular foundation on the surface of an isotropic soil for $\delta \leq 1.5$. To illustrate the coupled influence of anisotropy and poroelasticity on vertical vibrations, Figures 7.15(a) and 7.15(b) show the dimensionless amplitude Z and the dimensionless force transferred to soil, P_0/Q_0 . The response curve given by Richart (1962) is also shown ($E_h^* = E_v^* = 2.5$, $\nu_h = \nu_{vh} = 0.25$). In these figures, for the transversely isotropic elastic soil, the value of $E_v^* = 5$ ($n = 2$) is used. For poroelastic materials, the values of α_h , α_v , ρ_f^* , m_h^* , m_v^* and M^* are identical to the properties of Berea sandstone (Rice and Cleary, 1976), whereas the values of b_h^* and b_v^* equal to 2.3 and 11.5 are considered to illustrate the influence of b on the response. Figure 7.15 confirms that the degree of anisotropy has a major effect on the vertical response. Presence of poroelasticity also reduces the vertical amplitude as fluid friction serves as a damper and a reduction of displacement is seen as b_h^* and b_v^* increase. The influence of poroelasticity is

relatively higher in the case of isotropic soils compared to an anisotropic soil. The effects of poroelasticity and anisotropy on the vertical response become negligible for $\delta > 2.0$. The force transferred soil increases with frequency and reaches a peak value which is over the twice the static force for isotropic soils. The force transferred reaches an asymptotic value when $\delta > 2.0$. The results also show that force amplification with frequency is smaller for poroelastic and anisotropic soils.

7.3 Flexible Circular Foundation in Multi-Layered Half-Space

7.3.1 Formulation of interaction problem

Consider a flexible circular foundation under time-harmonic vertical loading embedded in a multi-layered transversely isotropic poroelastic half-space as shown in Figure 7.16. The formulation of dynamic interaction between a flexible circular plate and a homogeneous half-space outlined in Section 7.2 can be adopted for this problem, where only the influence functions in Eq. (7.10) are obtained by employing the exact stiffness matrix method outlined in Section 5.2.

7.3.2 Numerical solutions and discussions

The accuracy of the present study for dynamic response of a flexible circular foundation of radius a resting on a multi-layered transversely isotropic elastic half-space is examined next. Ai and Liu (2014) reported displacement profiles $w^*(r)$ of a circular plate, subjected to a uniformly distributed load of constant magnitude q_0 , resting on a multi-layered transversely isotropic half-space. The multi-layered half-space consists of the first and second layers with the same thickness of $3a$ overlying a homogeneous half-space. The normalized parameters are: $E_h^* = E_v^* = 3$ and for first layer; $E_h^* = E_v^* = 4$ for second layer; $E_h^* = E_v^* = 3$ for underlying half-space. In addition, ν_h and ν_{vh} are equal to 0.25 and G^* is equal to 1 for all layers, whereas other poroelastic parameters are set to be negligibly small. The material properties of foundation are $\gamma = 11.25$, and the normalized frequency is $\delta = 1$. By using $N_e = 32$ and

$N = 8$, it can be seen from Figures 7.17 that a very good agreement between the displacement profiles obtained from the present study and that reported by Ai and Liu (2014) is obtained for both real and imaginary parts.

Figures 7.18(a) and 7.18(b) respectively show the central displacement of permeable and impermeable flexible circular plates in multi-layered transversely isotropic poroelastic half-space under time-harmonic vertical loading. Both System A and System B, which correspond to a transversely isotropic and isotropic poroelastic media respectively, are presented in Figure 7.18. In addition, $\nu_p = 0.25$ and $\gamma = 10$ for the flexible plate and $N_e = 32$ and $N = 8$ with both surface ($h = 0$) and embedded ($h/a = 1$) foundations being considered. The influence of anisotropy is clearly seen on dynamic response of flexible foundations. Moreover, the embedded foundation ($h/a = 1$) is less stiff and less damped than surface foundation ($h = 0$) as illustrated in Figures 7.18(a) and 7.18(b). It is also found that central displacement of the foundation depends significantly on the hydraulic boundary conditions, where the impermeable contact surface makes the soil-foundation system stiffer and less damped when compared to the case of fully permeable condition. Figure 7.19 shows vertical displacement profiles of circular impermeable foundations at $h/a = 0$ and 1 for different systems, where $\gamma = 10$ and $\delta = 0.5$. It is also evident from Figure 7.19 that the effects of anisotropy and the level of embedment are clearly noted on the vertical displacement profiles of flexible foundations.

7.4 Conclusion

The discretization technique and the fundamental solutions obtained in Chapter 5 are used in the formulation of dynamic interaction between vertically loaded rigid and flexible circular foundations and transversely isotropic poroelastic soils presented in this chapter. The soil-structure interaction problems considered here are a rigid circular foundation on a homogeneous layer with rigid base, and a flexible circular foundation embedded in homogeneous and multi-layered half-spaces. Numerical results indicate that non-dimensional vertical compliances of circular foundation depend significantly on anisotropic material properties E_v and b_v . For a

rigid foundation on a homogeneous layer with rigid base, the thickness of the layer significantly influences the vertical compliance of a foundation, and it is found that for a layer with $h/a > 15$ this case could be investigated by considering the layer as a half-space. For a flexible foundation embedded in a half-space, the foundation flexibility is an important factor and the central displacement increases as the foundation becomes more flexible. It is also found that the foundation can be considered deeply buried when $h/a \geq 10$.

The response curves for the cases of a flexible circular foundation embedded in a homogeneous half-space show that the highest response corresponds to isotropic soils and the presence of poroelasticity reduces the foundation displacement for increasing values of the pore fluid friction. Anisotropy also reduces the displacement when $n > 1$ and the influence of poroelasticity on anisotropic soils is similar to isotropic soils. The force transferred to soil is amplified with increasing frequency but reaches an asymptotic value. A lower force is transferred in the case of poroelastic and anisotropic soils.

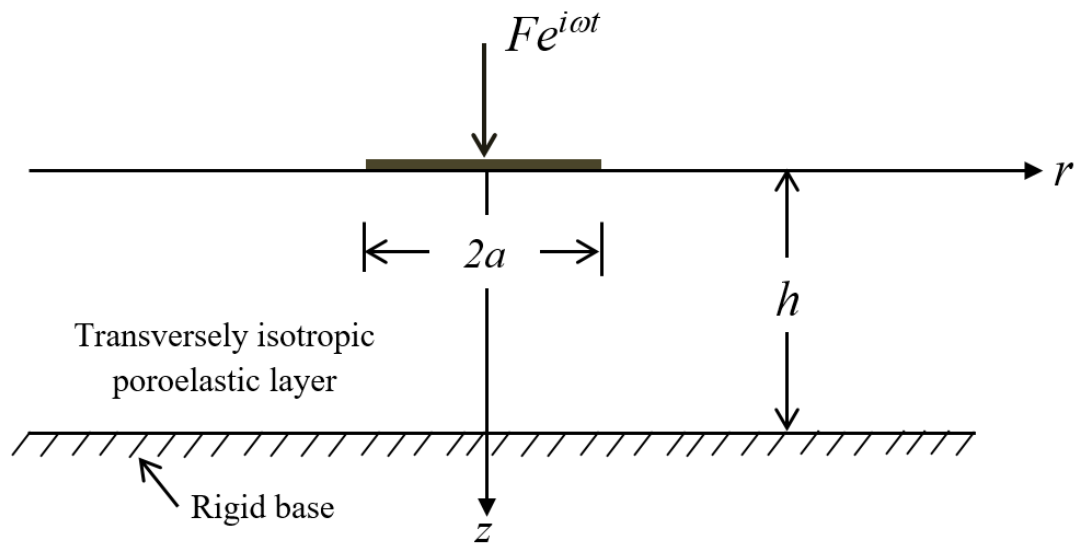


Figure 7.1 Rigid circular foundation on transversely isotropic poroelastic layer



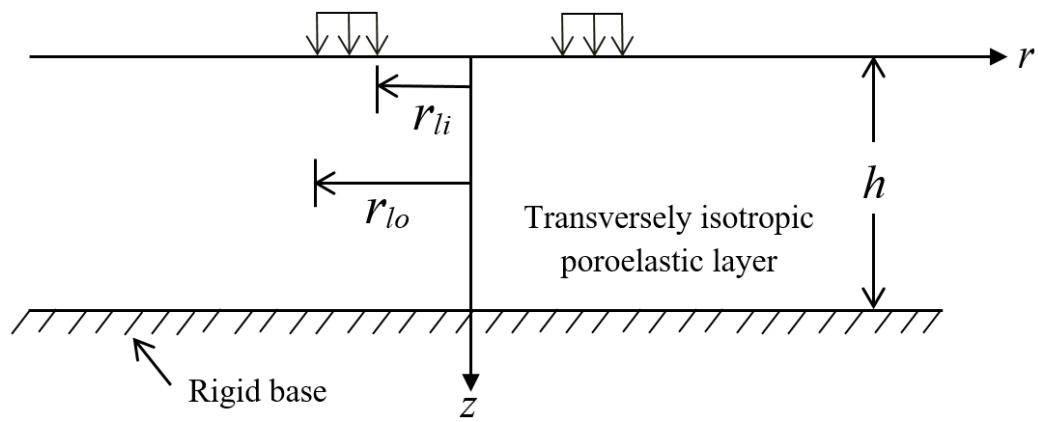
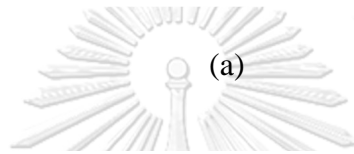
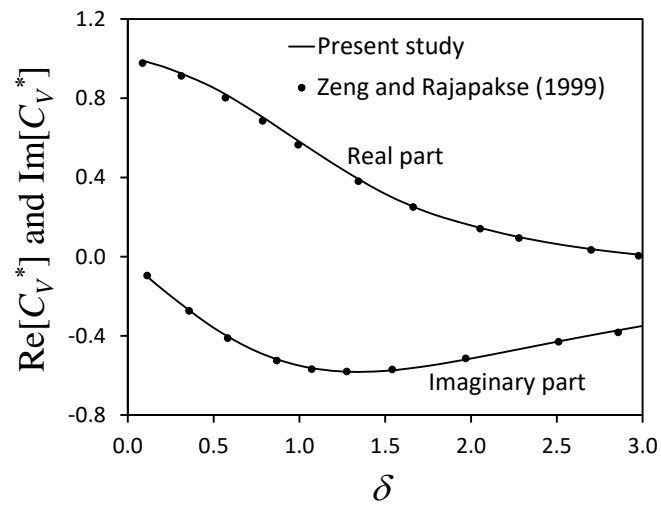
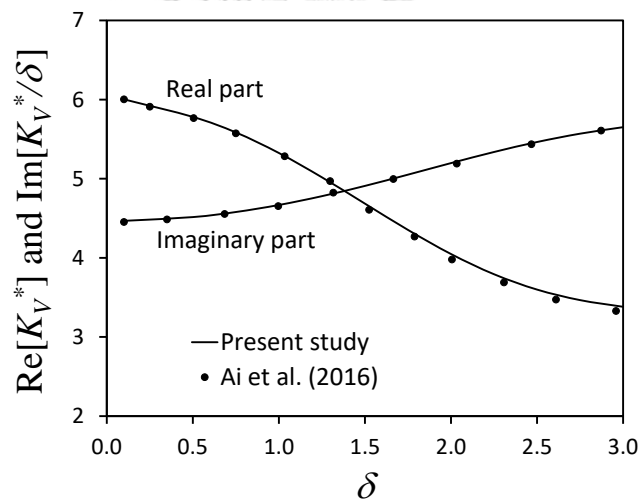


Figure 7.2 Unit vertical ring load f_z and applied ring fluid pressure f_p



(a)



(b)

Figure 7.3 Comparison with existing solutions for: (a) isotropic poroelastic half-space; (b) transversely isotropic elastic half-space

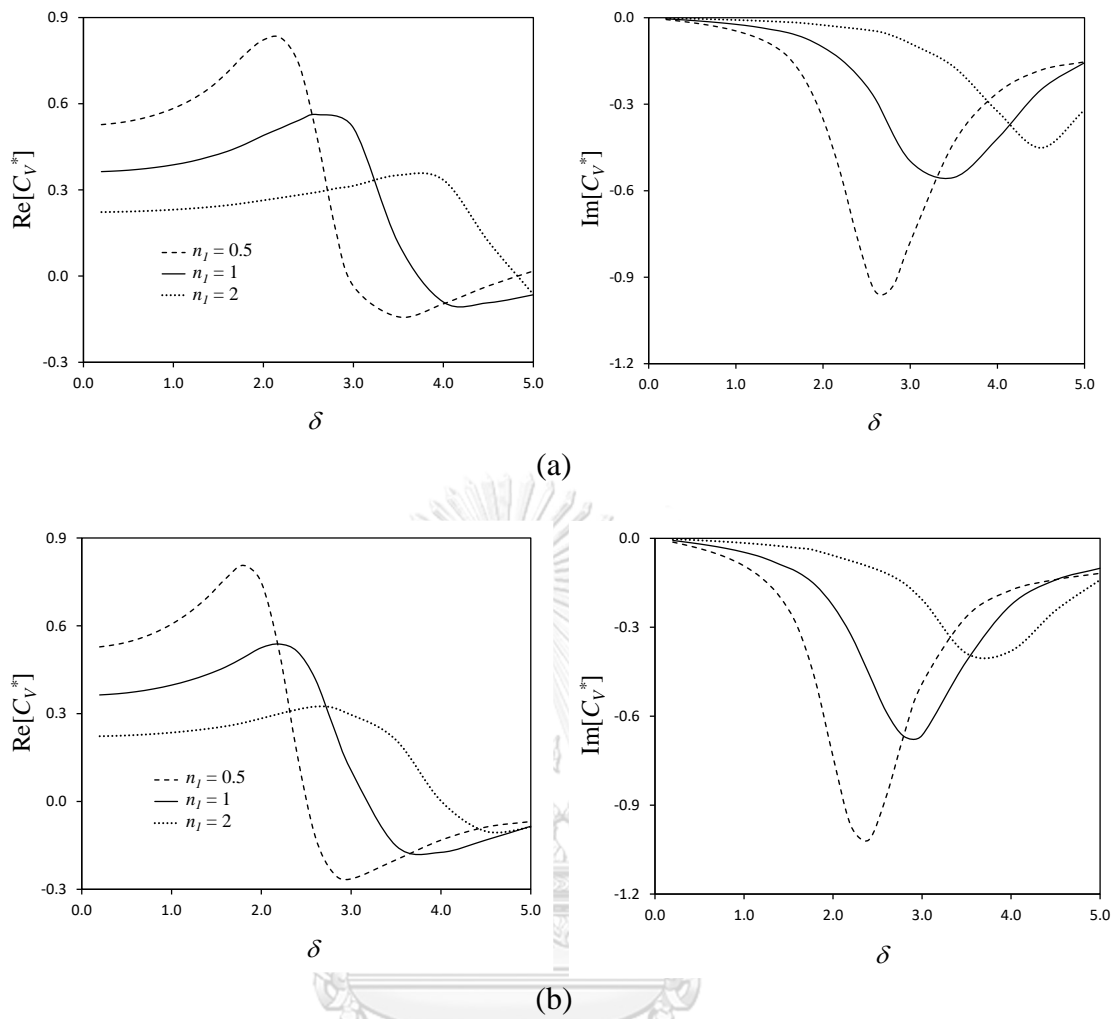


Figure 7.4 Influence of $n_1 = E_v/E_h$ on non-dimensional vertical compliance with $h/a = 1$ and $n_2 = 1$: (a) permeable foundation; (b) impermeable foundation

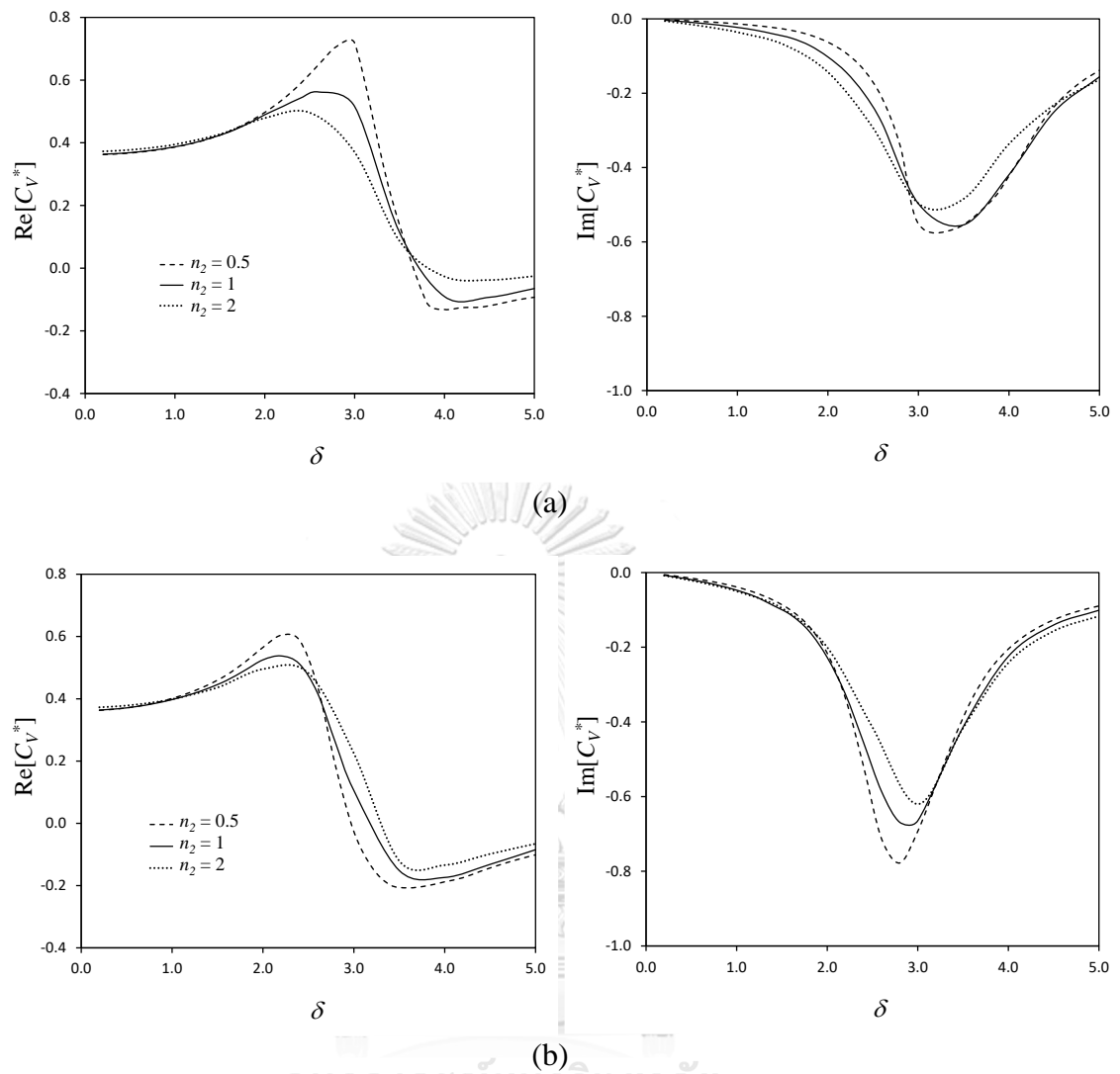


Figure 7.5 Influence of $n_2 = b_v/b_h$ on non-dimensional vertical compliance with $h/a = 1$ and $n_1 = 1$: (a) permeable foundation; (b) impermeable foundation

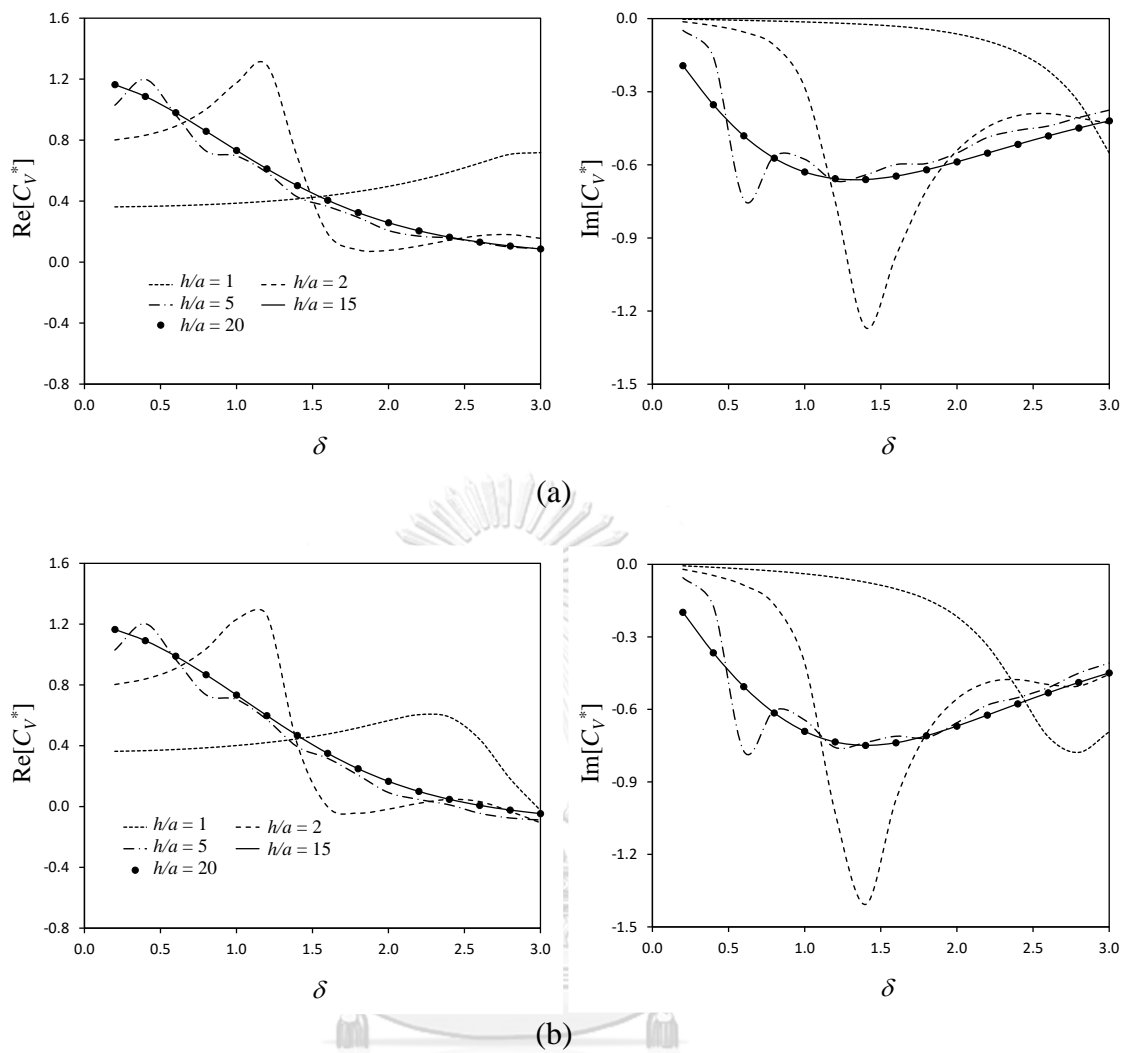


Figure 7.6 Influence of layer thickness on non-dimensional vertical compliance with $n_1 = n_2 = 0.5$: (a) permeable foundation; (b) impermeable foundation

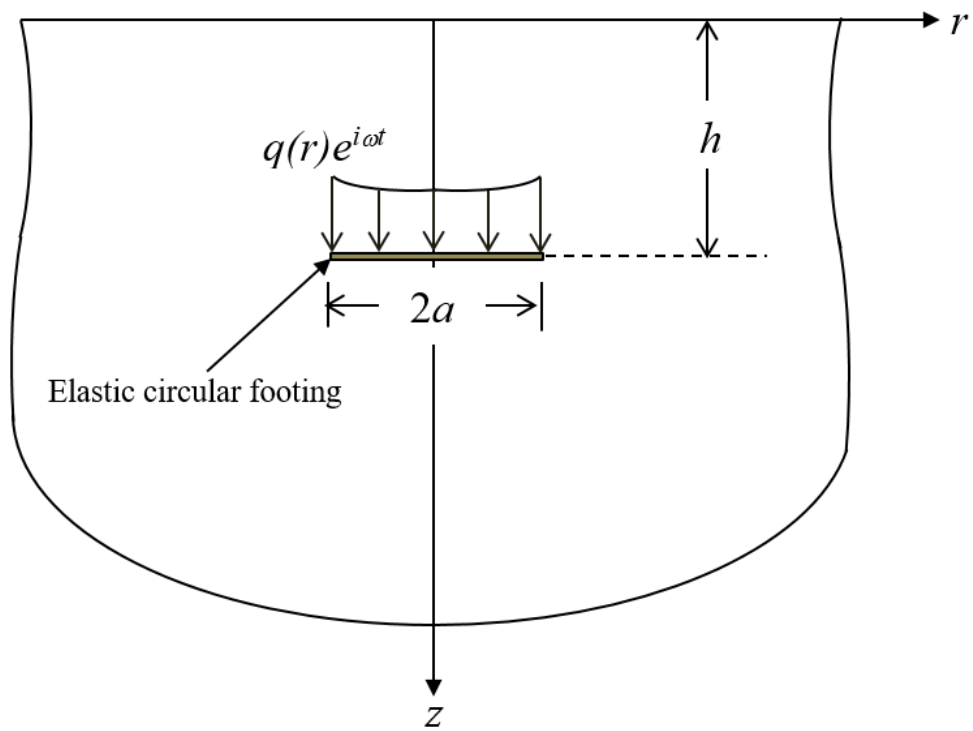


Figure 7.7 Vertically loaded circular foundation in a transversely isotropic poroelastic soil

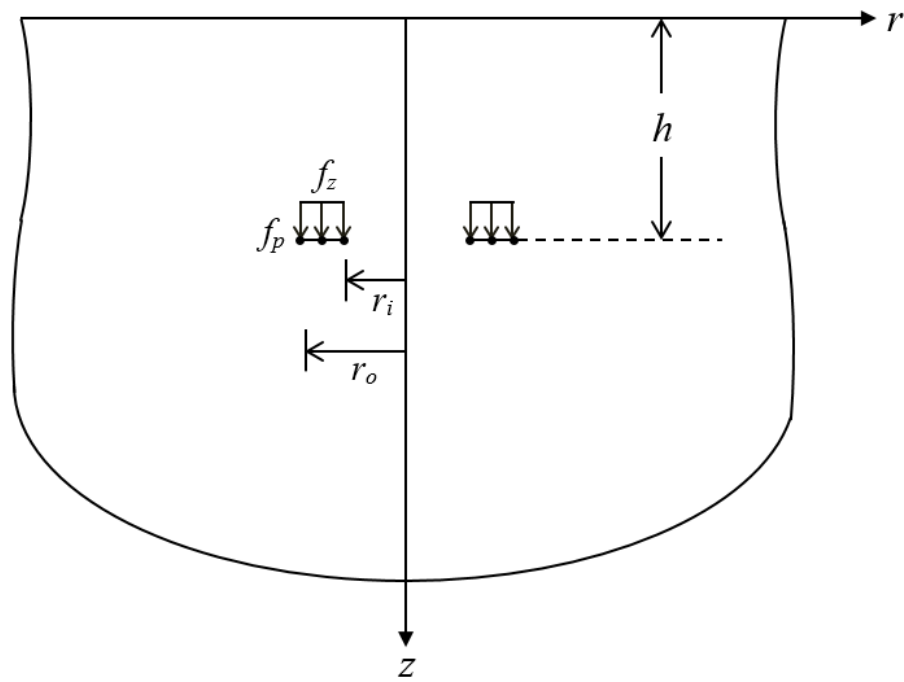


Figure 7.8 Vertical annular load f_z and annular fluid pressure f_p acting in the interior of soil half-space

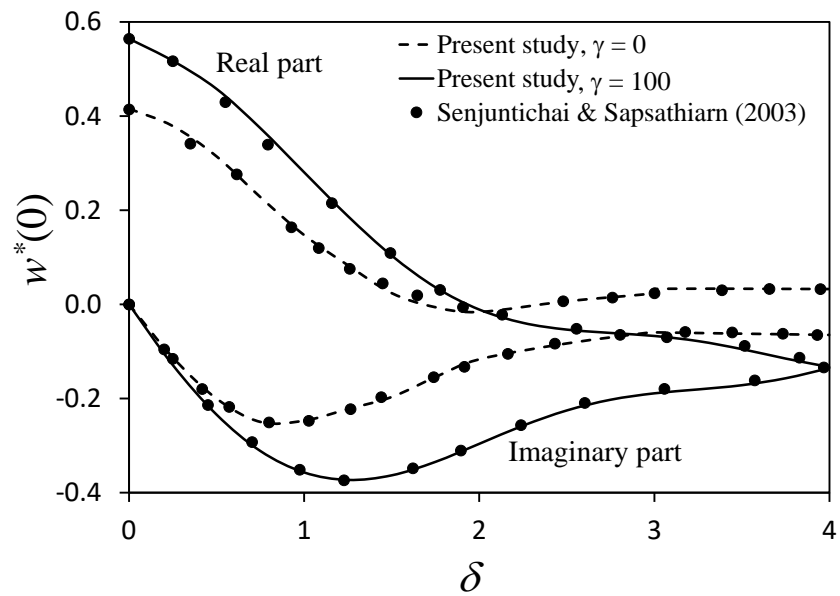


Figure 7.9 Comparison of central displacement of embedded foundations on isotropic poroelastic soil ($h/a = 1$)



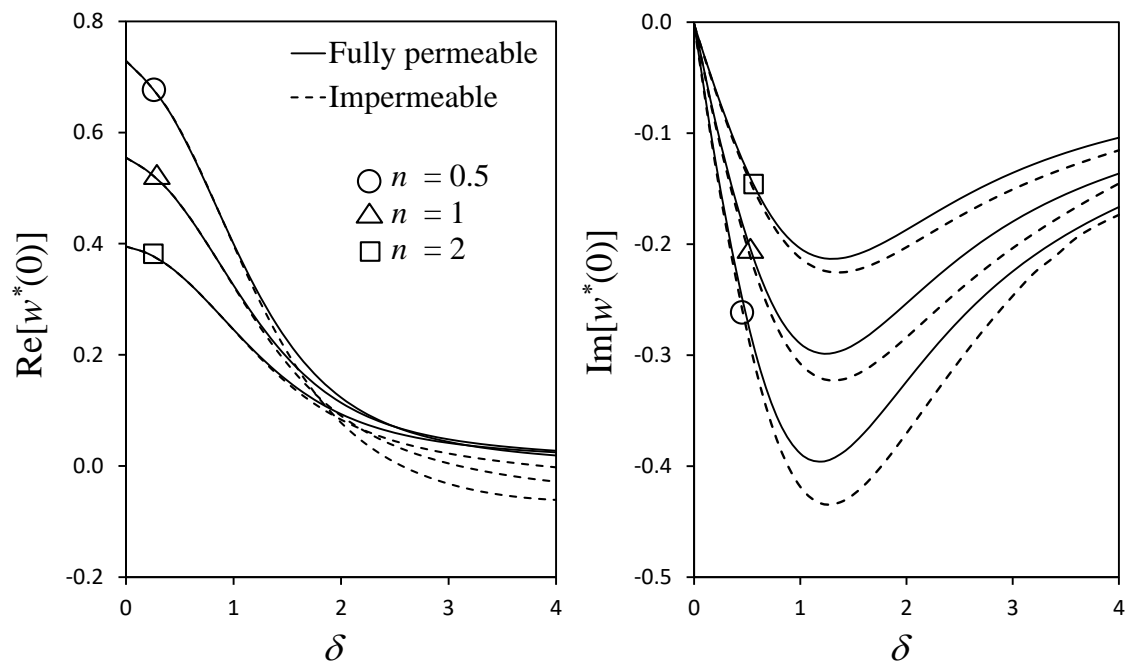


Figure 7.10 Effect of foundation permeability on vertical compliance of a rigid foundation ($h/a = 0$)



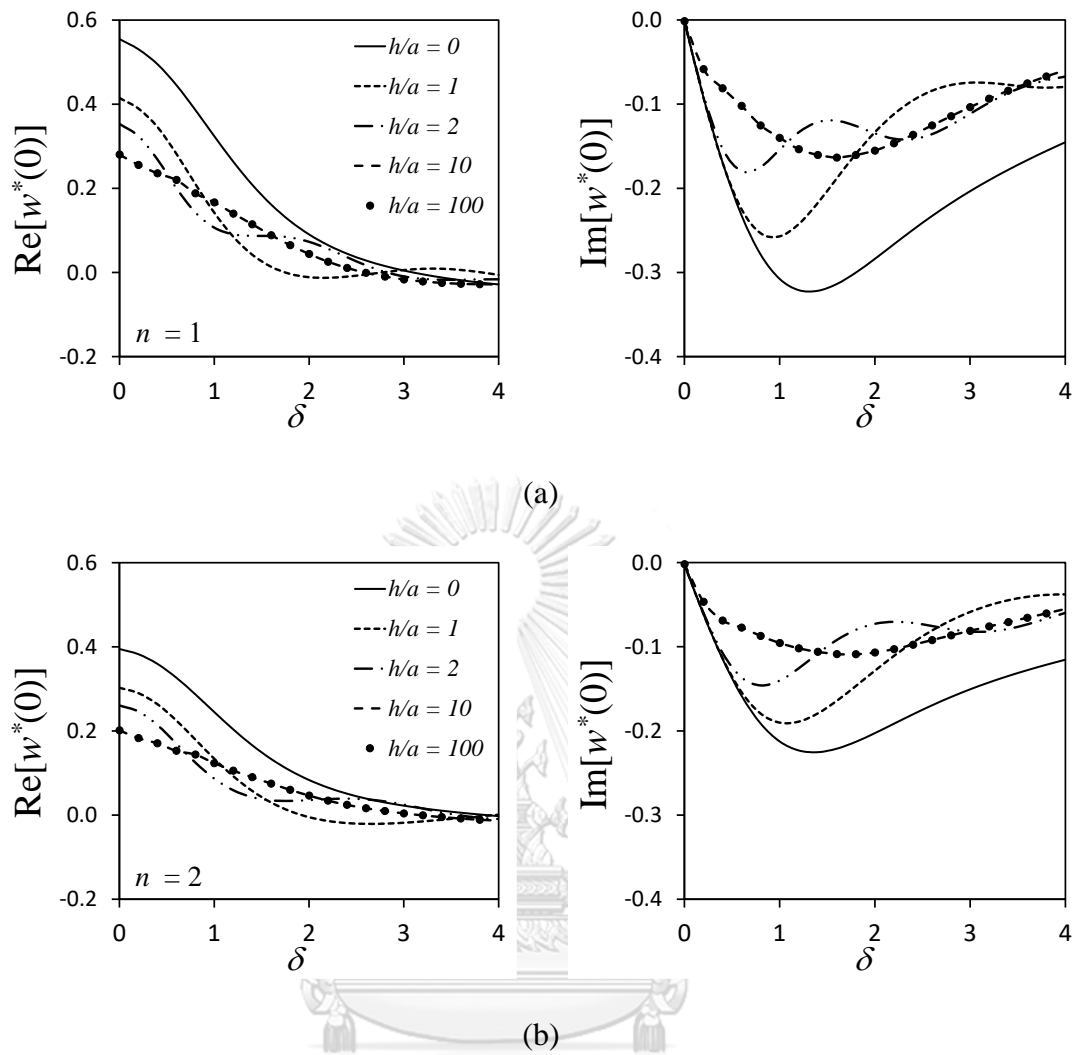


Figure 7.11 Central vertical compliance of a rigid impermeable foundation for different depths of embedment: (a) $n = 1$; (b) $n = 2$

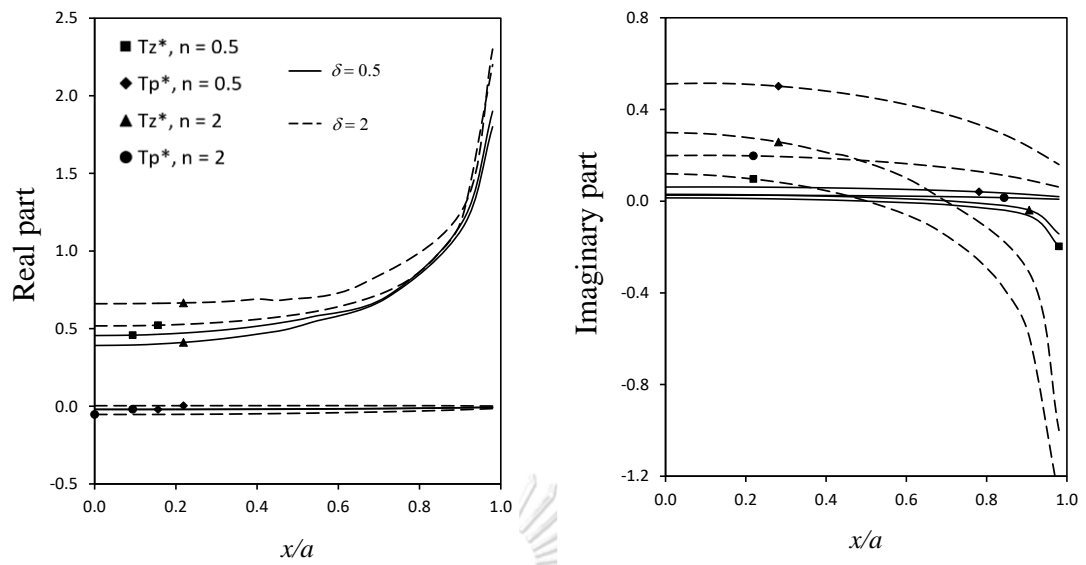


Figure 7.12 Profiles of vertical stress and pore pressure jumps under a rigid impermeable foundation with $h/a = 2$

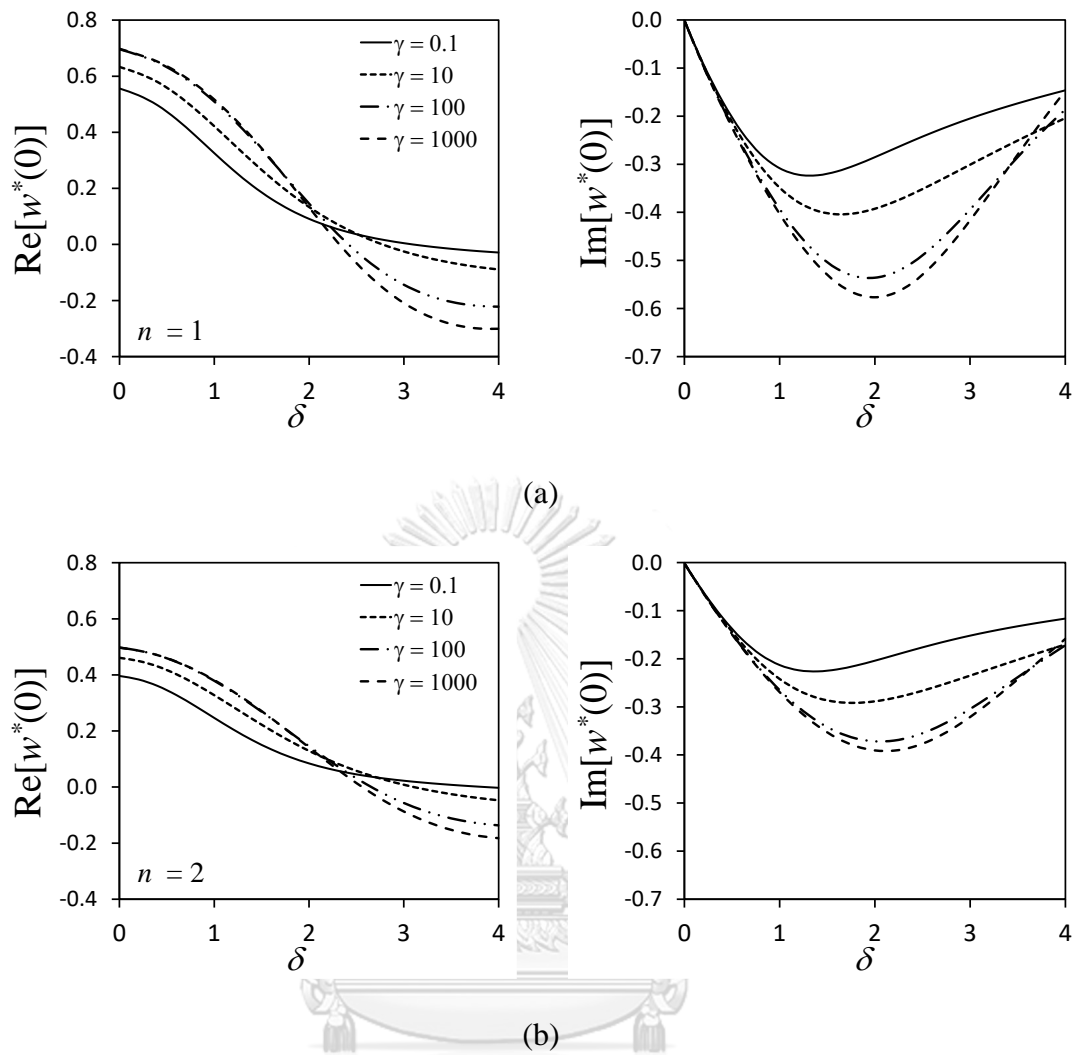


Figure 7.13 Central vertical compliance of a rigid impermeable foundation for different foundation flexibilities ($h/a = 0$): (a) $n = 1$; (b) $n = 2$

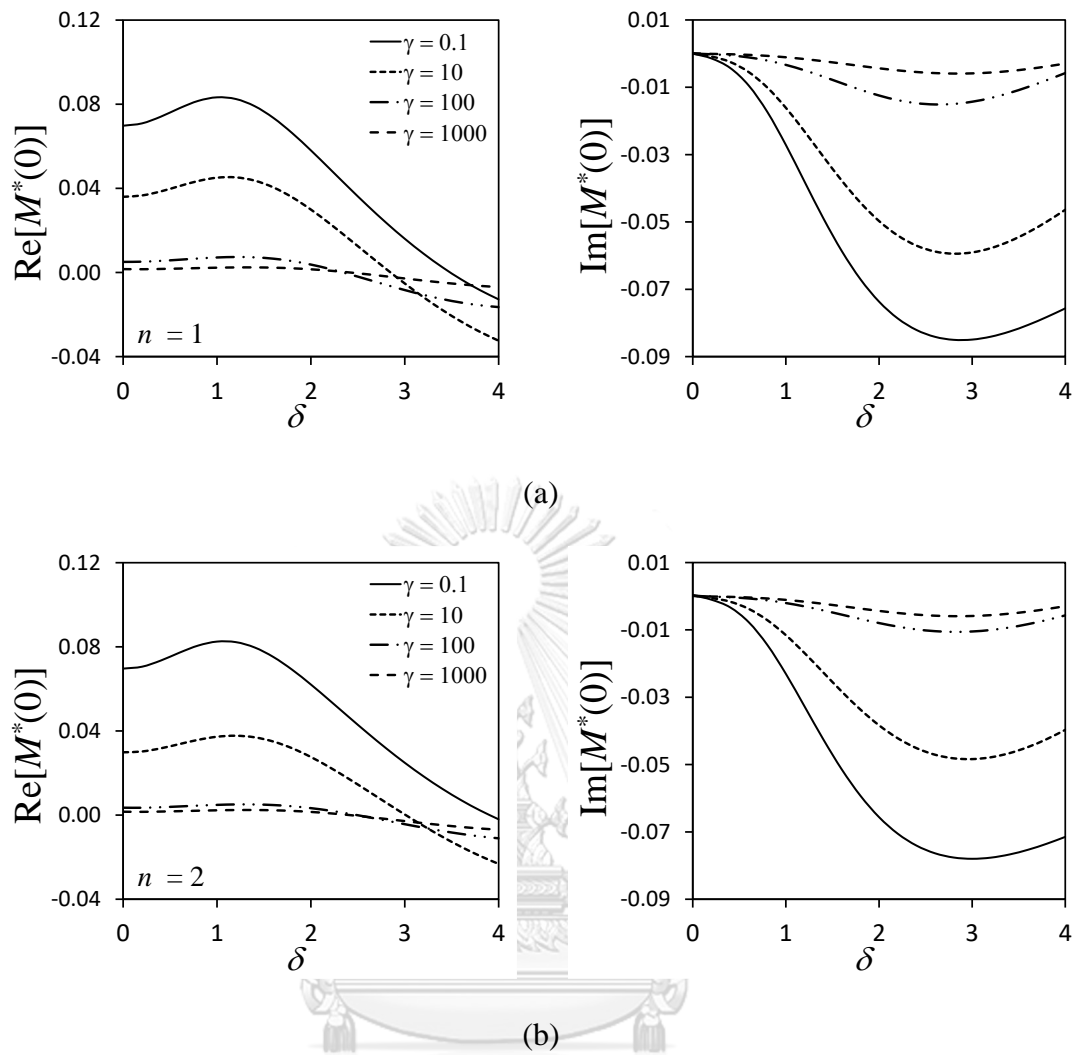
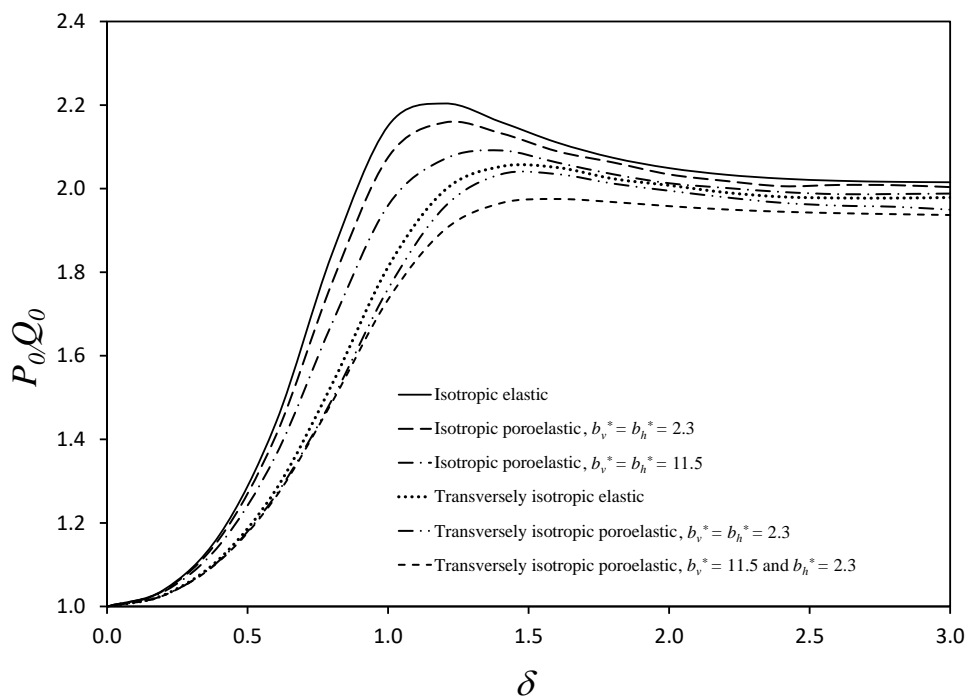
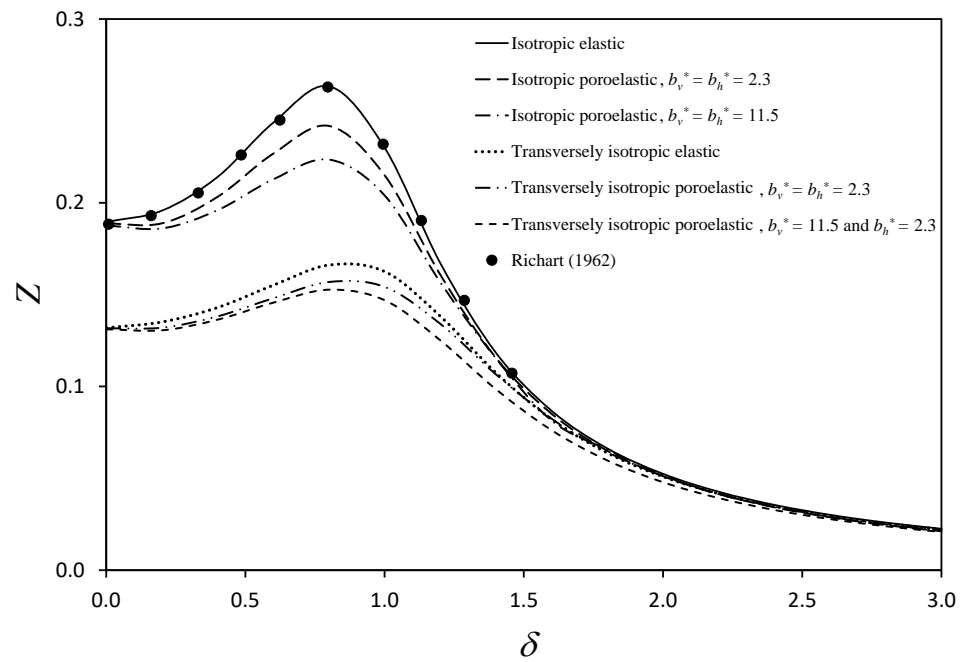


Figure 7.14 Bending moment at the center of foundation for different foundation flexibilities ($h/a = 0$): (a) $n = 1$; (b) $n = 2$



(b)

Figure 7.15 (a) Dimensionless amplitude of and (b) dimensionless force transferred to soil for a rigid impermeable massive foundation on different soils ($h/a = 0$)

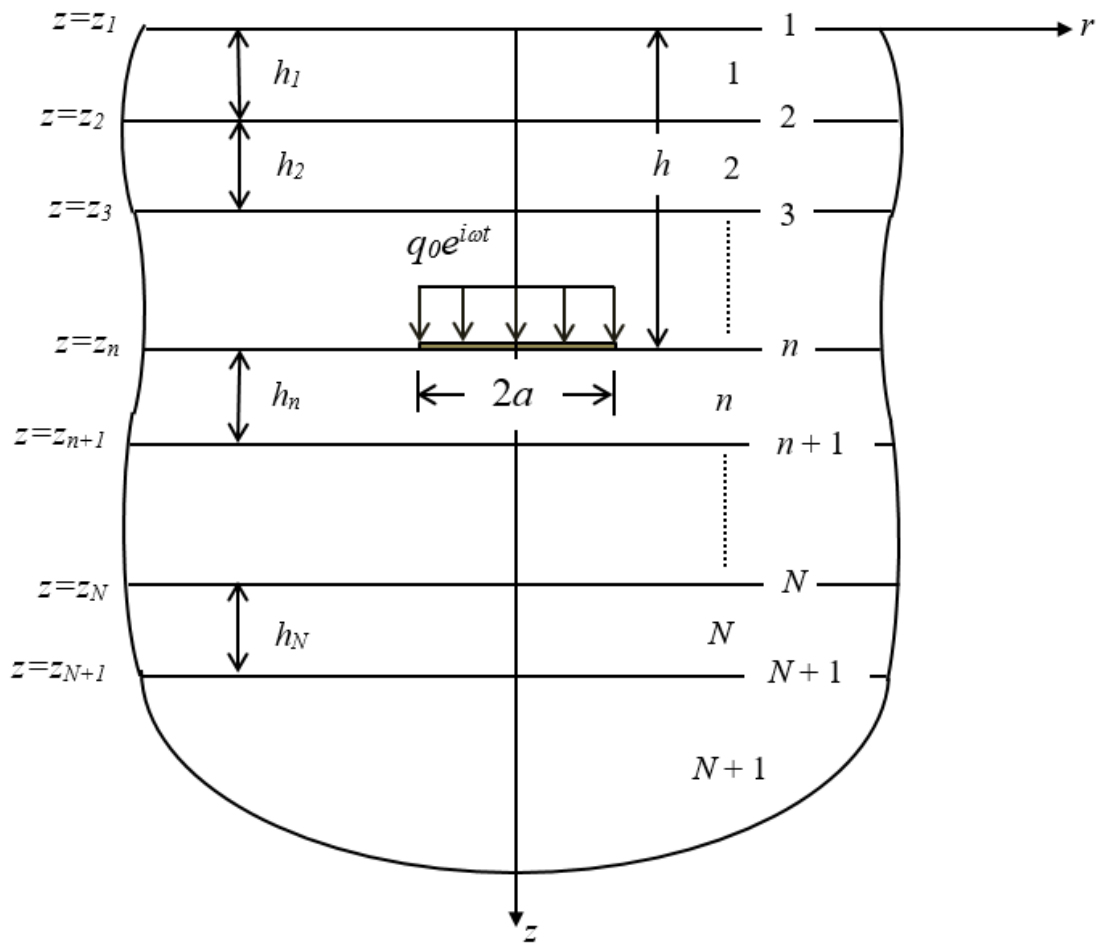


Figure 7.16 Vertically loaded circular foundation in a multi-layered transversely isotropic poroelastic half-space

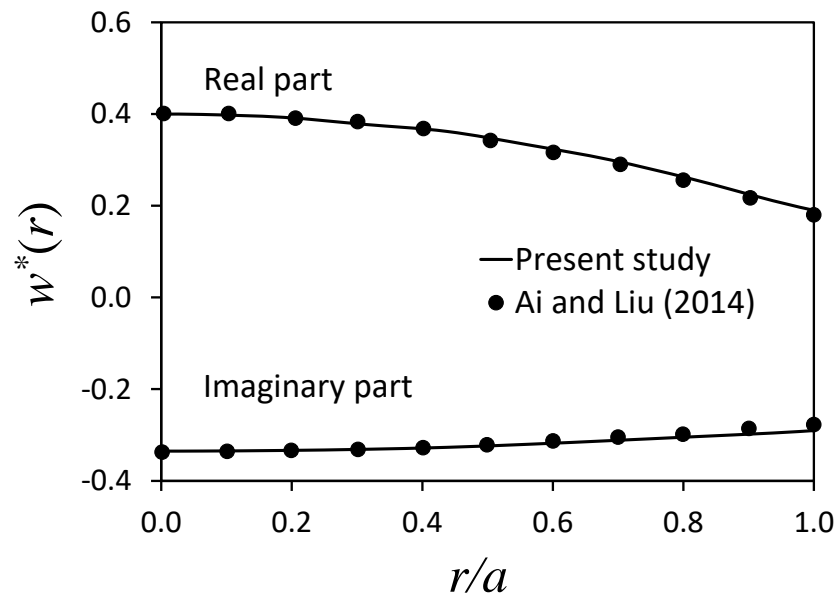


Figure 7.17 Comparison of displacement profile of flexible circular foundations on multilayered transversely isotropic elastic half-space



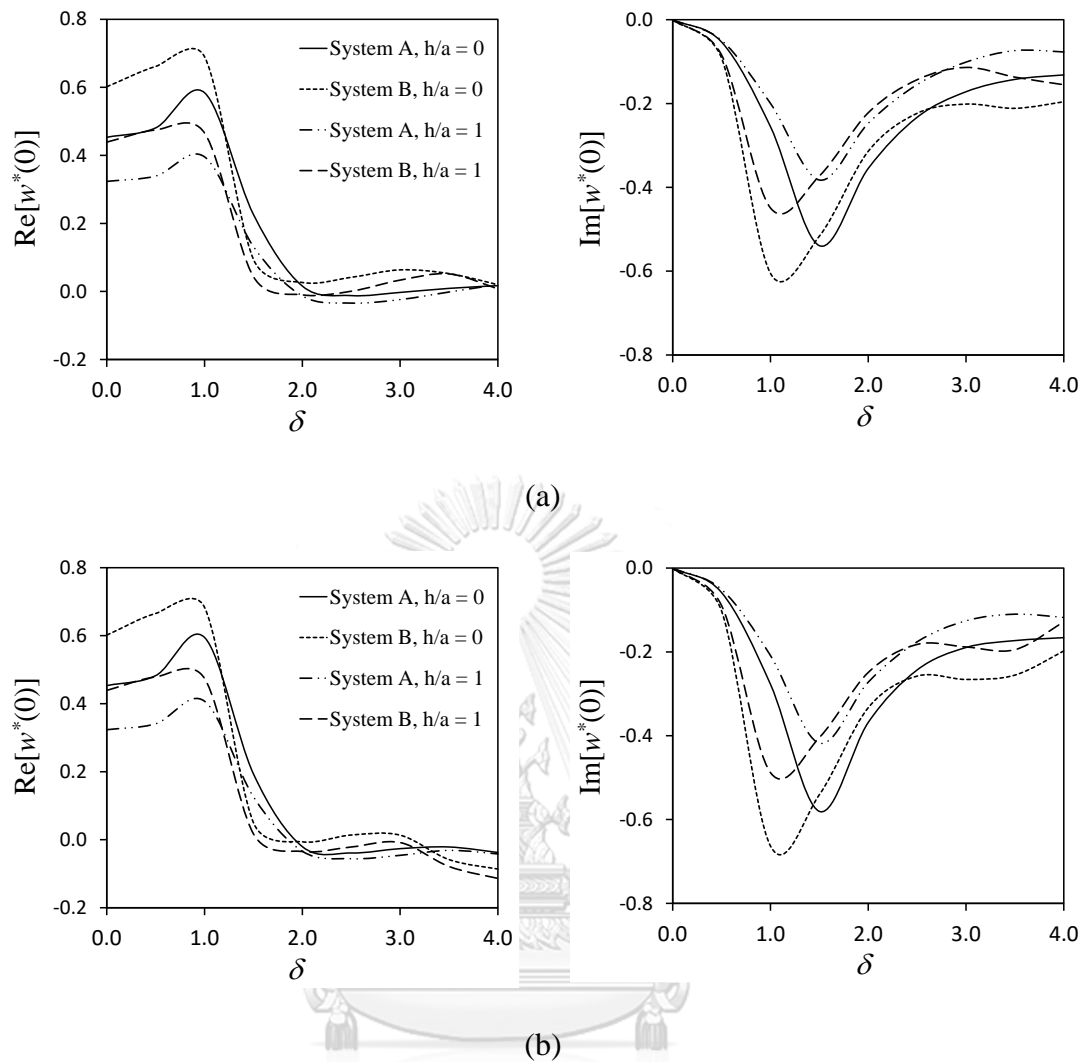


Figure 7.18 Central vertical displacement of a circular foundation at $h/a = 0$ and 1 for different systems, where $\gamma = 10$: (a) permeable; (b) impermeable

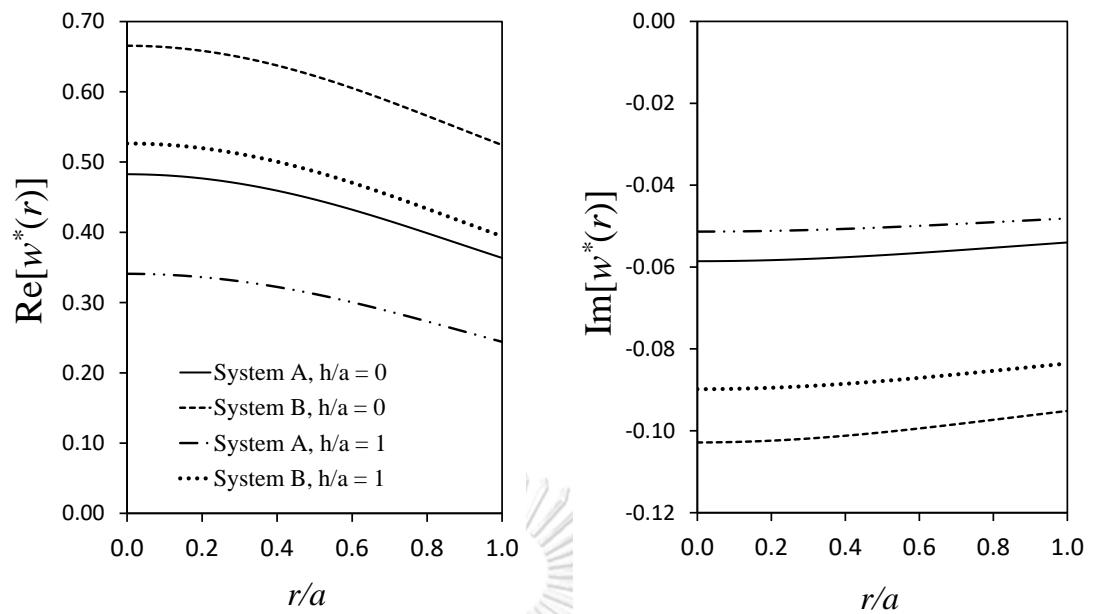


Figure 7.19 Vertical displacement profiles of a circular impermeable foundation at $h/a = 0$ and 1 for different systems, where $\gamma = 10$ and $\delta = 0.5$

CHAPTER 8 CONCLUSIONS

This dissertation presents poroelastodynamic fundamental solutions of transversely isotropic poroelastic materials. The general solutions for transversely isotropic poroelastic media under time-harmonic loading are derived analytically by applying appropriate integral transform techniques. The fundamental solutions of a homogeneous half-space under plane strain and axisymmetric deformations are then explicitly obtained by solving relevant boundary value-problems based on the derived general solutions. An exact stiffness matrix method is also employed to obtain the fundamental solutions of multi-layered transversely isotropic poroelastic media. Selected numerical results corresponding to dynamic response of transversely isotropic poroelastic media under time-harmonic loading. In addition, the obtained fundamental solutions are then employed in the analysis of various dynamic interaction problems between foundations and transversely isotropic poroelastic soils. Conclusions for each problems are given at the end of Chapter 4-7 based on the numerical results presented in those chapters. The major findings and conclusions of this study can be summarized as follows:

1. The fundamental solutions are obtained in the Fourier and Hankel transform spaces for plane strain and axisymmetric problems respectively. An exact stiffness matrix method is successfully applied to determine the fundamental solutions for multi-layered media. The numerical inversion of Fourier and Hankel transforms is carried out by employing an adaptive numerical quadrature scheme using a 21-point Gauss–Kronrod rule. Accuracy of the present numerical scheme is verified by comparing with various existing solutions for each problem. Numerical results indicate that anisotropic and poroelastic material properties have a significant influence on the dynamic response of transversely isotropic poroelastic media.
2. A semi-analytical discretization scheme is successfully adopted to investigate dynamic interaction problems between foundations and transversely isotropic poroelastic soils. Numerical results reveal that the

dynamic interaction between strip and circular foundations and transversely isotropic poroelastic soils are substantially different from the interaction with isotropic poroelastic soils. In addition, dynamic response of foundations also depends significantly on frequency of excitation, hydraulic boundary conditions, foundation flexibility, and distance between adjacent foundations.

The fundamental solutions obtained in this dissertation can be used to assess the accuracy of approximate methods such as finite element and boundary element methods that are applied to study more complicated problems in geotechnical engineering. In addition, the present solution scheme can also be extended to study other geomechanics problems such as arbitrary-shape foundations or laterally-loaded piles with the development of required fundamental functions that are related to three-dimension dynamic response of transversely isotropic poroelastic soils.

APPENDIX

Appendix A: Element of the layer stiffness matrix $\mathbf{K}^{(n)}$

1st row:

$$\begin{aligned}
 K_{11} = & \frac{1}{R} \left[(e_{1n}^m e_{2n}^p e_{3n}^m + e_{1n}^p e_{2n}^m e_{3n}^p) (-\varphi_1 \theta_8 - \varphi_2 \theta_6 + \varphi_3 \theta_5) \kappa_1 \right. \\
 & - (e_{1n}^p e_{2n}^p e_{3n}^m + e_{1n}^m e_{2n}^m e_{3n}^p) (\varphi_1 \theta_8 - \varphi_2 \theta_4 + \varphi_3 \theta_7) \kappa_2 \\
 & - (e_{1n}^m e_{2n}^m e_{3n}^m + e_{1n}^p e_{2n}^p e_{3n}^p) (\varphi_1 \theta_9 - \varphi_2 \theta_6 + \varphi_3 \theta_7) \kappa_3 \\
 & + (e_{1n}^p e_{2n}^m e_{3n}^m + e_{1n}^m e_{2n}^p e_{3n}^p) (-\varphi_1 \theta_9 - \varphi_2 \theta_4 + \varphi_3 \theta_5) \kappa_4 \\
 & + 4(e_{3n}^m + e_{3n}^p) (\varphi_3 \psi_1 \psi_2 \kappa_{14} + \varphi_2 \psi_1 \psi_3 \zeta_2 \theta_1 + \varphi_1 \psi_2 \psi_3 \zeta_1 \theta_2) \\
 & + 4(e_{2n}^m + e_{2n}^p) (\varphi_2 \psi_1 \psi_3 \kappa_{13} + \varphi_3 \psi_1 \psi_2 \zeta_3 \theta_3 - \varphi_1 \psi_2 \psi_3 \zeta_1 \theta_2) \\
 & \left. + 4(e_{1n}^m + e_{1n}^p) (\varphi_1 \psi_2 \psi_3 \kappa_{12} - \varphi_3 \psi_1 \psi_2 \zeta_3 \theta_3 - \varphi_2 \psi_1 \psi_3 \zeta_2 \theta_1) \right] \quad (A1)
 \end{aligned}$$

$$\begin{aligned}
 K_{12} = & \frac{-i}{R} \left[(e_{1n}^p e_{2n}^m e_{3n}^p - e_{1n}^m e_{2n}^p e_{3n}^m) (\varphi_1 \theta_2 + \varphi_2 \theta_1 + \varphi_3 \theta_3) \kappa_1 \right. \\
 & + (e_{1n}^p e_{2n}^p e_{3n}^m - e_{1n}^m e_{2n}^m e_{3n}^p) (-\varphi_1 \theta_2 + \varphi_2 \theta_1 + \varphi_3 \theta_3) \kappa_2 \\
 & + (e_{1n}^m e_{2n}^m e_{3n}^m - e_{1n}^p e_{2n}^p e_{3n}^p) (\varphi_1 \theta_2 - \varphi_2 \theta_1 + \varphi_3 \theta_3) \kappa_3 \\
 & + (e_{1n}^m e_{2n}^p e_{3n}^p - e_{1n}^p e_{2n}^m e_{3n}^m) (-\varphi_1 \theta_2 - \varphi_2 \theta_1 + \varphi_3 \theta_3) \kappa_9 \\
 & + 4(e_{3n}^m - e_{3n}^p) (\varphi_1 \psi_2 + \varphi_2 \psi_1) \theta_1 \theta_2 \\
 & + 4(e_{2n}^m - e_{2n}^p) (\varphi_1 \psi_3 + \varphi_3 \psi_1) \theta_2 \theta_3 \\
 & \left. + 4(e_{1n}^m - e_{1n}^p) (\varphi_3 \psi_2 + \varphi_2 \psi_3) \theta_1 \theta_3 \right] \quad (A2)
 \end{aligned}$$

$$\begin{aligned}
 K_{13} = & \frac{-i}{R} \left[-(e_{1n}^m e_{2n}^p e_{3n}^m + e_{1n}^p e_{2n}^m e_{3n}^p) (-\varphi_1 \theta_{10} + \varphi_2 \theta_{13} + \varphi_3 \theta_{14}) \kappa_{10} \right. \\
 & + (e_{1n}^p e_{2n}^p e_{3n}^m + e_{1n}^m e_{2n}^m e_{3n}^p) (-\varphi_1 \theta_{10} + \varphi_2 \theta_{12} + \varphi_3 \theta_{15}) \kappa_2 \\
 & + (e_{1n}^m e_{2n}^m e_{3n}^m + e_{1n}^p e_{2n}^p e_{3n}^p) (\varphi_1 \theta_{11} - \varphi_2 \theta_{13} + \varphi_3 \theta_{15}) \kappa_3 \\
 & - (e_{1n}^p e_{2n}^m e_{3n}^m + e_{1n}^m e_{2n}^p e_{3n}^p) (\varphi_1 \theta_{11} - \varphi_2 \theta_{12} + \varphi_3 \theta_{14}) \kappa_9 \\
 & - 4(e_{3n}^m + e_{3n}^p) (\varphi_3 \psi_1 \psi_2 \kappa_{15} - \varphi_2 \chi_2 \psi_1 \psi_3 \theta_1 - \varphi_1 \chi_1 \psi_2 \psi_3 \theta_2) \\
 & + 4(e_{2n}^m + e_{2n}^p) (\varphi_2 \psi_1 \psi_3 \kappa_{16} + \varphi_3 \chi_3 \psi_1 \psi_2 \theta_3 - \varphi_1 \chi_1 \psi_2 \psi_3 \theta_2) \\
 & \left. - 4(e_{1n}^m + e_{1n}^p) (\varphi_1 \psi_2 \psi_3 \kappa_{17} + \varphi_3 \chi_3 \psi_1 \psi_2 \theta_3 + \varphi_2 \chi_2 \psi_1 \psi_3 \theta_1) \right] \quad (A3)
 \end{aligned}$$

$$\begin{aligned}
K_{14} = & \frac{2}{R} \left[(e_{1n}^m e_{3n}^m + e_{1n}^p e_{3n}^p) (\varphi_3 \kappa_{22} - \varphi_1 \psi_2 \theta_2 + \varphi_2 \kappa_{11}) \theta_6 \right. \\
& + (e_{1n}^p e_{3n}^m + e_{1n}^m e_{3n}^p) (\varphi_3 \psi_2 \theta_3 - \varphi_1 \psi_2 \theta_2 + \varphi_2 \kappa_{19}) \theta_4 \\
& + (e_{2n}^m e_{3n}^m + e_{2n}^p e_{3n}^p) (\varphi_3 \psi_1 \theta_3 + \varphi_1 \kappa_5 + \varphi_2 \kappa_{23}) \theta_9 \\
& - (e_{2n}^p e_{3n}^m + e_{2n}^m e_{3n}^p) (\varphi_3 \psi_1 \theta_3 + \varphi_1 \kappa_7 + \varphi_2 \psi_1 \theta_1) \theta_8 \\
& + (e_{1n}^m e_{2n}^m + e_{1n}^p e_{2n}^p) (\varphi_3 \kappa_6 + \psi_3 \kappa_{20}) \theta_7 \\
& - (e_{1n}^p e_{2n}^m + e_{1n}^m e_{2n}^p) (\varphi_3 \kappa_8 - \psi_3 \kappa_{18}) \theta_5 \\
& \left. - 4(\varphi_3 \psi_1 \psi_2 \kappa_{14} + \varphi_2 \psi_1 \psi_3 \kappa_{13} + \varphi_1 \psi_2 \psi_3 \kappa_{12}) \right]
\end{aligned} \tag{A4}$$

$$\begin{aligned}
K_{15} = & \frac{2i}{R} \left[(e_{1n}^m e_{2n}^m - e_{1n}^p e_{2n}^p) (\psi_3 \kappa_{20} + \varphi_3 \kappa_6) \theta_3 \right. \\
& - (e_{2n}^m e_{3n}^m - e_{2n}^p e_{3n}^p) (\varphi_3 \kappa_{21} + \varphi_2 \psi_1 \theta_1 - \varphi_1 \kappa_5) \theta_2 \\
& + (e_{2n}^m e_{3n}^p - e_{2n}^p e_{3n}^m) (\varphi_3 \psi_1 \theta_3 + \varphi_2 \psi_1 \theta_1 + \varphi_1 \kappa_7) \theta_2 \\
& + (e_{1n}^m e_{2n}^p - e_{1n}^p e_{2n}^m) (\varphi_3 \kappa_8 - \psi_3 \kappa_{18}) \theta_3 \\
& + (e_{1n}^m e_{3n}^m) (\varphi_3 \kappa_{22} - \varphi_1 \psi_2 \theta_2 + \varphi_2 \kappa_{11}) \theta_1 \\
& + (e_{1n}^p e_{3n}^m) (\varphi_3 \psi_2 \theta_3 - \varphi_1 \psi_2 \theta_2 + \varphi_2 \kappa_{19}) \theta_1 \\
& + (e_{1n}^m e_{3n}^p) (\varphi_3 \kappa_{22} + \varphi_1 \psi_2 \theta_2 - \varphi_2 \kappa_{19}) \theta_1 \\
& \left. + (e_{1n}^p e_{3n}^p) (\varphi_3 \psi_2 \theta_3 + \varphi_1 \psi_2 \theta_2 - \varphi_2 \kappa_{11}) \theta_1 \right]
\end{aligned} \tag{A5}$$

$$\begin{aligned}
K_{16} = & \frac{-2i}{R} \left[(e_{2n}^p e_{3n}^m + e_{2n}^m e_{3n}^p) (\varphi_3 \kappa_{21} - \varphi_2 \psi_1 \theta_1 - \varphi_1 \kappa_7) \theta_{10} \right. \\
& + (e_{1n}^p e_{3n}^m + e_{1n}^m e_{3n}^p) (\varphi_3 \psi_2 \theta_3 - \varphi_1 \psi_2 \theta_2 + \varphi_2 \kappa_{19}) \theta_{12} \\
& + (e_{1n}^m e_{3n}^m + e_{1n}^p e_{3n}^p) (\varphi_3 \psi_2 \theta_3 + \varphi_1 \psi_2 \theta_2 - \varphi_2 \kappa_{11}) \theta_{13} \\
& - (e_{2n}^m e_{3n}^m + e_{2n}^p e_{3n}^p) (\varphi_3 \psi_1 \theta_3 + \varphi_2 \kappa_{23} + \varphi_1 \kappa_5) \theta_{11} \\
& - (e_{1n}^m e_{2n}^m + e_{1n}^p e_{2n}^p) (\psi_3 \kappa_{20} + \varphi_3 \kappa_6) \theta_{15} \\
& + (e_{1n}^p e_{2n}^m + e_{1n}^m e_{2n}^p) (\psi_3 \kappa_{18} - \varphi_3 \chi_3 \theta_5 + \varphi_3 \zeta_3 \theta_{14}) \theta_{14} \\
& \left. + 4(\varphi_3 \psi_1 \psi_2 \kappa_{15} + \varphi_2 \psi_1 \psi_3 \kappa_{16} + \varphi_1 \psi_2 \psi_3 \kappa_{17}) \right]
\end{aligned} \tag{A6}$$

2nd row:

$$\begin{aligned}
K_{22} = & \frac{-\mathcal{G}_1}{R} \left[(e_{1n}^p e_{2n}^m e_{3n}^m + e_{1n}^m e_{2n}^p e_{3n}^p) \kappa_4 + (e_{1n}^p e_{2n}^p e_{3n}^m + e_{1n}^m e_{2n}^m e_{3n}^p) \kappa_2 \right. \\
& \left. - (e_{1n}^m e_{2n}^m e_{3n}^m + e_{1n}^p e_{2n}^p e_{3n}^p) \kappa_3 + (e_{1n}^m e_{2n}^p e_{3n}^m + e_{1n}^p e_{2n}^m e_{3n}^p) \kappa_{10} \right]
\end{aligned} \tag{A7}$$

$$\begin{aligned}
K_{23} = & \frac{1}{R} \left[(e_{1n}^m e_{2n}^m e_{3n}^p - e_{1n}^p e_{2n}^p e_{3n}^m) (\eta_3 \theta_{15} - \eta_2 \theta_{12} + \eta_1 \theta_{10}) \kappa_2 \right. \\
& + (e_{1n}^p e_{2n}^p e_{3n}^p - e_{1n}^m e_{2n}^m e_{3n}^m) (\eta_3 \theta_{15} - \eta_2 \theta_{13} + \eta_1 \theta_{11}) \kappa_3 \\
& + (e_{1n}^p e_{2n}^m e_{3n}^m - e_{1n}^m e_{2n}^p e_{3n}^p) (\eta_3 \theta_{14} - \eta_2 \theta_{12} - \eta_1 \theta_{11}) \kappa_9 \\
& + (e_{1n}^m e_{2n}^p e_{3n}^m - e_{1n}^p e_{2n}^m e_{3n}^p) (\eta_3 \theta_{14} - \eta_2 \theta_{13} - \eta_1 \theta_{10}) \kappa_{10} \\
& + 4(e_{3n}^m - e_{3n}^p) (\chi_3 \mathcal{G}_2 + \eta_3 \kappa_{15}) \psi_1 \psi_2 \\
& + 4(e_{1n}^p - e_{1n}^m) (-\eta_3 \chi_1 \theta_3 - \eta_2 \chi_1 \theta_1 - \eta_1 \kappa_{17}) \psi_2 \psi_3 \\
& \left. + 4(e_{2n}^m - e_{2n}^p) (-\eta_3 \chi_2 \theta_3 + \eta_2 \kappa_{16} + \eta_1 \chi_2 \theta_2) \psi_1 \psi_3 \right]
\end{aligned} \tag{A8}$$

$$K_{24} = -K_{15} \tag{A9}$$

$$\begin{aligned}
K_{25} = & \frac{2\mathcal{G}_1}{R} \left[(e_{1n}^m e_{2n}^m + e_{1n}^p e_{2n}^p - e_{1n}^p e_{2n}^m - e_{1n}^m e_{2n}^p) \psi_3 \theta_3 \right. \\
& + (e_{1n}^p e_{3n}^m + e_{1n}^m e_{3n}^p - e_{1n}^m e_{3n}^m - e_{1n}^p e_{3n}^p) \psi_2 \theta_1 \\
& \left. + (e_{2n}^m e_{3n}^m + e_{2n}^p e_{3n}^p - e_{2n}^p e_{3n}^m - e_{2n}^m e_{3n}^p) \psi_1 \theta_2 \right]
\end{aligned} \tag{A10}$$

$$\begin{aligned}
K_{26} = & \frac{-2\mathcal{G}_1}{R} \left[(e_{1n}^p e_{2n}^p - e_{1n}^m e_{2n}^m) \psi_3 \theta_{15} + (e_{1n}^m e_{2n}^p - e_{1n}^p e_{2n}^m) \psi_3 \theta_{14} \right. \\
& + (e_{1n}^m e_{3n}^m - e_{1n}^p e_{3n}^p) \psi_2 \theta_{13} + (e_{1n}^p e_{3n}^m - e_{1n}^m e_{3n}^p) \psi_2 \theta_{12} \\
& \left. + (e_{2n}^p e_{3n}^p - e_{2n}^m e_{3n}^m) \psi_1 \theta_{11} + (e_{2n}^m e_{3n}^p - e_{2n}^p e_{3n}^m) \psi_1 \theta_{10} \right]
\end{aligned} \tag{A11}$$

3rd row:

$$\begin{aligned}
K_{33} = & \frac{1}{R} \left[-(e_{1n}^m e_{2n}^p e_{3n}^m + e_{1n}^p e_{2n}^m e_{3n}^p) (-\varpi_1 \theta_{10} \kappa_1 + \varpi_2 \theta_{13} \kappa_1 - \varpi_3 \theta_{14} \kappa_{10}) \right. \\
& + (e_{1n}^p e_{2n}^m e_{3n}^m + e_{1n}^m e_{2n}^p e_{3n}^p) (-\varpi_1 \theta_{11} \kappa_4 + \varpi_2 \theta_{12} \kappa_4 + \varpi_3 \theta_{14} \kappa_9) \\
& - (e_{1n}^p e_{2n}^p e_{3n}^m + e_{1n}^m e_{2n}^m e_{3n}^p) (-\varpi_1 \theta_{10} \kappa_2 + \varpi_2 \theta_{12} \kappa_2 + \varpi_3 \theta_{15} \kappa_2) \\
& + (e_{1n}^m e_{2n}^m e_{3n}^m + e_{1n}^p e_{2n}^p e_{3n}^p) (-\varpi_1 \theta_{11} \kappa_3 + \varpi_2 \theta_{13} \kappa_3 - \varpi_3 \theta_{15} \kappa_3) \\
& + 4(e_{3n}^m + e_{3n}^p) (-\varpi_1 \chi_1 \psi_2 \psi_3 \theta_2 - \varpi_2 \chi_2 \psi_1 \psi_3 \theta_1 + \varpi_3 \psi_1 \psi_2 \kappa_{15}) \\
& - 4(e_{2n}^m + e_{2n}^p) (-\varpi_1 \chi_1 \psi_2 \psi_3 \theta_2 - \varpi_2 \psi_1 \psi_3 \kappa_{16} + \varpi_3 \chi_3 \psi_1 \psi_2 \theta_3) \\
& \left. + 4(e_{1n}^m + e_{1n}^p) (\varpi_1 \psi_2 \psi_3 \kappa_{17} + \varpi_2 \chi_2 \psi_1 \psi_3 \theta_1 + \varpi_3 \chi_3 \psi_1 \psi_2 \theta_3) \right]
\end{aligned} \tag{A12}$$

$$K_{34} = K_{16} \tag{A13}$$

$$K_{35} = -K_{26} \tag{A14}$$

$$\begin{aligned}
K_{36} = & \frac{-2}{R} \left[(e_{1n}^m e_{3n}^m + e_{1n}^p e_{3n}^p) (\varpi_3 \psi_2 \theta_3 \theta_{13} - \varpi_2 \theta_{13} \kappa_{11} + \varpi_1 \psi_2 \theta_2 \theta_{13}) \right. \\
& + (e_{1n}^p e_{3n}^m + e_{1n}^m e_{3n}^p) (\varpi_3 \psi_2 \theta_3 \theta_{12} + \varpi_2 \theta_{12} (\zeta_2 \theta_{12} - \chi_2 \theta_4) - \varpi_1 \psi_2 \theta_2 \theta_{12}) \\
& + (e_{2n}^m e_{3n}^m + e_{2n}^p e_{3n}^p) (-\varpi_3 \psi_1 \theta_3 \theta_{11} + \varpi_2 \psi_1 \theta_1 \theta_{11} - \varpi_1 \theta_{11} \kappa_5) \\
& - (e_{2n}^p e_{3n}^m + e_{2n}^m e_{3n}^p) (\varpi_3 \psi_1 \theta_3 \theta_{10} + \varpi_2 \psi_1 \theta_1 \theta_{10} - \varpi_1 \theta_{10} (\zeta_1 \theta_{10} - \chi_1 \theta_8)) \\
& - (e_{1n}^m e_{2n}^m + e_{1n}^p e_{2n}^p) (\varpi_3 \theta_{15} \kappa_6 - \varpi_2 \psi_3 \theta_1 \theta_{15} + \varpi_1 \psi_3 \theta_2 \theta_{15}) \\
& + (e_{1n}^p e_{2n}^m + e_{1n}^m e_{2n}^p) (\varpi_3 \theta_{14} (\zeta_3 \theta_{14} - \chi_3 \theta_5) + \varpi_2 \psi_3 \theta_1 \theta_{14} + \varpi_1 \psi_3 \theta_2 \theta_{14}) \\
& \left. + 4(\varpi_3 \psi_1 \psi_2 \kappa_{15} + \varpi_2 \psi_1 \psi_3 \kappa_{16} + \varpi_1 \psi_2 \psi_3 \kappa_{17}) \right] \quad (A15)
\end{aligned}$$

4th row:

$$K_{44} = K_{11} \quad (A16)$$

$$K_{45} = -K_{12} \quad (A17)$$

$$K_{46} = K_{13} \quad (A18)$$

5th row:

$$K_{55} = K_{22} \quad (A19)$$

$$K_{56} = -K_{23} \quad (A20)$$

6th row:

$$K_{66} = K_{33} \quad (A21)$$

where

$$\begin{aligned}
R = & 8 \left[(e_{1n}^m - e_{1n}^p) \psi_2 \psi_3 \theta_1 \theta_3 - (e_{2n}^m - e_{2n}^p) \psi_1 \psi_3 \theta_2 \theta_3 + (e_{3n}^m - e_{3n}^p) \psi_1 \psi_2 \theta_1 \theta_2 \right] \\
& + (e_{1n}^p e_{2n}^m e_{3n}^p - e_{1n}^m e_{2n}^p e_{3n}^m) \kappa_1^2 + (e_{1n}^p e_{2n}^p e_{3n}^m - e_{1n}^m e_{2n}^m e_{3n}^p) \kappa_2^2 \\
& + (e_{1n}^m e_{2n}^m e_{3n}^m - e_{1n}^p e_{2n}^p e_{3n}^p) \kappa_3^2 + (e_{1n}^m e_{2n}^p e_{3n}^p - e_{1n}^p e_{2n}^m e_{3n}^m) \kappa_4^2 \quad (A22)
\end{aligned}$$

$$e_{in}^m = e^{-\lambda_i h_n}, \quad i=1,2,3, \quad n=1,2,\dots,N, \quad e_{in}^p = e^{\lambda_i h_n}, \quad i=1,2,3, \quad n=1,2,\dots,N \quad (A23)$$

$$\kappa_1 = \chi_3 \psi_2 \zeta_1 + \chi_2 \psi_3 \zeta_1 + \chi_3 \psi_1 \zeta_2 - \chi_1 \psi_3 \zeta_2 - \chi_2 \psi_1 \zeta_3 - \chi_1 \psi_2 \zeta_3 \quad (A24)$$

$$\kappa_2 = \chi_3 \psi_2 \zeta_1 + \chi_2 \psi_3 \zeta_1 - \chi_3 \psi_1 \zeta_2 - \chi_1 \psi_3 \zeta_2 + \chi_2 \psi_1 \zeta_3 - \chi_1 \psi_2 \zeta_3 \quad (A25)$$

$$\kappa_3 = \chi_3 \psi_2 \zeta_1 - \chi_2 \psi_3 \zeta_1 - \chi_3 \psi_1 \zeta_2 + \chi_1 \psi_3 \zeta_2 + \chi_2 \psi_1 \zeta_3 - \chi_1 \psi_2 \zeta_3 \quad (A26)$$

$$\kappa_4 = \chi_3 \psi_2 \zeta_1 - \chi_2 \psi_3 \zeta_1 + \chi_3 \psi_1 \zeta_2 + \chi_1 \psi_3 \zeta_2 - \chi_2 \psi_1 \zeta_3 - \chi_1 \psi_2 \zeta_3 \quad (A27)$$

$$\kappa_5 = \chi_3 \psi_2 \zeta_1 - \chi_2 \psi_3 \zeta_1 + \chi_1 \psi_3 \zeta_2 - \chi_1 \psi_2 \zeta_3 \quad (A28)$$

$$\kappa_6 = \chi_3 \psi_2 \zeta_1 - \chi_3 \psi_1 \zeta_2 + \chi_2 \psi_1 \zeta_3 - \chi_1 \psi_2 \zeta_3 \quad (\text{A29})$$

$$\kappa_7 = -\chi_3 \psi_2 \zeta_1 - \chi_2 \psi_3 \zeta_1 + \chi_1 \psi_3 \zeta_2 + \chi_1 \psi_2 \zeta_3 \quad (\text{A30})$$

$$\kappa_8 = \chi_3 \psi_2 \zeta_1 + \chi_3 \psi_1 \zeta_2 - \chi_2 \psi_1 \zeta_3 - \chi_1 \psi_2 \zeta_3 \quad (\text{A31})$$

$$\kappa_9 = -\chi_1 (\psi_3 \zeta_2 - \psi_2 \zeta_3) + \chi_2 (\psi_3 \zeta_1 + \psi_1 \zeta_3) - \chi_3 (\psi_2 \zeta_1 + \psi_1 \zeta_2) \quad (\text{A32})$$

$$\kappa_{10} = \chi_1 (\psi_3 \zeta_2 + \psi_2 \zeta_3) - \chi_2 (\psi_3 \zeta_1 - \psi_1 \zeta_3) - \chi_3 (\psi_2 \zeta_1 + \psi_1 \zeta_2) \quad (\text{A33})$$

$$\kappa_{11} = \chi_2 \psi_3 \zeta_1 + \chi_3 \psi_1 \zeta_2 - \chi_1 \psi_3 \zeta_2 - \chi_2 \psi_1 \zeta_3 \quad (\text{A34})$$

$$\kappa_{12} = \chi_3 \zeta_1 \zeta_2 + \chi_2 \zeta_1 \zeta_3 - 2\chi_1 \zeta_2 \zeta_3, \quad \kappa_{13} = \chi_3 \zeta_1 \zeta_2 - 2\chi_2 \zeta_1 \zeta_3 + \chi_1 \zeta_2 \zeta_3 \quad (\text{A35})$$

$$\kappa_{14} = -2\chi_3 \zeta_1 \zeta_2 + \chi_2 \zeta_1 \zeta_3 + \chi_1 \zeta_2 \zeta_3, \quad \kappa_{15} = \chi_2 \chi_3 \zeta_1 + \chi_1 \chi_3 \zeta_2 - 2\chi_1 \chi_2 \zeta_3 \quad (\text{A36})$$

$$\kappa_{16} = \chi_2 \chi_3 \zeta_1 - 2\chi_1 \chi_3 \zeta_2 + \chi_1 \chi_2 \zeta_3, \quad \kappa_{17} = -2\chi_2 \chi_3 \zeta_1 + \chi_1 \chi_3 \zeta_2 + \chi_1 \chi_2 \zeta_3 \quad (\text{A37})$$

$$\kappa_{18} = \varphi_2 \chi_3 \zeta_1 + \varphi_1 \chi_3 \zeta_2 - \varphi_2 \chi_1 \zeta_3 - \varphi_1 \chi_2 \zeta_3 \quad (\text{A38})$$

$$\kappa_{19} = -\chi_2 \psi_3 \zeta_1 + \chi_3 \psi_1 \zeta_2 - \chi_1 \psi_3 \zeta_2 - \chi_2 \psi_1 \zeta_3 \quad (\text{A39})$$

$$\kappa_{20} = -\varphi_2 \chi_3 \zeta_1 + \varphi_1 \chi_3 \zeta_2 + \varphi_2 \chi_1 \zeta_3 - \varphi_1 \chi_2 \zeta_3 \quad (\text{A40})$$

$$\kappa_{21} = -\chi_2 \psi_1 \zeta_1 + \chi_1 \psi_1 \zeta_2, \quad \kappa_{22} = -\chi_2 \psi_2 \zeta_1 + \chi_1 \psi_2 \zeta_2, \quad \kappa_{23} = -\chi_3 \psi_1 \zeta_1 + \chi_1 \psi_1 \zeta_3 \quad (\text{A41})$$

$$\theta_1 = \chi_3 \zeta_1 - \chi_1 \zeta_3, \quad \theta_2 = \chi_3 \zeta_2 - \chi_2 \zeta_3, \quad \theta_3 = \chi_2 \zeta_1 - \chi_1 \zeta_2, \quad \theta_4 = \psi_3 \zeta_1 + \psi_1 \zeta_3 \quad (\text{A42})$$

$$\theta_5 = \psi_2 \zeta_1 + \psi_1 \zeta_2, \quad \theta_6 = \psi_3 \zeta_1 - \psi_1 \zeta_3, \quad \theta_7 = \psi_2 \zeta_1 - \psi_1 \zeta_2, \quad \theta_8 = \psi_3 \zeta_2 + \psi_2 \zeta_3 \quad (\text{A43})$$

$$\theta_9 = \psi_3 \zeta_2 - \psi_2 \zeta_3, \quad \theta_{10} = \chi_3 \psi_2 + \chi_2 \psi_3 \quad (\text{A44})$$

$$\theta_{11} = \chi_3 \psi_2 - \chi_2 \psi_3, \quad \theta_{12} = \chi_3 \psi_1 + \chi_1 \psi_3 \quad (\text{A45})$$

$$\theta_{13} = \chi_3 \psi_1 - \chi_1 \psi_3, \quad \theta_{14} = \chi_2 \psi_1 + \chi_1 \psi_3, \quad \theta_{15} = \chi_2 \psi_1 - \chi_1 \psi_3 \quad (\text{A46})$$

$$\mathfrak{g}_1 = \eta_3 \chi_2 \zeta_1 - \eta_2 \chi_3 \zeta_1 - \eta_3 \chi_1 \zeta_2 + \eta_1 \chi_3 \zeta_2 + \eta_2 \chi_1 \zeta_3 - \eta_1 \chi_2 \zeta_3 \quad (\text{A47})$$

$$\mathfrak{g}_2 = -\eta_2 \chi_3 \zeta_1 + \eta_2 \chi_1 \zeta_3 - \eta_1 \chi_3 \zeta_2 + \eta_1 \chi_2 \zeta_3 \quad (\text{A48})$$

Appendix B: Element of the layer stiffness matrix $\mathbf{K}^{(n+1)}$

1st row:

$$\bar{K}_{11} = \frac{1}{H} (\varphi_3 \psi_2 \zeta_1 - \varphi_2 \psi_3 \zeta_1 - \varphi_3 \psi_1 \zeta_2 + \varphi_1 \psi_3 \zeta_2 + \varphi_2 \psi_1 \zeta_3 - \varphi_1 \psi_2 \zeta_3) \quad (\text{B1})$$

$$\bar{K}_{12} = \frac{i}{H} (\varphi_3 \chi_2 \zeta_1 - \varphi_2 \chi_3 \zeta_1 - \varphi_3 \chi_1 \zeta_2 + \varphi_1 \chi_3 \zeta_2 + \varphi_2 \chi_1 \zeta_3 - \varphi_1 \chi_2 \zeta_3) \quad (\text{B2})$$

$$\bar{K}_{13} = \frac{i}{H} (\varphi_3 \chi_2 \psi_1 - \varphi_2 \chi_3 \psi_1 - \varphi_3 \chi_1 \psi_2 + \varphi_1 \chi_3 \psi_2 + \varphi_2 \chi_1 \psi_3 - \varphi_1 \chi_2 \psi_3) \quad (\text{B3})$$

2nd row:

$$\bar{K}_{22} = \frac{-1}{H} (\eta_3 \chi_2 \zeta_1 - \eta_2 \chi_3 \zeta_1 - \eta_3 \chi_1 \zeta_2 + \eta_1 \chi_3 \zeta_2 + \eta_2 \chi_1 \zeta_3 - \eta_1 \chi_2 \zeta_3) \quad (\text{B4})$$

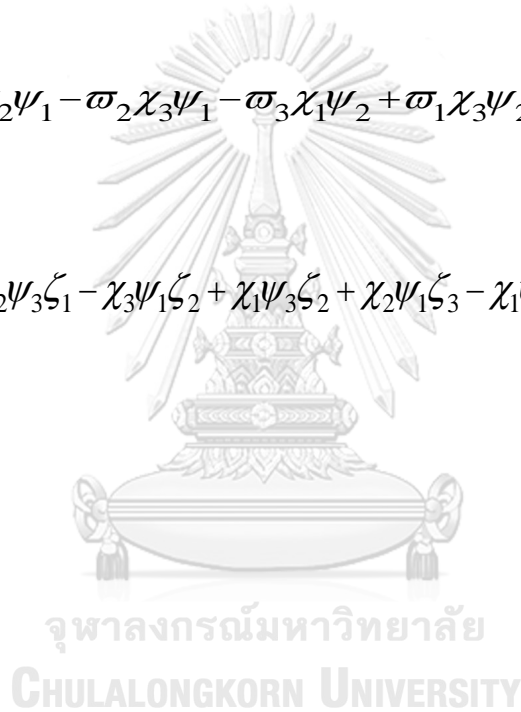
$$\bar{K}_{23} = \frac{-1}{H} (\eta_3 \chi_2 \psi_1 - \eta_2 \chi_3 \psi_1 - \eta_3 \chi_1 \psi_2 + \eta_1 \chi_3 \psi_2 + \eta_2 \chi_1 \psi_3 - \eta_1 \chi_2 \psi_3) \quad (\text{B5})$$

3rd row:

$$\bar{K}_{33} = \frac{1}{H} (\varpi_3 \chi_2 \psi_1 - \varpi_2 \chi_3 \psi_1 - \varpi_3 \chi_1 \psi_2 + \varpi_1 \chi_3 \psi_2 + \varpi_2 \chi_1 \psi_3 - \varpi_1 \chi_2 \psi_3) \quad (\text{B6})$$

where

$$H = \chi_3 \psi_2 \zeta_1 - \chi_2 \psi_3 \zeta_1 - \chi_3 \psi_1 \zeta_2 + \chi_1 \psi_3 \zeta_2 + \chi_2 \psi_1 \zeta_3 - \chi_1 \psi_2 \zeta_3 \quad (\text{B7})$$



REFERENCES



จุฬาลงกรณ์มหาวิทยาลัย
CHULALONGKORN UNIVERSITY

REFERENCES

- Ai, Z. Y., H. T. Li, and Y. F. Zhang. 2017. 'Vertical vibration of a massless flexible strip footing bonded to a transversely isotropic multilayered half-plane', *Soil Dynamics and Earthquake Engineering*, 92: 528-36.
- Ai, Z. Y., and Z. X. Li. 2014. 'Time-harmonic response of transversely isotropic multilayered half-space in a cylindrical coordinate system', *Soil Dynamics and Earthquake Engineering*, 66: 69-77.
- Ai, Z. Y., Z. X. Li, and N. R. Cang. 2014. 'Analytical layer-element solution to axisymmetric dynamic response of transversely isotropic multilayered half-space', *Soil Dynamics and Earthquake Engineering*, 60: 22-30.
- Ai, Z. Y., and C. L. Liu. 2014. 'Axisymmetric vibration of an elastic circular plate bonded on a transversely isotropic multilayered half-space', *Soil Dynamics and Earthquake Engineering*, 67: 257-63.
- Ai, Z. Y., C. L. Liu, and J. P. Jiang. 2016. 'Dynamic analysis of a vertically loaded rigid disc in a transversely isotropic multilayered half-space', *Meccanica*, 51: 1887-95.
- Ai, Z. Y., J. J. Mu, and G. P. Ren. 2018. '3D dynamic response of a transversely isotropic multilayered medium subjected to a moving load', *International Journal for Numerical and Analytical Methods in Geomechanics*, 42: 636-54.
- Ai, Z. Y., and L. H. Wang. 2017. 'Influences of Biot's compressible parameters on dynamic response of vertically loaded multilayered poroelastic soils', *Soil Dynamics and Earthquake Engineering*, 94: 7-12.
- Ai, Z. Y., and Y. F. Zhang. 2015. 'Plane strain dynamic response of a transversely isotropic multilayered half-plane', *Soil Dynamics and Earthquake Engineering*, 75: 211-19.
- . 2016. 'Vertical vibration of a rigid strip footing on a transversely isotropic multilayered half-plane', *Applied Mathematical Modelling*, 40: 10521-32.
- Amiri-Hezaveh, A., M. Eskandari-Ghadi, M. Rahimian, and A. K. Ghorbani-Tanha. 2013. 'Impedance Functions for Surface Rigid Rectangular Foundations on Transversely Isotropic Multilayer Half-Spaces', *Journal of Applied Mechanics-Transactions of the Asme*, 80.
- Ba, Z. N., Z. Q. Kang, and V. W. Lee. 2017. 'Plane strain dynamic responses of a multi-layered transversely isotropic saturated half-space', *International Journal of Engineering Science*, 119: 55-77.
- Biot, M. A. . 1941. 'General theory of three-dimensional consolidation', *Journal of Applied Physics*, 12: 155-64.
- . 1955. 'Theory of elasticity and consolidation for a porous anisotropic solid', *Journal of Applied Physics*, 26: 182-85.
- . 1956. 'Theory of propagation of elastic waves in a fluid-saturated porous solid. I. Low-frequency range', *Journal of the Acoustical Society of America*: 168-78.
- . 1962. 'Mechanics of deformation and acoustic propagation in porous media', *Journal of Applied Physics*, 33: 1482-98.

- Bougacha, S., J. L. Tassoulas, and J. M. Roesset. 1993. 'Analysis of Foundations on Fluid-Filled Poroelastic Stratum', *Journal of Engineering Mechanics-Asce*, 119: 1632-48.
- Cheng, A. H. D. 1997. 'Material coefficients of anisotropic poroelasticity', *International Journal of Rock Mechanics and Mining Sciences*, 34: 199-205.
- Das, B.M. 2011. *Principles of Soil Dynamics* (Cengage Learning: USA).
- Eskandari-Ghadi, M., and A. Ardeshir-Behrestaghi. 2010. 'Forced vertical vibration of rigid circular disc buried in an arbitrary depth of a transversely isotropic half space', *Soil Dynamics and Earthquake Engineering*, 30: 547-60.
- Eskandari-Ghadi, M., M. Fallahi, and A. Ardeshir-Behrestaghi. 2010. 'Forced Vertical Vibration of Rigid Circular Disc on a Transversely Isotropic Half-Space', *Journal of Engineering Mechanics*, 136: 913-22.
- Eskandari-Ghadi, M., S. M. Nabizadeh, and A. Ardeshir-Behrestaghi. 2014. 'Vertical and horizontal vibrations of a rigid disc on a multilayered transversely isotropic half-space', *Soil Dynamics and Earthquake Engineering*, 61-62: 135-39.
- Gazetas, G. 1981. 'Strip foundations on a cross-anisotropic soil layer subjected to dynamic loading', *Géotechnique*, 31: 161-79.
- Halpern, Marc R., and Paul Christiano. 1986a. 'Response of poroelastic halfspace to steady-state harmonic surface tractions', *International Journal for Numerical and Analytical Methods in Geomechanics*, 10: 609-32.
- . 1986b. 'Steady-state harmonic response of a rigid plate bearing on a liquid-saturated poroelastic halfspace', *Earthquake Engineering & Structural Dynamics*, 14: 439-54.
- Jin, B., and H. Liu. 1999. 'Vertical dynamic response of a disk on a saturated poroelastic half-space', *Soil Dynamics and Earthquake Engineering*, 18: 437-43.
- Kassir, M. K., K. K. Bandyopadhyay, and J. Xu. 1989. 'Vertical vibration of a circular footing on a saturated half-space', *International Journal of Engineering Science*, 27: 353-61.
- Kassir, Mumtaz K., and Xu Jimin. 1988. 'Interaction functions of a rigid strip bonded to saturated elastic half-space', *International Journal of Solids and Structures*, 24: 915-36.
- Khojasteh, A., M. Rahimian, M. Eskandari, and R. Y. S. Pak. 2008. 'Asymmetric wave propagation in a transversely isotropic half-space in displacement potentials', *International Journal of Engineering Science*, 46: 690-710.
- Khojasteh, A., M. Rahimian, M. Eskandari, and R. Y. S. Pak. 2011. 'Three-dimensional dynamic Green's functions for a multilayered transversely isotropic half-space', *International Journal of Solids and Structures*, 48: 1349-61.
- Khojasteh, A., M. Rahimian, R. Y. S. Pak, and M. Eskandari. 2008. 'Asymmetric dynamic Green's functions in a two-layered transversely isotropic half-space', *Journal of Engineering Mechanics-Asce*, 134: 777-87.
- Kirkner, David J. 1982. 'Vibration of a rigid disc on a transversely isotropic elastic half space', *International Journal for Numerical and Analytical Methods in Geomechanics*, 6: 293-306.

- Kumar, R., N. R. Garg, and A. Miglani. 2003. 'Elastodynamics of an axisymmetric problem in an anisotropic liquid-saturated porous medium', *Journal of Sound and Vibration*, 261: 697-714.
- . 2004. 'Dynamic behaviour of an anisotropic liquid-saturated porous medium in frequency domain', *Journal of Sound and Vibration*, 275: 877-91.
- Liu, K. S., X. Li, and X. N. Sun. 1997. 'A numerical method for axisymmetric wave propagation problem of anisotropic solids', *Computer Methods in Applied Mechanics and Engineering*, 145: 109-16.
- Liu, Z. X., J. W. Liang, and C. Q. Wu. 2015. 'Dynamic Green's function for a three-dimensional concentrated load in the interior of a poroelastic layered half-space using a modified stiffness matrix method', *Engineering Analysis with Boundary Elements*, 60: 51-66.
- Lu, J. F., and A. Hanyga. 2005. 'Fundamental solution for a layered porous half space subject to a vertical point force or a point fluid source', *Computational Mechanics*, 35: 376-91.
- Paul, S. 1976. 'On the displacements produced in a porous elastic half-space by an impulsive line load. (Non-dissipative case)', *Pure and Applied Geophysics PAGEOPH*, 114: 605-14.
- Philippacopoulos, A. J. 1989. 'Axisymmetric Vibration of Disk Resting on Saturated Layered Half-Space', *Journal of Engineering Mechanics*, 115: 2301-22.
- Philippacopoulos, A. J. . 1988. 'Lamb's problem for fluid-saturated, porous media', *Bulletin of the Seismological Society of America*, 78: 908–23.
- Piessens, R.; Doncker-Kapenga, E.; Überhuber, C. W.; Kahaner, D. K. 1983. *QUADPACK, A subroutine package for automatic integration* (Springer: Berlin).
- Pooladi, A., M. Rahimian, and R. Y. S. Pak. 2017. 'Poroelastodynamic potential method for transversely isotropic fluid-saturated poroelastic media', *Applied Mathematical Modelling*, 50: 177-99.
- Rahimian, M., M. Eskandari-Ghadi, R. Y. S. Pak, and A. Khojasteh. 2007. 'Elastodynamic Potential Method for Transversely Isotropic Solid', *Journal of Engineering Mechanics*, 133: 1134-45.
- Rajapakse, R. K. N. D., and T. Senjuntichai. 1995. 'Dynamic response of a multi-layered poroelastic medium', *Earthquake Engineering & Structural Dynamics*, 24: 703-22.
- Rajapakse, R. K. N. D., and Y. Wang. 1991. 'Elastodynamic Green's Functions of Orthotropic Half Plane', *Journal of Engineering Mechanics*, 117: 588-604.
- . 1993. 'Green's Functions for Transversely Isotropic Elastic Half Space', *Journal of Engineering Mechanics*, 119: 1724-46.
- Rice, J. R., and M. P. Cleary. 1976. 'Some basic stress-diffusion solutions for fluid saturated elastic porous media with compressible constituents', *Reviews of Geophysics and Space Physics*, 14: 227-41.
- Richart, F. E. . 1962. 'Foundation vibrations', *Trans. ASCE*: 863-98.
- Sahebkar, K., and M. Eskandari-Ghadi. 2016. 'Time-harmonic response of saturated porous transversely isotropic half-space under surface tractions', *Journal of Hydrology*, 537: 61-73.

- Senjuntichai, T., and W. Kaewjuea. 2008. 'Dynamic Response of Multiple Flexible Strips on a Multilayered Poroelastic Half-Plane', *Journal of Mechanics of Materials and Structures*, 3: 1885-901.
- Senjuntichai, T., S. Keawsawasvong, and R. Plangmal. 2018. 'Three-dimensional dynamic response of multilayered poroelastic media', *Marine Georesources & Geotechnology*: 1-14.
- Senjuntichai, T., and R. K. N. D. Rajapakse. 1994. 'Dynamic Greens-Functions of Homogeneous Poroelastic Half-Plane', *Journal of Engineering Mechanics-Asce*, 120: 2381-464.
- Senjuntichai, T., and Y. Sapsathiarn. 2003. 'Forced Vertical Vibration of Circular Plate in Multilayered Poroelastic Medium', *Journal of Engineering Mechanics*, 129: 1330-41.
- Senjuntichai, T.; Rajapakse, R. K. N. D. 1996. 'Dynamics of a rigid strip bonded to a multilayered poroelastic half-plane.' in A. P. S. Selvadurai (ed.), *Mechanics of Poroelastic Media* (Kluwer Dordrecht: Netherlands).
- Shodja, H. M., and M. Eskandari. 2007. 'Axisymmetric time-harmonic response of a transversely isotropic substrate-coating system', *International Journal of Engineering Science*, 45: 272-87.
- Sneddon, I. N. 1951. *Fourier Transforms* (McGraw-Hill: New York).
- Stoneley, R. 1949. 'The seismological implications of aeolotropy in continental structures', *Geophysical Supplements Monthly Notices of the Royal Astronomical Society*, 5: 343-53.
- Timoshenko, S. P.; Woinowsky-Krieger, S. . 1951. *Theory of Plates and Shells* (McGraw-Hill: New York).
- Wang, C. D., and J. J. Liao. 1999. 'Elastic solutions for a transversely isotropic half-space subjected to buried asymmetric-loads', *International Journal for Numerical and Analytical Methods in Geomechanics*, 23: 115-39.
- Wang, Y., and R. K. N. D. Rajapakse. 1994. 'An Exact Stiffness Method for Elastodynamics of a Layered Orthotropic Half-Plane', *Journal of Applied Mechanics-Transactions of the Asme*, 61: 339-48.
- Washizu, K. . 1982. *Variational Methods in Elasticity and Plasticity* (Pergamon: New York).
- Zeng, X., and R. K. N. D. Rajapakse. 1999. 'Vertical vibrations of a rigid disk embedded in a poroelastic medium', *International Journal for Numerical and Analytical Methods in Geomechanics*, 23: 2075-95.
- Zheng, P., B. Y. Ding, S. X. Zhao, and D. Ding. 2013. 'Dynamic Response of a Multilayered Poroelastic Half-Space to Harmonic Surface Traction', *Transport in Porous Media*, 99: 229-49.

VITA

NAME Suraparb Keawsawasvong

DATE OF BIRTH 28 February 1991

PLACE OF BIRTH Songkhla

INSTITUTIONS ATTENDED Bachelor of Engineering degree in Civil Engineering from Thammasat University in 2013 and Master of Engineering degree in Civil Engineering from Chulalongkorn University in 2015

PUBLICATION Keawsawasvong, S. and Senjuntichai, T. 2019. 'Poroelastodynamic fundamental solutions of transversely isotropic half-plane', Computers and Geotechnics, 106, 52-67.
Keawsawasvong, S. and Senjuntichai, T. 2018. 'Influence of anisotropic properties on vertical vibrations of circular foundation on saturated elastic layer', Mechanics Research Communications, 94, 102-109.